NEW INSIGHTS INTO THE CHARACTERISTICS AND CHEMISTRY OF ORGANIC AEROSOLS IN HONG KONG: TRANSITION FROM OUTDOOR TO INDOOR ENVIRONMENTS

HUO YUNXI

Ph.D.

The Hong Kong Polytechnic University

2025

The Hong Kong Polytechnic University

Department of Civil and Environmental Engineering

NEW INSIGHTS INTO THE CHARACTERISTICS AND CHEMISTRY OF ORGANIC AEROSOLS IN HONG KONG: TRANSITION FROM OUTDOOR TO INDOOR ENVIRONMENTS

HUO Yunxi

A Thesis Submitted to The Hong Kong Polytechnic University

in Partial Fulfillment of the Requirements for

the Degree of Doctor of Philosophy

April 2025

CERTIFICATE OF ORIGINALITY

I hereby declare that this thesis is my own work and that, to the best of my knowledge and belief, it reproduces no material previously published or written, nor material that has been accepted for the award of any other degree or diploma, except where due acknowledgment has been made in the text.

_____(Signed)

HUO Yunxi (Name of Student)

Abstract

Fine particulate matter ($PM_{2.5}$, define as particulate matter with an aerodynamic diameter of 2.5 micrometers or less) pollution has become a significant environmental and public health issue in densely populated megacities like Hong Kong. Recent studies indicate that secondary organic aerosols (SOA) are increasingly contributing to $PM_{2.5}$ levels, yet their sources and formation mechanisms remain insufficiently understood. Hong Kong, situated adjacent to the Pearl River Delta (PRD) region and the South China Sea, is influenced by both continental and marine air masses. This unique land-sea transitional zone may have an enhanced atmospheric oxidative capacity compared to typical urban areas, potentially facilitating SOA formation and the chemical evolution of organic aerosols (OA). Additionally, Hong Kong's urban environment is characterized by dense, tall buildings and limited living space per-capita, where numerous chemicals, predominantly organics, are present in indoor air. However, there is a lack of understanding regarding the composition and evolution of indoor organic compounds. In this study, we collected OA samples from both indoor and outdoor environments using advanced chemical analysis techniques. This approach allowed us to obtain a high time-resolution dataset of OA markers, providing new insights into the characteristics and chemical processes of SOA in outdoor air. Building on this knowledge, I further investigated the indoor environment, thereby addressing a critical knowledge gap in Hong Kong's indoor air quality research. The findings from this study enhance our understanding of the abundance and evolution of organic aerosols in both indoor and outdoor settings, and offer valuable guidance for developing effective air quality management strategies.

To explore the formation and evolution processes of SOA in the outdoor environment, a comprehensive sampling campaign was conducted at a regional background site in

Hong Kong. A central question in atmospheric chemistry is the extent to which anthropogenic emissions influence the formation of natural OA. To address this, a suite of state-of-the-art instruments was deployed to measure both bulk and speciated organic compounds in submicron particles. The study revealed that average carbon oxidation states ($\overline{OS}_C$) were higher at night in coastal air, contrasting with afternoon peaks in continental air. This suggests that aqueous reactions dominated in coastal air, as indicated by correlations between $\overline{OS}_C$, ozone and sulfate, while photochemical processes were more prevalent in continental air passing through the PRD region. The concentrations of ten speciated SOA markers were highest in continental air from the PRD, with high concentrations of anthropogenic SOA (ASOA) markers linked to precursor levels and intense photochemical reactions. A significant correlation (R^2 > 0.30) between these markers and total organics highlights the influence of anthropogenic emissions. In contrast, biogenic SOA (BSOA) markers derived from isoprene and monoterpenes were not directly explained by precursor levels. Detailed analysis showed that isoprene-derived SOA (iSOA) formation was influenced by aqueous reactions and potential aerosol seed formation. Elevated nighttime levels of 2-methyltetrols, differing from other SOA markers, were potentially linked to variations in relative humidity and/or gas-to-particle partitioning. Monoterpene-derived SOA (mSOA) formation was facilitated by in-situ photochemical processes in continental air, transforming fresh products into aged ones. Integrating bulk and molecular-level OA data, this study found that BSOA suppressed ASOA levels in coastal air, with SO_2 levels promoting BSOA formation. In two continental clusters, comparable levels of BSOA and ASOA were observed, but continental air traveling through the PRD region experienced higher atmospheric oxidation, favoring ASOA production. Hydroxyl dicarboxylic acids (OHDCA), important constituents of SOA, were observed at notable levels, with malic acid (a typical OHDCA species) concentrations reaching up to 533 ng m^{-3}. In coastal air, OHDCA correlated well with sulfate (R^2=0.48) during periods of

higher relative humidity (RH) and droplet-mode sulfate size distribution, suggesting aqueous formation. In short-range continental air, OHDCA levels rose significantly from morning to early afternoon (406 ng m^{-3}), correlating with corrected ozone levels considering titration loss (O_3_corr, sum of ozone and nitrogen dioxide). underscoring the role of gas-phase photochemistry in regulating OHDCA formation. The elevated OHDCA was likely attributed to aqueous photooxidation, with dominant factors varying under different atmospheric conditions. The precursors of OHDCA may include biogenic emissions, as indicated by correlations of OHDCA with 2-methylglyceric acid (bihourly data) and isoprene and monoterpenes (daily average data). However, anthropogenic aromatics might also contribute, especially in short-range continental air. These findings provide valuable observational evidence for refining simulations of OHDCA formation and its impact on air quality and climate.

To understand the emission characteristics and evolution processes of indoor OA, a detailed sampling campaign was carried out in a typical apartment in Hong Kong. While numerous studies have highlighted the adverse health effects of indoor particulate matters (PM), the molecular compositions and emission characteristics of PM-bound organic matter (OM) indoors remain poorly understood. This group of species is particularly critical due to its high concentration and complexity in indoor PM. In the Hong Kong residence where typical activities were performed at normal frequency and intensity, it was observed that these activities significantly elevated both the total concentration and the fraction of OM in indoor PM. However, during undisturbed periods-when no high-emission activities were occurring, though residual effects from previous activities might persist-the concentration of total PM-bound OM outdoors (10.3 ± 0.7 μg m^{-3}) exceeded that indoors (8.2 ± 0.1 μg m^{-3}). Indoor activities involving combustion or high-temperature processes significantly increased the indoor-to-outdoor (I/O) ratios for many organic species. In addition, factors such as gas-to-particle partitioning, secondary formation, carry-over (residues of pollutants in the air),

and re-emission modulated the I/O ratios of certain compounds. We obtained detailed emission profiles of speciated organics for five indoor activities within a residence. During undisturbed periods, the indoor contribution to PM-bound OM was estimated to be no higher than 13.1%. However, carry-over and/or re-emission were evident for certain compounds emitted from cigarette smoking and incense burning. Clear evidence of the aging of indoor cooking emissions was observed, suggesting the presence of indoor heterogeneous chemistry. Kinetic analysis indicated that the effective rate constants for oleic acid indoors are higher than those outdoors, likely due to elevated indoor temperatures accelerating reaction rates. Despite lower ozone levels indoors, the lifetime of oleic acid is comparable to that outdoors, implying the presence of undiscovered oxidants in indoor air. These findings enhance our understanding of the emissions and airborne fate of speciated organics in indoor PM.

Overall, this study comprehensively explored the characteristics and formation chemistry of OA in both indoor and outdoor environments in Hong Kong. Through online measurements, we identified key factors driving SOA formation in this land-sea transitional zone and examined the behavior of indoor OA in compact living spaces. The findings of this PhD thesis highlight the significant roles of aqueous and photochemical reactions in outdoor SOA formation. In addition, the study reveals the emission characteristics and evolution processes of indoor OA influenced by human activities. These results not only deepen our understanding of SOA formation in densely populated urban settings but also provide valuable insights for improving air quality management and mitigating health risks associated with particulate matter pollution.

THE NOVELTY OF THIS STUDY

In this PhD study, I deployed advanced mass spectrometry to conduct sampling campaigns in both indoor and outdoor environments in Hong Kong, characterizing the composition of OA from bulk to molecular levels. The SOA formation process in the outdoor environment was investigated utilizing a highly time-resolved dataset, identifying key influencing factors. This study is the first to provide field evidence that anthropogenic emissions can significantly affect SOA formation in Hong Kong, revealing that human-related air pollutants have a substantial impact on PM-bound organics. I also explored the formation process and potential precursors of notably high levels of climate-relevant OHDCA, proposing for the first time that different factors dominate their aqueous photochemical formation depending on the air masses reaching Hong Kong. The findings suggest that while the precursors of OHDCA mainly originated from biogenic sources, in air masses traveling through the PRD region, these precursors were also associated with anthropogenic emissions. Addressing the longstanding issue of indoor air pollution in Hong Kong, I examined the chemistry of outdoor OA within Hong Kong homes to better understand indoor OA. For the first time, I obtained emission profiles of particle-bound speciated organics for high-emission indoor activities, clearly identifying organic tracers. For the first time, I quantified the dynamic contributions of these activities, as well as outdoor air filtration, to the total PM-bound organics indoors. Furthermore, the chemical aging of indoor cooking emissions was explored and the kinetic parameters were calculated and compared with outdoor samples, which highlighted the importance of indoor heterogeneous chemistry.

RESEARCH OUTPUTS

1. **Huo, Yunxi**, Xiaopu Lyu, Dawen Yao, Beining Zhou, Qi Yuan, Shun-cheng Lee, and Hai Guo. "Exploring the formation of high levels of hydroxyl dicarboxylic acids at an urban background site in South China." Journal of Geophysical Research: Atmospheres 129, no. 6 (2024): e2023JD040096.

2. **Huo, Yunxi**, Dawen Yao, and Hai Guo. "Differences in aerosol chemistry at a regional background site in Hong Kong before and during the COVID-19 pandemic." Science of the Total Environment 926 (2024): 171990.

3. **Huo, Yunxi**, Hai Guo, Xiaopu Lyu, and Dawen Yao. "Emission characteristics, sources, and airborne fate of speciated organics in particulate matters in a Hong Kong residence." Indoor air 32, no. 3 (2022): e13017.

4. **Huo, Yunxi**, Xiaopu Lyu, Dawen Yao, and Hai Guo. "Characteristics of secondary organic molecular markers at a regional background site in Hong Kong: interplay between natural and anthropogenic emissions." (in preparation).

5. Lyu, Xiaopu, **Yunxi Huo**, Jin Yang, Dawen Yao, Kaimin Li, Haoxian Lu, Yangzong Zeren, and Hai Guo. "Real-time molecular characterization of air pollutants in a Hong Kong residence: Implication of indoor source emissions and heterogeneous chemistry." Indoor Air 31, no. 5 (2021): 1340-1352.

6. Li, Hongyong, Xiaopu Lyu, Likun Xue, **Yunxi Huo**, Tianshu Chen, Dawen Yao, Haoxian Lu, Beining Zhou, and Hai Guo. "Hydroxyl dicarboxylic acids at a mountainous site in Hong Kong: formation mechanisms and implications for particle growth." ACS Environmental Au (2025).

7. Li, Hongyong, Xiaopu Lyu, Likun Xue, **Yunxi Huo**, Dawen Yao, Haoxian Lu, and Hai Guo. "In situ measurement of organic aerosol molecular markers in urban Hong Kong during a summer period: temporal variations and source apportionment." Atmospheric Chemistry and Physics 24, no. 12 (2024): 7085-7100.

8. Yao, Dawen, Hai Guo, Xiaopu Lyu, Haoxian Lu, and **Yunxi Huo**. "Secondary organic aerosol formation at an urban background site on the coastline of South China: Precursors and aging processes." Environmental Pollution 309 (2022): 119778.

9. Lyu, Xiaopu, Hai Guo, Dawen Yao, Haoxian Lu, **Yunxi Huo**, Wen Xu, Nathan Kreisberg et al. "In situ measurements of molecular markers facilitate understanding of dynamic sources of atmospheric organic aerosols." Environmental Science & Technology 54, no. 18 (2020): 11058-11069.

10. Zeng, Lewei, Kaimin Li, Hai Guo, Beining Zhou, Xiaopu Lyu, **Yunxi Huo**, Erik Uhde et al. "Contributions of indoor household activities to inhalation health risks induced by gaseous air pollutants in Hong Kong home." Aerosol and Air Quality Research 23, no. 9 (2023): 230063.

11. Xia, Men, Tao Wang, Zhe Wang, Yi Chen, Xiang Peng, **Yunxi Huo**, Weihao Wang et al. "Pollution-derived Br_2 boosts oxidation power of the coastal atmosphere." Environmental Science & Technology 56, no. 17 (2022): 12055-12065.

ACKNOWLEDGEMENTS

Time flies like an arrow; nearly seven years have passed since I first arrived in Hong Kong. As a teenager, I was always fascinated by Hong Kong's culture and dreamed of living here. Looking back, I could never have imagined being fortunate enough to complete my PhD in this vibrant city. This unforgettable journey would not have been possible without the guidance and support of my PhD supervisor, Professor Guo Hai. I still vividly remember my first interview in his office. The regret of not being selected for the research postgraduate program during my undergraduate years lingered in my heart, and I felt like a drowning person at that time. Perhaps Professor Guo did not realize that his PhD offer was a lifeline for me. I am deeply grateful to him for providing a platform that allowed me to turn the tide during a low point in my life. Throughout my PhD studies, Professor Guo's broad-mindedness pardoned my naive ideas and words, giving me the freedom to complete my research. I often felt inadequate, striving to work hard so as not to disappoint him. His rigorous attitude and insightful understanding of scientific research helped me navigate challenges. As I write this, his care and support come vividly to mind. It is because of his unwavering support that I was able to complete my dissertation.

I want to express my gratitude to my parents and family first. I have always been a child who loves freedom, often unwilling to follow established traditions or expectations, which inevitably led to conflicts. However, I am most grateful that my parents chose to support and understand me after moments of hesitation and tension. I hope to one day create a more beautiful world to repay them. I also want to thank my grandparents. Though they are slow in speech, their love has been a guiding light through dark times whenever I felt sad.

I also want to express my deepest appreciation to my old friends, whose happiness and support have been crucial throughout my journey. To my college debate team friends-

Qing QING, Xudong FANG, Jinyu SHENG, Fuyi CHEN, and Benjin JIN-the memories we shared have always helped me through times of loneliness and hardship. I especially want to thank Qing QING, who has been my pillar since we met. No matter the time or situation, you have always been there for me. Thank you for sharing the joys and beauty of life and for standing by me through tough times. I want to thank the friends I grew up with either. Although the pandemic has limited our opportunities to meet, you always warmly welcome me back whenever I return home. My dear friends, thank you for being a part of my life, and may our friendship last forever.

Last, I would like to sincerely thank all my group mates: Dr. Xiaopu LYU, Dr. Dawen YAO, Dr, Haoxian LU, Dr. Zeren YANGZONG, Dr. Jingcui XU, Dr. Cunteng WANG, Dr. Yu WANG, Mr. Hongyong LI, Miss Beining ZHOU, and Miss Jin YANG. I am deeply grateful for their support in discussing my research and for the leisure time we shared. Special appreciation goes to Dr. Xiaopu LYU, whose invaluable assistance greatly enhanced my studies and helped me become a better PhD student. The time we spent together will always be a cherished memory. I would also like to thank our scientific officers, Mr. Jazz CHAN and Mr. Steven POON, for their technical support during my studies and sampling campaigns. Additionally, I extend my gratitude to the CAPRAM team at TROPOS and the people I met in Germany: Professor Herrmann, Dr. Andreas, Dr. Erik, Dr. Lin HE, Dr. Liang WEN, Miss Yaru WANG, and Mr. Yifan YANG. Meeting them during the pandemic, a particularly challenging period for my research, was a blessing. Their kindness and warmth lifted my spirits and made a difficult time more bearable. The three months I spent at TROPOS are an unforgettable part of my PhD journey.

It is challenging to encapsulate learning and growth from my six years of PhD study in just a few hundred words. While I may not consider myself an outstanding PhD graduate, I have done my best to complete this academic journey. If there is one lesson

that stands out above all else, it is the importance of perseverance-never giving up and always striving for excellence. I believe this lesson will benefit me throughout my life.

Table of Contents

Abbreviations

Abbreviations	Full names
2-MGA	2-methylglyceric acid
2-MTs	2-methyltetrols
3-HDGA	3-hydroxy-4,4-dimethylglutaric acid
AC	Air conditioners
ALWC	Aerosol liquid water content
AMS	Aerosol mass spectrometry
AOC	Atmospheric oxidation capacity
aqSOA	Aqueous secondary organic aerosol
ASOA	Anthropogenic secondary organic aerosol
AVOCs	Anthropogenic volatile organic compounds
BBOA	Biomass-burning OA
BSOA	Biogenic secondary organic aerosol
BTEX	Sum of toluene, benzene, ethylbenzene and xylenes
BVOCs	Biogenic volatile organic compounds
CFD	Computational fluid dynamics
Cl	Chlorine
Cl^-	Chloride
CMAQ	Community Multiscale Air Quality
CMB	Chemical Mass Balance
CO	Carbon monoxide
COA	Cooking-related OAs
CPCA	Custom principal component analysis
CTD	Collection-Thermal Desorption
DHOPA	2,3-dihydroxy-4-oxopentanoic acid
E-AIM	Extended AIM Aerosol Thermodynamics Model
EC	Elemental carbon

GC-MS	Gas chromatography-mass spectrometry
HEPA	High efficiency particulate air
HMML	Hydroxymethel-methyl-α-lactone
HO_2	Hydroperoxyl
HOA	Hydrocarbon-like OA
HT	Hok Tsui
HYSPLIT	Hybrid Single-Particle Lagrangian Integrated Trajectory
I/O	Indoor-to-outdoor
IEPOX	Isoprene epoxydiols
iSOA	Isoprene-derived SOA
ISs	Internal standards
*j*NO2	Photolysis frequency of NO_2
LO-OOA	Less oxidized oxygenated organic aerosol
LVOOA	Low-volatility oxygenated organic aerosol
MBTCA	3-methyl-1,2,3-butanetricarboxylic acid
MDLs	Method detection limits
MO-OOA	More oxidized oxygenated organic aerosol
mSOA	Monoterpene-derived SOA
MSTFA	N-Methyl-N-(trimethylsilyl) trifluoroacetamide
NH_4^+	Ammonium
NO	Nitrogen monoxide
NO_2	Nitrogen dioxide
NO_3	Nitrate radicals
NO_3^-	Nitrate
NO_x	Nitrogen oxides
NR-PM_1	Non-refractory sub-micron particulate matter
O:C	Oxygen-to-carbon
O_3	Ozone
O_3_corr	Sum of ozone and nitrogen dioxide

OA	Organic aerosol
OC	Organic carbon
OH	Hydroxyl
OHDCA	Hydroxyl dicarboxylic acids
OM	Organic matter
OOA	Oxygenated OA
$\overline{OS}_C$	Carbon oxidation state
P/M ratio	Ratio of pinic acid to MBTCA
PA	Pinic acid
PAHs	Polycyclic aromatic hydrocarbons
PM_1-OM	Total organics in PM_1
PM	Particulate matters
$PM_{2.5}$	Atmospheric particulate matter with an aerodynamic diameter of or less than 2.5 μm
PM_1	Atmospheric particulate matter with an aerodynamic diameter of or less than 1 μm
PM_{10}	Atmospheric particulate matter with an aerodynamic diameter of or less than 10 μm
PMF	Positive Matrix Factorization
PNA	Pinonic acid
POA	Primary organic aerosol
PRD	Pearl River Delta
PTR	Proton Transfer Reaction-Time of flight-Mass Spectrometer
R^2	Coefficient of determination
RH	Relative humidity
RIE	Relative ionization efficiencies
RO_2	Peroxy radicals
ROC	Reactive organic carbon
S/IVOCs	Semi-/inter-volatile organic compounds
SO_2	Sulfur dioxide

SO_4^{2-}	Sulfate
SOA	Secondary organic aerosols
SVOOA	Semi-volatile oxygenated organic aerosol
SV-TAG	The dual-cell semi-volatile thermal desorption aerosol gas chromatograph
TAG	Thermal-desorption Aerosol Gas-chromatograph
VBS	Volatility basis set
VCPs	Volatile chemical products
VOCs	Volatile organic compounds

Lists of Figures

Lists of Tables

Chapter 1 Introduction

1.1 Background

With rapid urbanization and industrialization, air quality has become a significant public concern. Previous epidemiological studies have warned that air pollutants are associated with various acute and chronic health effects, which vary depending on the pollutant constituents (Li et al., 2003, Manisalidis et al., 2020). Particulate air pollution, particularly fine particulate matters ($PM_{2.5}$), is consistently linked to serious health effects, such as adverse respiratory and cardiopulmonary morbidity (Feng et al., 2016, Englert, 2004). Moreover, some components in $PM_{2.5}$ can scatter and absorb solar and territorial radiation, thereby modulating climate by affecting the atmospheric abundance and distribution of trace gases on both global and regional scales (Tai et al., 2010, Goldstein et al., 2009).

Previous studies have demonstrated that $PM_{2.5}$ is a complex mixture of chemical compositions, including organics, inorganic ions, heavy metals, and trace elements. Although heavy metals and trace elements account for only a small proportion of $PM_{2.5}$ mass concentration (Chow et al., 2022, Liu et al., 2018), the sources and formation of inorganics in $PM_{2.5}$ have been extensively investigated (Zhang et al., 2012, Schlesinger, 2007). Organics, also known as organic aerosols (OA) or organic matter (OM), constitute the largest portion of $PM_{2.5}$, ranging from 20% to 90% (Jimenez et al., 2009, Kanakidou et al., 2005). The composition of OA is characterized by a wide variety of organic compounds containing carbon, hydrogen, oxygen, nitrogen, and sulfur atoms, influenced by factors such as emission sources, meteorological conditions, and land cover. Based on their origins, OA can be classified as either primary organic aerosol (POA) or secondary organic aerosol (SOA) (Kroll and Seinfeld, 2008, Jang et al., 2002). POA is directly emitted from natural sources (e.g., pollen, wildfires, and volcanic

eruption) and anthropogenic sources (e.g., cooking, stationary, and traffic emission), while SOA forms in the atmosphere through complex chemical processes involving the oxidation of volatile organic compounds (VOCs) and semi-/inter-volatile organic compounds (S/IVOCs) (Ziemann and Atkinson, 2012, Ervens et al., 2011). The shift in volatility is a key driver for multiphase reactions that generate SOA, yet the mechanisms of these physicochemical processes remain incompletely understood (Murphy et al., 2011, Lane et al., 2008). Furthermore, the complex blend of SOA precursors, with numerous functional groups and molecular configurations, complicates the understanding of SOA formation (Goldstein and Galbally, 2007). Recent modeling efforts have incorporated the volatility basis set (VBS) approach into emission inventories to better account for precursors, resulting in improved agreement between measured and simulated SOA concentrations (Shrivastava et al., 2011, Tsimpidi et al., 2010). However, the VBS approach often lumps species with the same saturation vapor pressure into a single bin and assumes a constant mass increase within that bin, posing challenges in accurately reproducing both SOA mass and the oxygen-to-carbon (O:C) ratio in some simulation scenarios (Hodzic et al., 2010). Therefore, it is crucial to obtain more molecular-level information from field studies to better characterize and constrain emissions, oxidation mechanisms, and subsequent changes in OA composition.

Characterizing and identifying the speciation of OA involves various analytical tools, which can be broadly categorized into offline and online techniques. Offline techniques typically involve filter-based sample collection, allowing for the analysis of the physical and chemical properties of OA using a range of instruments (Hallquist et al., 2009). However, these methods require sampling periods of hours or days, making them inadequate for capturing rapid changes in OA evolution processes. To address this limitation, online techniques such as Aerosol Mass Spectrometry (AMS) and Thermal-

desorption Aerosol Gas-chromatograph (TAG) have been developed (DeCarlo et al., 2006, Williams et al., 2006). AMS can measure the size-resolved mass concentration of non-refractory fine particle components (PM_1, particulate matter with an aerodynamic diameter less than 1 micrometer, and $PM_{2.5}$), including total organics and inorganics (sulfate, nitrate, ammonium, and chloride). The mass spectrum matrix obtained from AMS can be decomposed into several OA factors (e.g., hydrocarbon-like OA (HOA), oxygenated OA (OOA), cooking-related OA (COA), biomass-burning OA (BBOA)) to reflect influences from various sources or atmospheric processes. However, AMS provides information only on bulk and fragmented organics, as molecules undergo fragmentation without pre-separation, limiting its ability to offer specific molecular information on OA composition. To meet the growing demand for highly time-resolved molecular-level measurements, researchers at the University of California, Berkeley, developed the TAG instrument. This emerging technique is designed for in-situ analysis of speciated OA markers in particles. To date, TAG has been increasingly applied in field OA studies worldwide, including in America (Chan et al., 2016, Zhao et al., 2013, Williams et al., 2010), the Amazon Forest (Yee et al., 2020, De Sá et al., 2017), Shanghai (Zhang et al., 2021, He et al., 2020, Wang et al., 2020), and Hong Kong (Wang et al., 2022b, Lyu et al., 2020), as well as in chamber experiments (Bertrand et al., 2018, Fortenberry et al., 2018, Leavey et al., 2017, Lambe et al., 2009). Recent studies have also applied AMS and TAG to investigate indoor OA components (Katz et al., 2021, Lyu et al., 2021, Lunderberg et al., 2020, Kristensen et al., 2019, Lunderberg et al., 2019), examining their sources, evolution, and dynamic behaviors under rapidly changing conditions such as temperature, ventilation, and outdoor air pollution. Compared to AMS, TAG has a lower time resolution (with a minimal time interval of about 1h), and lacks the capability to measure total organics and size-resolved concentrations. Therefore, combining TAG and AMS is currently necessary to achieve a more comprehensive characterization of OA components and enhance our

understanding of their formation chemistry.

Hong Kong, one of the most densely populated cities globally, faces air pollution challenges related to PM from various local sources such as traffic and cooking (Yao et al., 2021, Lee et al., 2015). In addition, meteorological factors, particularly northerly winds in autumn, transport air masses from heavily polluted regions such as the PRD region, further influencing PM levels (Louie et al., 2005). As a coastal city in a subtropical area, Hong Kong experiences higher temperatures and relative humidity, which can enhance photochemical and aqueous processes for SOA formation. Over the past decade, background fine particle levels at a remote site (Tap Mun) have significantly decreased from 30 μg m^{-3} in 2013 to 12 μg m^{-3} in 2023 (HKEPD). However, a comparison of AMS measurements at two rural sites (HKUST and Hok Tsui) in 2011 and 2020 showed stable SOA concentrations, with 5.2 μg m^{-3} in 2011 and 5.0 μg m^{-3} in 2020, despite a decline in NR-PM_1 levels from15.9 μg m^{-3} in 2011 to 12.3 μg m^{-3} in 2020 (Yao et al., 2022, Li et al., 2015). These observations suggest that SOA components are becoming a dominant factor in fine particle pollution. Stringent emission reduction measures have decreased VOCs precursors for SOA formation (Tan et al., 2023, Huang et al., 2015b). Recent studies indicate that anthropogenic emissions (e.g., NO_x and SO_2) can enhance SOA formation (Shrivastava et al., 2019, Xu et al., 2015, Shilling et al., 2013), but these processes have not been thoroughly investigated in Hong Kong. Therefore, there is a pressing need to study SOA chemistry in the region. Besides, previous studies have highlighted that cooking is an important contributor to OA in urban Hong Kong (Yao et al., 2021). Since most cooking emissions originate indoors, it is essential to investigate the indoor environment. Recently, the adverse health impacts of indoor PM have also gained increasing attention (Kumar et al., 2023, Li et al., 2017). Given the limited living space per capital in Hong Kong, indoor air quality studies are essential. Previous research has demonstrated that outdoor PM can

infiltrate indoor spaces, worsening indoor air quality (Long and Sarnat, 2004). High-emission activities such as incense burning and traditional Chinese cooking are common in daily life of Hong Kong residents. However, past studies on indoor air quality in Hong Kong have primarily focused on species with known health risks or their physical dynamics through computational fluid dynamics (CFD) simulations (Chen et al., 2020, Chang et al., 2007). Recent research highlights indoor heterogeneous reactions leading to SOA formation (Abbatt and Wang, 2020, Petrick et al., 2011), yet the composition and evolution of airborne particles indoors remain understudied compared to outdoor environments. This knowledge gap is concerning in Hong Kong, where residents spend most of their time in confined indoor spaces.

In this PhD study, we integrated high-resolution measurements from TAG and AMS to investigate the characteristics and chemistry of OA at both bulk and molecular levels. We identified and quantified a series of OA markers, exploring the impact of anthropogenic emissions on SOA formation in a regional background. During the sampling campaign in Hong Kong, we observed high levels of speciated SOA and studied their formation mechanisms. Additionally, we examined the molecular characteristics of OA within a Hong Kong apartment and compiled emission profiles of typical indoor activities. The evolution processes of certain indoor activities were further explored. The findings of this study provide valuable insights into the speciation and chemical evolution of OA in both outdoor and indoor environments in Hong Kong.

1.2 Organization

This thesis is organized into six chapters, each summarized as follows:

Chapter 1: This chapter provides the research background, highlights current knowledge gaps, and outlines the organization of the study.

Chapter 2: This chapter reviews previous studies on the formation chemistry of atmospheric aerosols, the development and application of TAG, and past research on OA in Hong Kong. It summarizes the limitations of previous studies and establishes the research objectives for this study.

Chapter 3: This chapter details the sampling sites, instruments, and models used in the study.

Chapter 4: This chapter presents findings from a field observation conducted at a regional background site. It discussed the characteristics of typical SOA tracers observed during the campaign, with a focus on the anthropogenic influence on SOA formation. Notably, high levels of OHDCA were detected, prompting further investigation into their formation mechanisms and potential precursors under varying atmospheric conditions.

Chapter 5: This chapter details the results of a field observation conducted in an apartment, designed to replicate the daily activities of typical Hong Kong families. Emission profiles of particle-bound speciated organics were determined for high-emission indoor activities, with clear identification of organic tracers. The indoor evolution of source-emitted aerosols was further explored using the identified OA tracers.

Chapter 6: This chapter summarizes the major conclusions of the study, discusses its limitations, and offers suggestions for future research.

Chapter 2 Literature review

2.1 Chemical components in atmospheric aerosols

2.1.1 Overview of chemical compositions

Atmospheric aerosols are a complex mixture of components, including heavy metals, trace elements, inorganic ions (i.e., sulfate, nitrate, ammonium, and chloride), and organics. Aerosols that are directly emitted from natural sources, such as wildfires and volcanoes, or from anthropogenic sources, such as industry, traffic, and livestock, are known as primary aerosols (Zhao et al., 2021, Yu et al., 2013). In addition, atmospheric heterogenous reactions can lead to secondary aerosol formation (Ziemann and Atkinson, 2012). Primary aerosols typically contain significant amounts of elements (e.g., iron, silicon, sodium, and chlorine), whereas secondary aerosols are predominantly composed of organic and inorganic species such as sulfate, nitrate, and ammonium. It has been reported that secondary formation processes are the predominant drivers of haze days in China, with organic and inorganic aerosols together contributing up to 77% of $PM_{2.5}$ concentrations (Huang et al., 2014). Evidence also suggests that inorganic components in aerosols can contribute to SOA formation. For instance, Kulmala et al. (2000) indicated that the nucleation of sulfuric acid and ammonia is an efficient pathway for new particle formation, providing condensation sites for organic vapors. The abundance of inorganic species in aerosols can also affect particle acidity; Surratt et al. (2007) demonstrated that the yield of isoprene-derived SOA is positively correlated with increased aerosol acidity. Furthermore, aerosols containing nitrate- and/or sulfate exhibit strong hygroscopic properties, facilitating aqueous-phase reactions that generate oxidized SOA species (Shi et al., 2008).

2.1.2 Organic aerosol in the atmosphere

2.1.2.1 Identification of OA sources

Chemical Mass Balance (CMB) and Positive Matrix Factorization (PMF) are two widely used receptor models for the source apportionment of OA (Schauer et al., 1996, Paatero and Tapper, 1994). Both models utilize mathematical algorithms to calculate source contributions, operating under the assumption that the input OA markers originate from multiple sources with distinct source profiles (Reff et al., 2007, Hopke, 2003). The key difference between these models lies in their approach to source profiles: the CMB model requires prior knowledge of source profiles and cannot resolve unknown or undefined sources. In contrast, the PMF model derives source profiles directly from the input datasets, making it more user-friendly for studies focused on source apportionment.

The PMF model identifies sources by analyzing variations in input data and interpreting the sources based on distinctive tracers within source profiles. Its first application to aerosol studies in Hong Kong focused on identifying sources of ions and elements (Lee et al., 1999, Xie et al., 1999). Typically, major aerosol components inputted into PMF include organic carbon (OC), elemental carbon (EC), inorganic ions, and elements measured using traditional filter-based methods (Amato et al., 2009, Heo et al., 2009, Song et al., 2006). However, PMF can struggle to fully separate sources with similar temporal variations when indicative tracers are absent. To address this, Wang et al. (2017b) demonstrated that incorporating specific tracers into the PMF model significantly improves the estimation of SOA contributions. The performance of PMF is also influenced by the time resolution of input data (McGuire et al., 2014). Traditional filter-based measurements, which often cover extended periods, can reduce data variability and increase rotational ambiguity (Paatero and Hopke, 2009). Advances in online mass spectrometry techniques (e.g., AMS and TAG) have mitigated this issue, allowing PMF to resolve rapid changes in source emissions over shorter periods. Zhang

et al. (2005a) developed a custom principal component analysis (CPCA) method for AMS datasets, successfully characterizing HOA and OOA factors (Zhang et al., 2005b). Lanz et al. (2007) applied PMF to AMS spectra, separating the OOA factor into two components with different volatilities. Lane et al. (2008) further refined this approach by combining the multilinear engine method with PMF to resolve three OA factors: HOA, OOA, and wood combustion aerosol. AMS can also identify signals from sources such as sea salt (Ovadnevaite et al., 2012), organosulfate compounds (Huang et al., 2015a), and nanoplastic particles (Niu et al., 2024) using surrogate or authentic standards. However, AMS characterizes only the bulk OA spectra without pre-separation, necessitating deconvolution of the organic matrix to extract source and evolution information. Additionally, AMS source apportionment results are primarily interpreted based on lab-determined source profiles and atomic ratios, which can limit the accurate definition of some natural or anthropogenic sources in the real atmosphere. To overcome this limitation, Prof. Goldstein's group has developed a new online instrument capable of in-situ measurement of speciated OA markers (Williams et al., 2006). Wang et al. (2018) evaluated the performance of PMF model using averaged TAG data over intervals of 1, 4, and 6 hours, finding that higher time resolution resulted in more stable and distinct source profiles.

2.1.2.2 Chemistry of SOA formation

Secondary Organic Aerosols (SOA) constitute a significant portion of OA in most regions, raising concerns about their health and climate impacts (Pye et al., 2021, Zhu et al., 2017). The predominant mechanism for SOA formation involves the gas-phase oxidation of VOCs, resulting in lower-volatility products that partition into the condensed phase (Finlayson-Pitts and Pitts Jr, 1999). VOCs, crucial precursors for SOA formation, originate from both biogenic (BVOCs) and anthropogenic (AVOCs) sources. Globally, BVOCs account for 75-90% of total VOCs emissions and contribute up to 50%

SOA formation (Hoffmann et al., 1997, Guenther et al., 1995). Isoprene and monoterpenes are the most abundant BVOCs, with isoprene being the most prevalent (Surratt et al., 2010, Paulot et al., 2009, Claeys et al., 2004). It is well-established that isoprene produces different products under varying NO_x conditions (Carlton et al., 2009). Elevated NO_x levels shift isoprene oxidation from the hydroperoxyl (HO_2) pathway, forming isoprene epoxydiols (IEPOX) and eventually 2-methyltetrols (2-MTs) and C_5-alkenetriols, to the NO/NO_2 pathway, resulting in hydroxymethel-methyl-α-lactone (HMML) and 2-methylglyceric acid (2-MGA) (Kroll et al., 2006, Kroll et al., 2005, Claeys et al., 2004). Monoterpenes, of the second most prevalent BVOCs, exhibit diverse atmospheric reactivity (Heald et al., 2008, Yu et al., 1999). Among them, α-pinene contributes approximately 15% of global SOA mass (Heald et al., 2008). Kamens et al. (1999) first described the gas-phase reaction of α-pinene with ozone, estimating that 20-40% of reacted α-pinene carbon transitions to the aerosol phase. Kamens and Jaoui (2001) identified pinic acid (PA) and pinonic acid (PNA) as primary products of α-pinene ozonolysis. Subsequent reactions involving PNA and OH radicals can produce 3-methyl-1,2,3-butanetricarboxylic acid (MBTCA) (Szmigielski et al., 2007). In addition to α-pinene, the molecular structure of monoterpene isomers affects SOA yields, with exocylic double bonds (adjacent to ring skeleton) yielding more SOA than endocyclic ones (Friedman and Farmer, 2018). Although BVOCs dominate global VOC emissions, AVOCs play a crucial role in urban SOA formation. Low-chain alkanes and alkenes are abundant AVOCs, but their oxidation products mainly remain in the gas phase, contributing only 20% to urban SOA (Ziemann, 2011, Volkamer et al., 2006, Carter and Atkinson, 1985). In contrast, aromatic AVOCs, though less abundant, produce oxidized products that partition into particles, yielding higher SOA (Volkamer et al., 2006). Key AVOC sources include vehicle emissions, solvent use, and industry, with emerging sources like volatile chemical products (VCPs) from indoor cleansers, detergents, pesticides, and personal care products (Pennington et al., 2021, McDonald

et al., 2018). At the molecular level, 2,3-dihydroxy-4-oxopentanoic acid (DHOPA) is a typical anthropogenic SOA tracer from toluene oxidation (Al-Naiema and Stone, 2017). Nitromonoaromatics and phthalic acids are also products of aromatic VOCs and naphthalene photooxidation, though they can also originate from primary emissions such as vehicles and biomass burning (Iinuma et al., 2010, Kawamura and Kaplan, 1987a). More field studies are needed to evaluate AVOC-related SOA tracers concerning abundance, origins, and atmospheric behavior. Recent research highlights the significant influence of interactions between biogenic and anthropogenic emissions on SOA formation. Weber et al. (2007) first emphasized the impact of anthropogenic components on SOA formation. Goldstein et al. (2009) suggested that heterogeneous oxidation of BVOCs in the presence of NO_x and sulfate significantly affects summer aerosol optical thickness in the United States. Xu et al. (2015) found that SOA formation from isoprene and monoterpenes is influenced by SO_2 and NO_x emissions, with sulfate, rather than aerosol liquid water content (ALWC), directly controlling isoprene SOA formation. Edwards et al. (2017) observed that nighttime oxidation of BVOCs is limited by NO_x when the NO_x to BVOCs ratio is below 0.5. Zhang et al. (2018) demonstrated that NO_x plays a central role in monoterpene SOA formation, with reductions in NO_x leading to decreased SOA formation. Pye et al. (2013) used a Community Multiscale Air Quality (CMAQ) model to predict that a 25% reduction in SO_x (SO_2 + SO_4^{2-}) could significantly decrease isoprene aerosol levels. Marais et al. (2016) showed that a 34% reduction in NO_x emissions could increase isoprene SOA by 7%, while a 48% reduction in SO_2 could decrease it by 35%. In the PRD region, He et al. (2018a) explored isoprene SOA formation pathways, revealing sulfate's crucial role. Ding et al. (2019) measured other typical BSOA compounds derived from the oxidation of monoterpenes and β-caryophyllene, identifying a strong correlation between BSOA and both sulfate and O_x in this heavily polluted region. A study at a mountain site in the PRD region observed high BSOA tracer concentrations, which increased with the

arrival of anthropogenic pollutants, e.g., SO_2 and NO_2 due to enhanced aerosol acidity (Ma et al., 2024). Despite its urban density, Hong Kong has a rich and diverse vegetation cover (78%). During autumn and winter, air masses from the northern continent bring significant anthropogenic pollution to Hong Kong, but the impact on SOA formation has received little attention.

Recent studies have highlighted aqueous phase chemistry as a crucial mechanism in SOA formation, which may help resolve discrepancies between observed and model-predicted SOA concentrations (Heald et al., 2005). Generally, soluble VOCs and SVOCs can partition into the aqueous phase, a process typically described by Henry's Law (McNeill, 2015). Within this phase, they undergo chemical reactions to form aqueous SOA (aqSOA), which is a highly oxidized component. Efforts have been made to identify aqSOA at the molecular level to better understand its formation processes and contributions to particulate matters (Ye et al., 2020, Yu et al., 2014, Yu et al., 2005). For example, studies have identified oxalic acid as an important component of aqSOA, potentially contributing to the higher oxidation states observed in ambient OA (Charbouillot et al., 2012). Given the important role of aqueous reactions in SOA formation, further investigation into the molecular-level details of aqSOA and its formation processes is essential.

Moreover, recent research has increasingly focused on indoor SOA chemistry due to the unique indoor environment characterized by relatively stagnant air, low light levels, and potentially overlooked radical sources. The mechanisms behind the formation of indoor secondary organics remain not fully understood. Mattila et al. (2020a) discovered that cleaning with bleach can trigger the oxidation of terpenes indoors, leading to the production of oxidized VOCs and subsequent SOA formation. In a follow-up study, Mattila et al. (2020b) employed a kinetic model to demonstrate that bleach-related compounds can alter the levels of hydroxyl (OH) and chlorine (Cl)

radicals, thereby influencing indoor SOA formation through multiphase chemistry. Wang et al. (2020) highlighted the significance of surface-gas interactions for indoor pollutants, noting that compounds considered fully volatile outdoors behave as semivolatile indoors, with a greater presence on surfaces than in the air. Mattila et al. (2022) examined the reactive organic carbon (ROC) budget in indoor and outdoor air, finding higher ROC concentrations indoors and identifying activities such as cooking and cleaning as significant contributors to indoor ROC levels. Reidy et al. (2023) reported elevated OH radical concentrations during indoor cooking, which contribute to SOA growth. Zhou et al. (2023) explored the multiphase oxidation of unsaturated oils indoors, underscoring the critical role of ozonolysis reactions. Faty et al. (2024) highlighted the importance of multiphase reactions in determining the chemical fate of reactive low-volatility compounds indoors.

2.2 The development and application of TAG

The first TAG was developed by Prof. Goldstein's group at UC Berkeley to enable in-situ measurements of speciated markers in atmospheric aerosols (Williams et al., 2006). The core component of TAG is the Collection-Thermal Desorption (CTD) cell, which collects particles and thermally desorbs them to release speciated OA components. However, this initial version did not fully recover oxygenated and polar OA markers. In 2008, Goldstein et al. (2008)introduced the 2D-TAG, which improved separation capabilities by an order of magnitude over the original version. Building on this, Zhao et al. (2013) developed the SV-TAG by improving the inlet system and CTD cell, allowing for the simultaneous measurement of gaseous and condensed phase organic species. This advancement facilitated the observation of gas-to-particle partitioning processes of speciated S/IVOCs. Despite these improvements, all three TAG versions faced challenges in measuring polar and oxidized organic compounds. To address this, Isaacman et al. (2014) optimized TAG with an in-situ derivatization method. More

recently, Wernis et al. (2021) developed the c-TAG, extending the measurement range of organic compounds. This latest version provides hourly data on speciated VOCs and bihourly data on I/SVOCs within a single measurement cycle, offering a more comprehensive view of atmospheric oxidation and partitioning processes.

With advancements in the TAG instrument, its applications in the OA study have expanded globally. The initial use of TAG was to identify sources of observed OAs and to differentiate bulk OM measured by the AMS (Williams et al., 2007). A subsequent chamber study (Lambe et al., 2009) measured the effective rate constants and uptake coefficients of diesel-emitted POA markers with OH radicals, providing valuable insights into OA evolution processes in vehicle emissions. Williams et al. (2010) pioneered the measurement of the transition of speciated organics from vapor to particle phase in real-world environments, partially bridging the gap between chamber studies and field measurements. The first application of SV-TAG successfully quantified speciated SVOCs in the vapor phase, offering important insights into gas-to-particle partitioning theory (Zhao et al., 2013). In field observations, Isaacman-VanWertz et al. (2016) demonstrated that traditional equilibrium partitioning models failed to predict the particle fraction of high vapor-pressure compounds, suggesting more oxidation products should be found in the condensed phase. During the Green Ocean Amazon campaign, Yee et al. (2018) identified oxidation products derived from β-caryophyllene and estimated their contribution to total OA mass, revealing the abundance of sesquiterpene oxidation products in the Amazonian Forest. Yee et al. (2020) also examined the impact of anthropogenic emissions on isoprene-derived SOA formation by analyzing tracer correlations and ratios. In China, Lyu et al. (2020) investigated the prevalence and variability of OA markers and source contributions at a coastal background site in Hong Kong. Studies by He et al. (2020), Wang et al. (2020) and Zhang et al. (2021) reported the characteristics and evolution of OA, assessing its health

risks in urban Shanghai. Wang and Yu (2021) used online data to reveal the heterogeneous ozone oxidation rates of cooking-emitted OA markers, such as oleic and linoleic acid, in the real atmosphere. Moreover, Huang et al. (2021) compared AMS-resolved source contributions with results that included molecular markers measured by TAG to identify AMS spectral profiles and tracer ions for the oxygenated cooking OA factor. Highly time-resolved datasets have enabled researchers to study OA variations over short periods. For instance, during the COVID-19 pandemic, Wang et al. (2022c) investigated the effects of lockdown measures on OA sources and secondary formation processes, while Wang et al. (2022b) explored the chemical evolution of typical SOA tracers during $PM_{2.5}$ episodes in Hong Kong. Importantly, variations in OA markers recorded by online measurements and larger datasets obtained in short time frames can be processed using the Bayesian inference approach, a practical tool to differentiate primary and secondary organic carbon in fine particles (Liao et al., 2023). Beyond outdoor studies, TAG has been increasingly applied to study indoor organic compounds in submicron particles (Katz et al., 2021, Lunderberg et al., 2020, Lunderberg et al., 2019, Kristensen et al., 2019). These studies investigate the sources, evolution, and dynamic behaviors of indoor organics under varying conditions, such as temperature, ventilation, and outdoor air pollution, through designed experiments. For example, the first deployment of TAG in a California residence revealed continuous emissions of semi-volatile organic compounds (SVOCs) from static indoor sources, with SVOC abundances remaining nearly unaffected by the number of occupants (Kristensen et al., 2019). Utilizing fast response data measured by TAG, Lunderberg et al. (2019) demonstrated that indoor air temperature and particle loading are key factors influencing the gas-particle partitioning of diethylhexyl phthalate indoors. Overall, TAG has proven to be a powerful tool in studying both outdoor and indoor condensed organics.

2.3 OA studies in Hong Kong

Hong Kong is a transitional region where air quality is influenced by air masses from both continental and marine origins. With vegetation covering 70% of the area and significant urban sources such as cooking and traffic emissions, the city emits abundant VOCs and oxidants, which have a high potential to form secondary air pollutants like ozone and SOA. Despite the prevalence of small living spaces and the fact that people spend most of their time indoors, indoor air pollution receives less attention. The subtropical climate, characterized by warmth and humidity year-round, results in the extensive and prolonged use of air conditioning systems. Additionally, outdoor air pollution from local sources, such as vehicle exhausts, and regional transport becomes particularly significant during the cooler seasons.

In Hong Kong, previous outdoor studies have concentrated on the source apportionment of OA. Cao et al. (2003) utilized the OC/EC ratio method to estimate the SOC budget in $PM_{2.5}$ samples from three sites in Hong Kong, finding that SOC contributed slightly more to total OC in summer than in winter. Yuan et al. (2006) applied the PMF model to PM_{10} data from the Hong Kong monitoring network, resolving a SOC source with an annual average concentration of 4.25 μg m^{-3}, accounting for 46% of total OC. This study also revealed a clear seasonal variation in SOC concentrations, with higher levels in winter (7.05 μg m^{-3}) compared to summer (1.66 μg m^{-3}). Zheng et al. (2006) analyzed $PM_{2.5}$ samples from roadside, urban, and rural sites in Hong Kong, identifying specific organic markers such as PAHs, steranes, hopanes, resin acids, cholesterol, and levoglucosan using off-line GC-MS. The CMB model was employed to apportion sources of POC and SOC to $PM_{2.5}$, showing that the annual SOC percentage was 6%, 21%, and 51% at roadside, urban, and rural sites, respectively. Hu et al. (2008) characterized SOA markers in $PM_{2.5}$ samples from four sites in Hong Kong, finding significantly higher concentrations on days influenced by regional transport.

Monoterpenes and β-caryophyllene-derived SOA were major contributors to $PM_{2.5}$ in summer, indicating the impact of biogenic emissions. Hu et al. (2010) further applied the PMF model to determine the secondary OC contribution to total OC, revealing that biomass-burning-related SOA accounted for 20% of the resolved SOA factor in regional transport air masses, highlighting the impact of biomass-burning aerosols. In the same dataset, Hu and Yu (2013) found that the concentration of a speciated SOA marker, malic acid, was the highest reported globally, likely due to significant emissions of monoterpenes and β-caryophyllene. Lyu et al. (2017) analyzed SOA markers from a mountain site in Hong Kong, finding that estimated biogenic secondary OC (0.60 ± 0.18 μg m^{-3}) was higher than secondary OC from anthropogenic emissions (0.26 ± 0.20 μg m^{-3}). Their results indicated that, in addition to regional transport influences, local ship emissions significantly enhanced secondary OC loading in Hong Kong. Cheng et al. (2021) collected one-year $PM_{2.5}$ samples and analyzed organic markers using off-line GC-MS. The PMF-predicted secondary formation factor contributed over 50% to OC, with NO_x processing playing a crucial role in SOA production during both day and night. The study also indicated that particles positively affected SOC derived from aging biomass burning plumes.

With the advancement of in-situ techniques, high-time resolution instruments such as the AMS and TAG have been extensively applied in OA studies in Hong Kong. Lee et al. (2013) conducted the first AMS measurements in the region, identifying three OA sources, two of which were linked to SOA formation. They observed a higher fraction of oxygenated organic aerosol and elevated O: C ratios in air masses from coastal and continental regions, associated with significant photochemical reactions and particle aging. Li et al. (2013) used AMS to demonstrate the evolution of OA during foggy and hazy days. Moreover, a seasonal study using AMS at a Hong Kong supersite revealed that secondary organic species dominated (~80%) the organic portion, with locally

produced SOA being prevalent in spring and summer (Li et al., 2015). Qin et al. (2016) reported that aerosol evolution in Hong Kong exhibited a distinct sea-land breeze pattern, with semi-volatile oxygenated organic aerosol (SVOOA) transforming into low-volatility oxygenated organic aerosol (LVOOA) during later photochemical periods. Liu et al. (2019) investigated in-situ SOA formation at a roadside site, indicating significant secondary PM production from motor vehicle emissions. Lyu et al. (2020) conducted dynamic source apportionment of organics in fine particles at a regional background site, revealing complex source changes in this transitional area. Yao et al. (2021) highlighted that cooking has become a source of OA comparable to vehicle emissions in urban Hong Kong. Yao et al. (2022) demonstrated that photochemical and aqueous processes can be intertwined in the formation of MO-OOA at a regional background site in Hong Kong. Wang et al. (2022b) documented the variation and chemical evolution of SOA tracers during $PM_{2.5}$ episodes.

Despite extensive efforts by the aerosol research community, studies on indoor OA in Hong Kong remain limited. Pervious indoor studies in the region have primarily focused on the concentrations, emissions and sources of criteria air pollutants and VOCs, examining prevalent housing types and common residential activities (Guo et al., 2009, Lee et al., 2002a, Lee et al., 2002b). A handful of studies have investigated speciated PM-bound species, these have been restricted to a few categories of organics with known health risks, such as such as polycyclic aromatic hydrocarbons (PAHs) and carbonyls (Chen et al., 2020, Cao et al., 2005, Chao and Wong, 2002). Moreover, the analysis has been constrained by the low time resolution of data resulting from long-duration sampling methods.

2.4 Limitations of previous studies

As discussed above, air quality in Hong Kong is significantly influenced by mesoscale

circulation and local emissions. Traditional filter-based measurements have struggled with low time resolution, missing rapid changes in the evolution of OA. While AMS has improved upon these limitations by measuring total and fragmented organics, it still falls short in identifying specific molecules, which is crucial for understanding sources and formation processes. Despite recent reductions in primarily emitted pollutants due to control policies, Hong Kong's extensive vegetation, covering over 70% of the area, leads to substantial emissions of BVOCs. These emissions may contribute to the persistent formation of SOA, potentially explaining why SOA concentrations have not significantly decreased. Pilot studies have highlighted the dominant role of SOA in fine particles, with malic acid concentrations being the highest reported globally, though its formation chemistry remains unclear. In addition, indoor air quality in Hong Kong is a growing concern, particularly given the limited residential space. With PM pollution identified as a major global health risk (Brauer et al. (2024) and people spending over 90% of their time indoors (Seguel et al., 2017), there is a notable gap in research on indoor OA sources and evolution in Hong Kong.

2.5 Research objectives

This thesis aims to characterize OA in both outdoor and indoor environments in Hong Kong through in-situ measurements with time resolutions ranging from minutes to hours. By focusing on source-specific and high-abundance OA tracers, the study seeks to gain deeper insights into their formation chemistry. The major objectives of this PhD study are as follows:

1) To investigate the influence of biogenic-anthropogenic interactions on the formation of SOA in Hong Kong.

2) To explore the sources, formation processes, and potential precursors of high-level OHDCA, such as malic acid, in Hong Kong.

3) To analyze the composition and emission characteristics of OA in real indoor environments in Hong Kong.

4) To examine the chemical evolution processes of OA emitted from typical indoor activities.

Chapter 3 Methodology

3.1 Description of sampling sites

In this PhD study, fine particle samples were collected from both outdoor and indoor environments in Hong Kong using AMS and TAG. The outdoor sampling campaign was conducted from September to November 2020 at a coastal background site, i.e., Hok Tsui. The indoor sampling campaign took place from November to December 2019 in a rented apartment. During both sampling campaigns, data on other gaseous air pollutants (e.g., trace gases and typical VOCs) and meteorological parameters were simultaneously measured.

3.1.1 Hok Tsui site

The Hok Tsui (HT) regional background site (22.209 N, 114.253 E) is situated at the southeastern tip of Hong Kong Island, overlooking the South China Sea (Figure 3.1). The sampling period coincided with the time of year when photochemical air pollution is most severe and ozone (O_3) levels peak in Hong Kong. During autumn, prevailing northerly winds in South China transport continental air to the site (Ho et al., 2003). As a result, air pollution observed at HT is influenced by both local emissions and air masses from inland areas such as the PRD region. These meteorological and geographical characteristics make HT an ideal location for studying SOA formation processes. The sampling inlet was positioned approximately 1 meter above the roof of a one-story building (~3 meters high), and a $PM_{2.5}$ cyclone (URG corporation) was used to filter out larger particles from the air entering the instruments. Further details about the sampling site can be found in our previous work (Yao et al., 2022, Lyu et al., 2020).

A suite of online instruments was utilized to simultaneously measure air pollutants in both gaseous and condensed phases. The non-refractory components of submicron

particulate matter (PM_1) were analyzed using High Resolution-Time of Flight-Aerosol Mass Spectrometry. Additionally, a TAG was used to measure speciated OA markers in fine particulate matter ($PM_{2.5}$). The TAG, manufactured by Aerodyne Research Inc., integrates sample collection, online derivatization, thermal desorption, and chemical analysis within a single operational cycle (Lyu et al., 2020). VOCs were measured using a Proton Transfer Reaction-Time of Flight-Mass Spectrometer (PTR). Furthermore, carbon monoxide (CO), nitric oxide (NO), NO_2, O_3, SO_2, $PM_{2.5}$, and meteorological parameters were continuously monitored by the Hong Kong Environmental Protection Department (Table 3.1).

Table 3. 1. Online monitoring instrument for trace gases, $PM_{2.5}$, and NO_2 photolysis frequency

Item	**Instrument**	**Model**
Ozone (O_3)	Ecotech UV Absorption Ozone Analyzer	EC9810B/S10
Sulfur dioxide (SO_2)	Teledyne Advanced Pollution Instrumentation (API) Trace-level UV Fluorescence SO_2 Analyzer	T100U
Carbon monoxide (CO)	Teledyne API Gas Filter Correlation CO Analyzer	T300
NO, nitrogen dioxide (NO_2), nitrogen oxide (NO_x)	Teledyne API Trace-level, Photolytic, True NO_2/NO/NO_x Analyzer	T200UP
$PM_{2.5}$	Tapered Element Oscillating Microbalance (TEOM)	Thermo Scientific™ 1405
Photolysis frequency of NO_2 (jNO_2)	MetCon Filter Radiometer	-

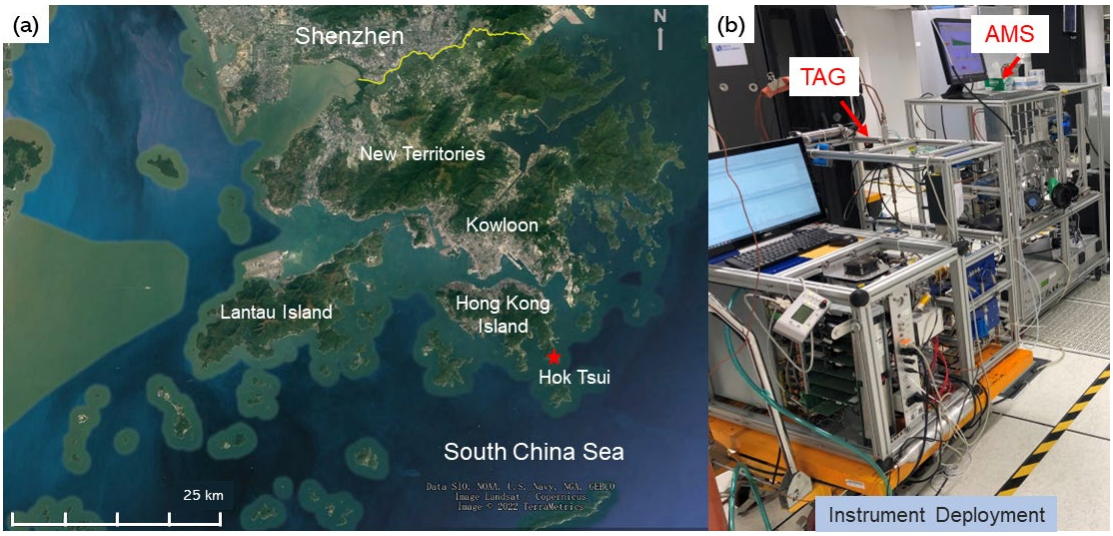

Figure 3. 1. (a) Location of the sampling site (HT, indicated by a red asterisk) in Hong Kong; and (b) Deployment of the main PM measurement instruments on site. The yellow line in (a) marks the boundary between Shenzhen and Hong Kong.

3.1.2 Indoor sampling site

An intensive sampling campaign was conducted in a rented residential apartment where the instruments were deployed, and specific activities were carried out. The apartment, located in a residential area of Kowloon, Hong Kong, had a saleable area of 25.4 m² and included one living room, two bedrooms, a washroom, and a kitchen. The surrounding area was primarily residential and commercial, with a highway, several streets, numerous restaurants, many funeral service worships, and two funeral parlors nearby. Figure 3.2 shows the location and layout of the apartment. For ventilation, the apartment was equipped with three air conditioners (AC), an exhaust fan, and a range hood. To maintain a suitable temperature for both the operation of the instruments and occupant comfort, at least one AC was kept on throughout the sampling campaign. All instruments were placed in the living room, and indoor and outdoor samples were collected alternately every other hour. Pre-cleaned copper tubing, 2-3 meters in length, was used as sampling lines to minimize the loss of charged particles. A cyclone (URG

Corporation) with a cut size of 2.5 μm was installed on the sampling line before the TAG and AMS to remove larger particles from the samples.

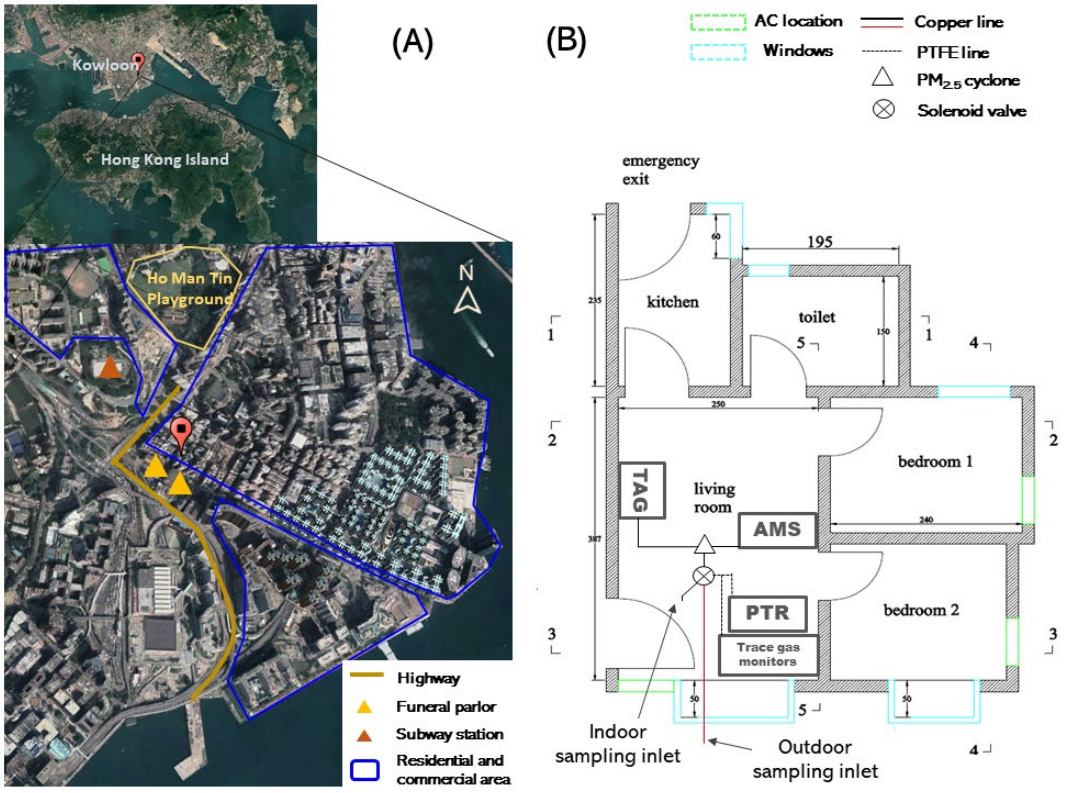

Figure 3. 2. Location of the sampling site (A) and layout of the apartment (B). AC: air conditioner; PTFE: polytetrafluoroethylene; PTR: proton transfer reaction mass spectrometry; $PM_{2.5}$: particulate matter with an aerodynamic diameter of no more than 2.5 μm.

3.2 Instrumentation

3.2.1 Description of the TAG

The TAG instrument used in this study is a highly specialized tool designed for fully automated sampling, handling, and analysis. It operates with a time resolution of 1 to 2 hours. During operation, the airflow first passes through a multichannel carbon denuder

to remove gaseous organics. Particle samples are then collected on a CTD cell for thermal desorption analysis. Polar organic components with -OH and -COOH functional groups in fine particles are derivatized using saturated N-Methyl-N-(trimethylsilyl) trifluoroacetamide (MSTFA) carried by a helium flow at 300°C. All desorbed organics are purged to a mini-column to trap the targeted compounds, which are then directed to a low-polarity gas chromatograph column coupled with a time-of-flight mass spectrometer deploying electron impact ionization for chemical analysis (EI-ToF-MS, Tofwerk). It is important to note that our TAG is capable of measuring condensed organics in $PM_{2.5}$ within the volatility range of C_{16}–C_{36} *n*-alkanes, but it cannot measure gas-phase organics like some SV-TAG instruments. To monitor and correct for changes in instrument response and peak shifts, internal standards (ISs) were added to each sample and subjected to the same procedures of sample transfer and analysis. The mix of ISs included 26 deuterated organic compounds with a wide range of volatility and chemical structures analogous to the target compounds. Authentic or surrogate standards, prepared in 5 concentration gradients and mixed with a fixed amount of ISs, were analyzed in the same manner as the samples to create standard curves. Peak fitting and integration for target compounds and ISs were performed using the **T**AG **E**xplo**R**er and i**N**tegration package software (TERN, version 2.2.18) on Igor Pro (version 7.0.8.1, WaveMetrics). The peak areas of all target compounds and authentic/surrogate standards were scaled relative to their corresponding ISs. By interpolating the IS-scaled peak areas of target compounds from the standard curves, we determined the mass of individual compounds collected, which were then converted to concentrations. The detailed workflow and operation of the TAG used in this study are described in Lyu et al. (2020). In Hong Kong, previous investigations into the characteristics of OA have demonstrated that organic compounds, especially typical OA markers and water-soluble organic carbon, are predominantly concentrated in particles within the 0.1-1 μm size range. This observation provides a strong basis for integrating

results obtained from both TAG and AMS analyses (Yu et al., 2004, Zheng et al., 2008).

3.2.2 Description of the HR-ToF-AMS

The non-refectory components in PM_1, including total organics, sulfate (SO_4^{2-}), nitrate (NO_3^-), ammonium (NH_4^+), and chloride (Cl^-), were measured using an Aerodyne HR-ToF-AMS (DeCarlo et al., 2006, Jayne et al., 2000). During both sampling campaigns, the AMS alternated between W mode and V+ ePToF mode every 4 to 5 minutes. The approximately 2-minute average data acquired in W mode were used for analyses in this study. The sampling flow rate and e-PToF size were calibrated before the sampling campaign. The sampling flow rate and e-PToF size were calibrated prior to the sampling campaign. Ionization efficiency was calibrated for m/z 30 and m/z 46 by injecting pure ammonium nitrate particles with a size of 350 nm, followed the method established by AMS developer. The default relative ionization efficiencies (RIE) used were 4, 1.2, 1.1, 1.3, and 1.4 for ammonium, sulfate, nitrate, chloride, and organics, respectively. To obtain background mass spectra and determine instrumental method detection limits (MDLs), particle-free filtered ambient air was sampled every two days for approximately 60 minutes using an inline high efficiency particulate air (HEPA) filter. The MDLs were determined to be 0.211, 0.022, 0.020, 0.013, and 0.013 μg m^{-3} for organics, sulfate, nitrate, ammonium, and chloride, respectively. The data collected by the AMS were processed using the Tof-AMS Analysis Toolkit 1.59D and Tof-AMS HR Analysis 1.19D, both based on WaveMetrics Igor Pro version 6.37.

3.2.3 Description of the PTR-MS

For VOC measurements, a PTR instrument was used. In this study, the PTR utilized H_3O^+ as the primary reagent ion, with the drift tube maintained under controlled conditions: a pressure of 3.8 mbar, a temperature of 60 °C, and a voltage of 900 V.

Ambient air was drawn through a Teflon sampling tube using an external pump at a constant flow rate of 3 m^3 min^{-1}, with a small fraction of sampled air (200 mL min^{-1}) analyzed by the instrument. A range of VOC species were quantified using standard gas. Calibrations were performed at room temperature, and the response factors were adjusted for relative humidity. The coefficient of determination (R^2) for all calibration curves was above 0.9.

3.3 Model configurations

3.3.1 Hybrid Single-Particle Lagrangian Integrated Trajectory (HYSPLIT) model

The 72-hr backward trajectories of air masses arriving at the HT site were simulated every 2 hours using the Hybrid Single-Particle Lagrangian Integrated Trajectory (HYSPLIT) model. All trajectories started from a point 300 m above the HT site, situated in the middle to lower part of the marine boundary layer (Jury and Walker, 1988, Wang et al., 2019). Based on model clustering, three types of air masses were identified: coastal air (CL1), short-range continental air (CL2), and long-range continental air (CL3), as shown in Figure 3.3. These accounted for 49%, 38%, and 13% of the total air masses by frequency, respectively. The CL2 trajectories were primarily confined to eastern and southern China, such as the PRD region, while CL3 trajectories extended to northern China and even Mongolia within 72 hours. As expected, the coastal CL1 was characterized by the highest temperature, relative humidity, and aerosol liquid water content (ALWC). CL2 contained higher levels of anthropogenic air pollutants, including sulfate, nitrate, CO, SO_2, and NO_x. In contrast, CL3 brought the coldest air from northern China to Hong Kong and had the lowest levels of ALWC and sulfate. Further, the earlier period of the CL1 segments, marked as Stage I,

significantly differed from the later period, Stage II, with much higher levels of OHDCA and ALWC. The CL2 segments in October, marked as Stage III, featured a higher photolysis frequency of NO_2 (jNO_2) than those in November, marked as Stage IV. These stages also differed in terms of O_3_corr. While the average O_3_corr was lower in Stage III, the daytime increase of O_3_corr from morning to afternoon was much larger than in Stage IV (37.2 ppbv *vs*. 25.9 ppbv), implying differences in daytime photochemical intensity. This division of stages aids in discussing OHDCA formation. Table 3.2 lists the segments of different clusters and stages.

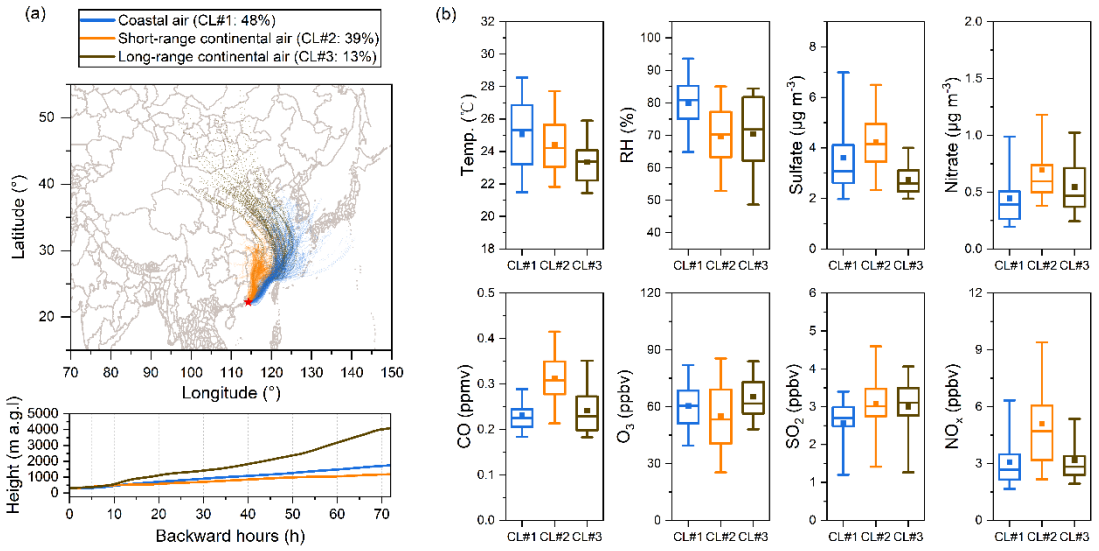

Figure 3. 3. Distribution of the 72 - hr backward trajectories of air masses arriving at HT at 300 m above ground level (a). Percentages in brackets indicating the frequency of each specific type of air mass within the total air masses; Box plot of selected meteorological parameters and air pollutants (b). In this plot, the square and line within each box denote the mean and median values, respectively. The upper (lower) boundary of the box corresponds to the 75th (25th) percentile, while the top and bottom whiskers indicate the 95th and 5th percentiles, respectively.

Table 3. 2. Allocation of date segments to different clusters and stages.

Cluster	Stage	Date segments
CL1	Stage I	Sep. 27 – Oct. 6
	Stage II	Oct. 11 – Oct. 16; Oct. 26 – Nov. 1; Nov. 12 – Nov. 17
CL2	Stage III	Oct. 6 – Oct. 11; Oct. 17 – Oct. 21
	Stage IV	Oct. 22 – Oct. 24; Nov. 2 – Nov. 3; Nov. 7 – Nov. 10
CL3	-	Oct. 24 – Oct. 25; Nov. 4 – Nov. 6; Nov. 11

3.3.2 Extended AIM Aerosol Thermodynamics Model (E-AIM)

ALWC was calculated as a function of particulate matter compositions and meteorological conditions. The model inputs included ionic compositions measured by the AMS, specifically sulfate, nitrate, and chloride, along with temperature and relative humidity. The model assumed particle neutrality by using ammonium to balance the excess anions and cations. The estimated ammonium levels showed excellent agreement with observed values, with a slope of 0.97 and an R^2 of 0.99.

The ALWC in fine particles was determined using the method outlined by Isaacman-VanWertz et al. (2016). The E-AIM model, developed to characterize the partitioning of gas, liquid, and solid phases in aerosol systems, was used for this purpose (http://www.aim.env.uea.ac.uk/aim/aim.php). Specifically, the E-AIM IV model (Wexler and Clegg, 2002) was employed to calculate the ALWC, taking into account the effects of inorganic chemical components. The model inputs included ionic compositions measured by the AMS, such as sulfate, nitrate, and chloride, as well as temperature and relative humidity. The model assumed particle neutrality by using

ammonium to balance the excess anions and cations. The estimated and observed ammonium levels showed strong agreement, with a slope of 0.97 and an R^2 of 0.99. Additionally, the extra water uptake by hygroscopic organics was calculated using the following equation:

$$Wo = \frac{V_{org}(0.29(O{:}C))}{\frac{100}{RH\%}-1}$$

where V_{org} is the organic mass divided by its density, which is assumed to be 1.4 g cm^{-3}, as per Isaacman-VanWertz et al. (2016). The O: C ratio refers to the oxygen-to-carbon ratio of fine particles measured by the AMS. The hygroscopicity is assumed to be 0.29, based on (Massoli et al., 2010). RH denotes the relative humidity throughout the sampling campaign.

In this study, the calculated ALWC is limited to PM_1, as the AMS data were used as input. It is important to note that the AMS cannot detect sea-salt chloride. During the HT sampling campaign, we also calculated the ALWC using concentrations of water-soluble ions from 28 daily $PM_{2.5}$ filter samples. Although there was a difference in average values, which was expected, the ALWC derived from the two data sets showed a moderate correlation (R^2 = 0.52). Additionally, the relationships of ALWC between different types of air masses remained consistent across both data sets.

Chapter 4 Characteristics and formation chemistry of secondary organic molecular markers at a regional background site in South China

4.1 Introduction

Atmospheric OA plays a paramount role in affecting air quality and climate (Seinfeld and Pandis, 2016). SOA constitutes a considerable fraction of OA, exerting significant impacts on radiative effects and cloud droplet activation (Huang et al., 2014). The formation of SOA involves the gas-phase oxidation of organic compounds, leading to the production of low-volatility products, as well as multiphase chemistry that encompasses heterogeneous processes (Kroll and Seinfeld, 2008). Globally, biogenic sources emit more VOC than anthropogenic sources, and so does the resulting SOA, e.g., 39.5 Tg a^{-1} of BSOA versus 24.6 Tg a^{-1} of ASOA, according to Kelly et al. (2018). Observational evidence indicated the influence of anthropogenic air pollutants, e.g., nitrogen oxides (NO_x) and sulfur dioxides (SO_2), on the formation of BSOA (Hoyle et al., 2011). For this reason, a modelling study demonstrated that isoprene SOA can increase as NO_x decrease but decrease as SO_2 decrease (Marais et al., 2016). In East Asia, a large fraction of BSOA (78%) was affected by anthropogenic sources during its formation (Matsui et al., 2014).

Over the past few decades, many studies have focused on the anthropogenic impacts on the formation of isoprene and monoterpenes SOA, given the high emissions, reactivity, and SOA yields of the VOCs precursors (Hoyle et al., 2011, Shilling et al., 2013). For example, NO_x strongly affects SOA chemistry by altering the fate of peroxy radicals (RO_2) formed through VOCs oxidation (Kroll and Seinfeld, 2008). Increased NO_x levels have been shown to redirect the oxidation pathway of isoprene from the

hydroperoxyl (HO_2) channel, which would otherwise yield isoprene epoxydiols (IEPOX) and eventually 2-methyltetrols (2-MTs) and C_5-alkenetriols, to the NO_x-channel that leads to the formation of hydroxymethel-methyl-α-lactone (HMML) and subsequently 2-methylglyceric acid (2-MGA) (Carlton et al., 2009, Claeys et al., 2004, Kroll et al., 2005). Monoterpenes are a diverse class of BVOCs, with isomers that exhibit a wide range of reactivities with oxidants, leading to the formation of SOA (Griffin et al., 1999). Studies have also indicated that NO_x could suppress SOA formation from α-pinene and β-pinene by reducing hydroxyl radical (OH) concentrations and inhibiting new particle formation (Sarrafzadeh et al., 2016, Wildt et al., 2014). Conversely, SO_2 leads to the formation of sulfate and acidic particles, which enhance SOA production from isoprene and monoterpenes through the salting-in effect and acid-catalyzed reactions (Offenberg et al., 2009, Xu et al., 2016). Besides, anthropogenic VOCs emissions indirectly stimulate SOA formation by increasing O_3 levels and atmospheric oxidation capacity (AOC) in urban areas (Srivastava et al., 2022, Wu et al., 2020a).

In Hong Kong, high concentrations of small molecule OHDCA, such as malic acid and tartaric acid, have been observed (Lyu et al., 2020, Hu and Yu, 2013). Due to the high proportion of polar functional groups, that is, hydroxyl (OH) and carboxyl, in the molecules, OHDCA is expected to be more soluble than oxalic acid (the most studied analog of OHDCA) and may play critical roles in affecting the physical and chemical properties of ambient aerosols. It has been indicated that the viscosity of OA particles increases with the addition of the OH group, which may further alter ice nucleation pathways and radiation intensity of cirrus layers (Reid et al., 2018, Rothfuss and Petters, 2017). Like the presence of oxalic acid in cloud condensation nuclei, OHDCA may also affect weather and climate through its involvement in cloud formation (Ramanathan et al., 2001, Novakov and Penner, 1993). However, modeling studies generally

underestimate the abundance of dicarboxylic acids in the atmosphere (Zhu et al., 2020, Ervens et al., 2004). Such modeling flaws may be the result of improper representation of their formation and degradation chemistry (Carlton et al., 2009, Varga et al., 2007). OHDCA species in the atmosphere are generally considered as secondary products (Kawamura and Bikkina, 2016, Yao et al., 2004). In laboratory reaction systems, they were detected in ozonolysis of cycloalkanes and photooxidation of anthropogenic VOCs, such as toluene, but the yields were fairly low, that is, 0.05%–0.1% (Sato et al., 2007, Gao et al., 2004). Malic acid, an OHDCA representative, was frequently observed in field campaigns and was proposed to be a late-generation photochemical oxidation product of unsaturated fatty acids and biogenic hydrocarbons (Kawamura and Ikushima, 1993). Besides, it was considered to be formed via aqueous reactions involving hydroxylation of dicarboxylic acids with similar structures (Kawamura et al., 1996b). For example, succinic acid was suspected to be an earlier generation product of malic acid, due to the good consistency between them across many observations (Kourtchev et al., 2009, Kawamura et al., 1996a). Chamber studies indicated more efficient oxidation of succinic acid in aqueous phase than in gas phase (Carlton et al., 2007).

Previous offline studies in Hong Kong have highlighted the significant role of nitrate radicals (NO_3) in the formation of monoterpene-derived SOA (Cheng et al., 2021). However, the influence of the NO_x cycle on SOA formation is limited by the low temporal resolution of the data. A handful of studies have attempted to reveal the anthropogenic influence on SOA formation based on online measurement techniques, such as AMS. For example, Huang et al. (2015a) observed that air masses originating from continental regions can promote the formation of high-molecular-weight organosulfates, as detected using AMS. Since the AMS only measures bulk OA or fragmentation, exploring anthropogenic effects on SOA chemistry without molecular-level OA composition remains challenging. Besides, Hu and Yu (2013) have reported

high levels of malic acid in Hong Kong and speculated its formation through aqueous photodegradation of biogenic hydrocarbons, based on the correlations with SOA tracers in daily samples. However, the aqueous processes were not substantiated by observational evidence limited by low-time resolution data. Moreover, other mechanisms that may also be involved in malic acid formation, for example, photochemical oxidation, were not discussed. Recently, we measured more OHDCA species at a higher time resolution (i.e., 1.5 hr) with a TAG in the urban background atmosphere of Hong Kong. The preliminary study demonstrated that OHDCA formation was related to the levels of titration-corrected ozone (O_3_corr), which was calculated as the sum of O_3 and NO_2, and could be facilitated by SO_2 in marine air (Lyu et al., 2020). While these studies shed light on OHDCA chemistry, the major mechanisms and precursors that lead to OHDCA formation under varying atmospheric conditions remain unresolved.

In this chapter, a highly time-resolved dataset of chemical compositions of submicron particles was obtained at a regional background site in South China known for receiving continental air masses and coastal outflow. The unique geographic location of this site provided an opportunity to investigate potential interactions between biogenic and anthropogenic emissions. The combination of AMS and TAG data outlined a relatively complete composition pattern of OA. The typical SOA tracers derived from biogenic VOCs (isoprene and monoterpenes) and anthropogenic VOCs (e.g., aromatics) were quantitatively analyzed. Moreover, the OHDCA chemistry, including formation mechanisms and potential precursors, was explored in the real atmosphere.

4.2 Overview of measurements

Figure 4.1 shows the time series of NR-PM_1 compositions, a subset of speciated OA markers, criteria air pollutants and meteorological parameters labeled by the type of air

masses. A detailed statistical summary of the concentrations of quantified OA markers and other aerosol components is available in Table 4.1. Throughout the field measurements, the mass concentration of NR-PM_1 ranged from 3.9 to 44.7 μg m^{-3}, with an average value of 12.2 ± 0.5 μg m^{-3}. The concentrations were roughly consistent with those reported at other supersites in HK, such as 15 μg m^{-3} at HKUST in 2011 (Li et al., 2015). The mean concentration of NR-PM_1 in the CL2 air (21.3 ± 1.5 μg m^{-3}) was significantly higher than that in the other two types of air masses (10.5 ± 0.6 μg m^{-3} in CL1 and 16.1 ± 2.7 μg m^{-3} for CL3). It was even comparable to that observed at a roadside site in HK (26.1 ± 0.7 μg m^{-3}) (Yao et al., 2021). The comparisons highlight the impacts of anthropogenic emissions in the upwind urban areas on particulate matter pollution in the background atmosphere.

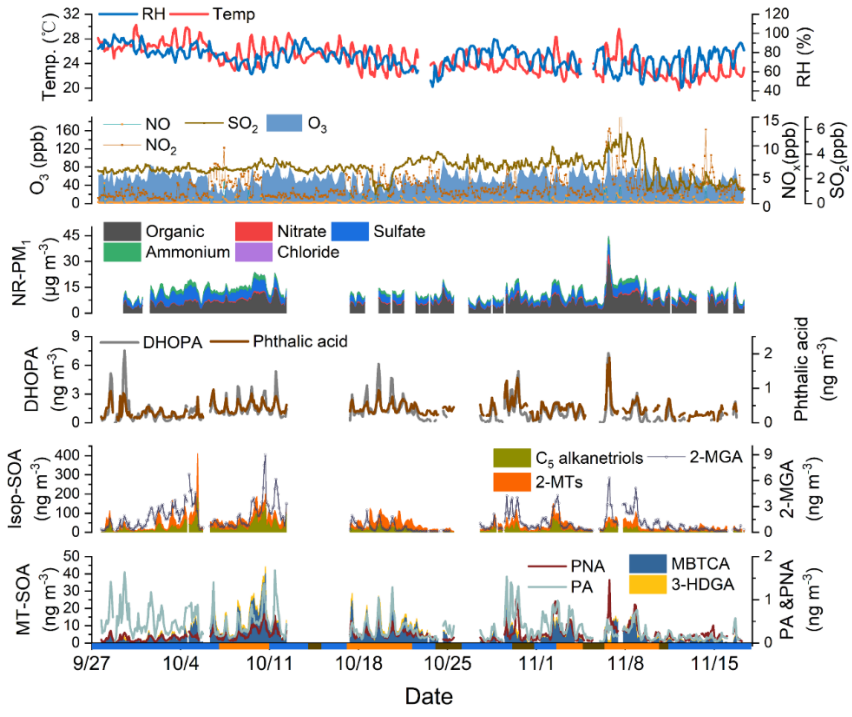

Figure 4. 1. Time series of main NR-PM_1 components, selected SOA tracers and meteorological parameters. Full names of SOA tracers are shown in Table 4.1. The blue, orange and brown bars at the bottom represent the CL1, CL2 and CL3 air, respectively. Missing data is due to instrument maintenance.

Table 4. 1. Detailed information on submicron particle concentrations, quantified major OA compounds, and their VOC precursors in the three groups of air masses throughout the campaign.

Compounds	**CL#1**			**CL#2**			**CL#3**		
	Min.-Max.	**Mean**	**95%CI**	**Min.-Max.**	**Mean**	**95%CI**	**Min.-Max.**	**Mean**	**95%CI**
Meteorological parameters									
Temperature (℃)	19.7-30.3	25.1	0.3	21.1-29.6	24.4	0.2	21.0-26.6	23.4	0.3
Relative humidity (RH, %)	43.1-99.0	80.2	1.0	49.0-88.4	69.7	1.3	44.4-86.1	70.5	2.7
Criteria pollutant (ppb; ppm for CO)									
nitrogen oxide (NO)	0.1-3.0	0.3	0.04	0.08-5.6	0.4	0.05	0.08-3.4	0.2	0.09
nitrogen dioxides (NO_2)	0.2-13.3	2.5	0.3	0.4-26.2	4.45	0.5	0.4-11.2	2.4	0.4
ammonia (NH_3)	1.7-142.9	11.4	2.3	6.2-292.4	13.7	4.3	5.6-14.3	8.6	0.4
sulfur dioxide (SO_2)	0.8-26.6	10.5	0.6	6.7-66.0	21.3	1.5	3.9-50.2	16.1	2.7
ozone (O_3)	21.6-89.8	51.0	2.0	14.9-149.5	46.0	2.6	32.9-92.1	56.4	2.6

O_3_corr (O_3 + NO_2)	35.5-97.9	62.4	1.3	27.1-185.3	59.1	2.8	46.7-165.3	67.4	3.4
carbon monoxide (CO)	0.2-0.8	0.2	0.006	0.2-0.5	0.3	0.01	0.1-0.4	0.2	0.01
Submicron particles and their major components measured by AMS (μg m^{-3})									
$PM_{2.5}$	1.4-48.0	14.7	0.8	10.8-68.8	21.5	1.1	7.7-35.7	19.1	1.8
NR-PM_1	0.8-26.6	10.5	0.6	6.7-66.0	21.3	1.5	3.9-50.2	16.1	2.7
PM_1-OM	0.9-13.7	4.8	0.3	3.0-28.6	7.7	0.5	1.8-13.8	5.5	0.6
Sulfate	0.4-8.6	3.8	0.2	2.0-7.5	4.2	0.2	1.8-4.4	2.7	0.2
Nitrate	0.1-2.3	0.4	0.0	0.3-5.3	0.7	0.1	0.2-1.1	0.5	0.1
Ammonium	0.3-3.3	1.5	0.1	0.9-4.3	1.9	0.1	0.7-2.1	1.2	0.1
Chloride	0.017-0.2	0.1	0.0	0.030-0.3	0.1	0.0	0.046-0.2	0.1	0.0
OA tracers measured by TAG (ng m^{-3})									
Oleic acid	0.2-9.5	1.7	0.2	0.5-30.0	5.2	0.7	0.5-6.3	1.8	0.3
Adipic acid	0.4-5.4	1.3	0.1	0.5-13.8	1.8	0.2	0.5-3.3	1.4	0.2

Azelaic acid	0.1-7.3	1.9	0.2	0.6-8.7	3.1	0.2	0.2-5.9	2.2	0.3
3-hydrobenzoic acid	0.2-0.9	0.5	0.0	0.3-1.0	0.5	0.0	0.3-1.0	0.5	0.0
4-hydrobenzoic acid	0.1-0.9	0.3	0.0	0.2-1.0	0.4	0.0	0.1-1.6	0.5	0.1
Phthalic acid	0.05-1.2	0.3	0.0	0.1-1.9	0.5	0.0	0.1-0.7	0.4	0.0
Isophthalic acid	0.2-5.4	2.2	0.1	0.6-4.4	2.4	0.1	1.0-3.8	2.0	0.2
Terephthalic acid	0.4-17.4	6.3	0.4	0.02-11.3	4.8	0.2	1.1-15.7	5.7	0.8
2,3-dihydroxy-4-oxopentanoic acid (DHOPA)	0.02-7.5	1.0	0.2	0.1-7.3	1.6	0.2	0.0-2.2	0.6	0.2
Isoprene-derived SOA tracers									
2-methylglyceric acid (2-MGA)	0.1-6.7	1.2	0.2	0.1-9.0	1.5	0.2	0.1-1.4	0.4	0.1
2-methylthreitol (2-MT-1)	0.5-67.9	6.2	0.8	2.8-24.8	9.6	0.6	2.0-9.0	4.3	0.4
2-methylerythritol (2-MT-2)	1.1-162.2	16.3	2.2	5.5-67.7	26.8	2.0	4.3-20.9	10.2	1.0
cis-2-methyl-1,3,4-trihydroxy-1-butene (C_5 alkanetriols-1)	0.03-10.0	0.8	0.2	0.02-10.0	1.0	0.1	0.04-1.8	0.3	0.1
3-methyl-2,3,4-trihydroxy-1-butene (C_5 alkanetriols-2)	0.1-20.4	1.3	0.3	0.04-13.5	1.6	0.2	0.1-2.0	0.4	0.1

trans-2-methy-1,3,4-trihydroxy-1-butene (C_5 alkanetriols-3)	0.2-150.2	11.8	2.3	0.9-122.3	19.4	2.6	0.6-11.2	2.6	0.5
Monoterpene-derived SOA tracers									
Pinic acid	0.04-1.7	0.4	0.0	0.1-1.4	0.4	0.0	0.03-0.5	0.2	0.0
Pinonic acid	0.01-0.6	0.1	0.0	0.04-1.5	0.3	0.0	0.03-0.2	0.1	0.0
3-hydroxy-4,4-dimethylglutaric acid (3-HDGA)	0.1-3.4	0.7	0.1	0.2-5.5	1.8	0.1	0.1-1.0	0.5	0.1
3-methyl-1,2,3-butanetricarboxylic acid (MBTCA)	0.1-19.3	2.6	0.4	0.05-40.2	8.7	1.0	0.1-7.6	2.4	0.6
VOC precursors (ppb)									
BTEX (sum of toluene, benzene, ethylbenzene and xylenes)	0.2-3.8	0.9	0.1	0.4-9.3	1.9	0.06	0.2-4.1	1.0	0.2
Isoprene	0.01-0.6	0.1	0.02	0.05-0.8	0.2	0.02	0.03-0.3	0.1	0.02
MVK + MACR	0.02-0.26	0.1	0.01	0.05-0.67	0.2	0.02	0.02-0.22	0.1	0.01
(MVK + MACR) / isoprene	---	0.70	0.39	---	0.85	0.51	---	0.84	0.49
Monoterpene	0.004-0.07	0.03	0.003	0.01-0.08	0.03	0.003	0.01-0.07	0.02	0.003

The total organics (PM_1-OM) contributed more than half to the NR-PM_1 in both CL2 (53%) and CL3 air (55%), whereas in the CL1 air the contribution dropped to 45%. Sulfate was second only to NR-PM_1 among all types of air, followed by nitrate, ammonium and chloride. Similar patterns were also identified in previous studies in this region (He et al., 2011, Xiao et al., 2011, Li et al., 2015). The aging degree of OA was assessed using the oxygen-to-carbon atomic ratio (O: C) and carbon oxidation state ($\overline{OS}_C$ = 2 × O: C - H: C), where H:C is the hydrogen-to-carbon atomic ratio. Higher O: C ratios indicate that aerosols have experienced higher levels of atmospheric aging, signifying more SOA formation. Interestingly, the highest O: C ratio (0.81 ± 0.01) and $\overline{OS}_C$ (0.23 ± 0.04) were observed in CL1. Moderate correlations between $\overline{OS}_C$ and O_3_corr were identified for the CL1 (R^2=0.40) and CL2 (R^2=0.30) instead of CL3 (R^2=0.1), indicating photochemical aging and explaining the increase in $\overline{OS}_C$ from the morning to the early or later afternoon. Moreover, the peak of $\overline{OS}_C$ in the CL1 was several hours later than in the other two types of air, leading to a lager gap in the diurnal profile from the late afternoon to midnight. This trend is consistent with the diurnal profile of ALWC (Figure 4.2), indicating that aqueous processes contribute to aerosol oxidation. Compared to the other two clusters, CL3 exhibited a weaker correlation with ozone and ALWC, suggesting that photochemistry and aqueous phase reaction was not the dominant factor in the aerosol aging process.

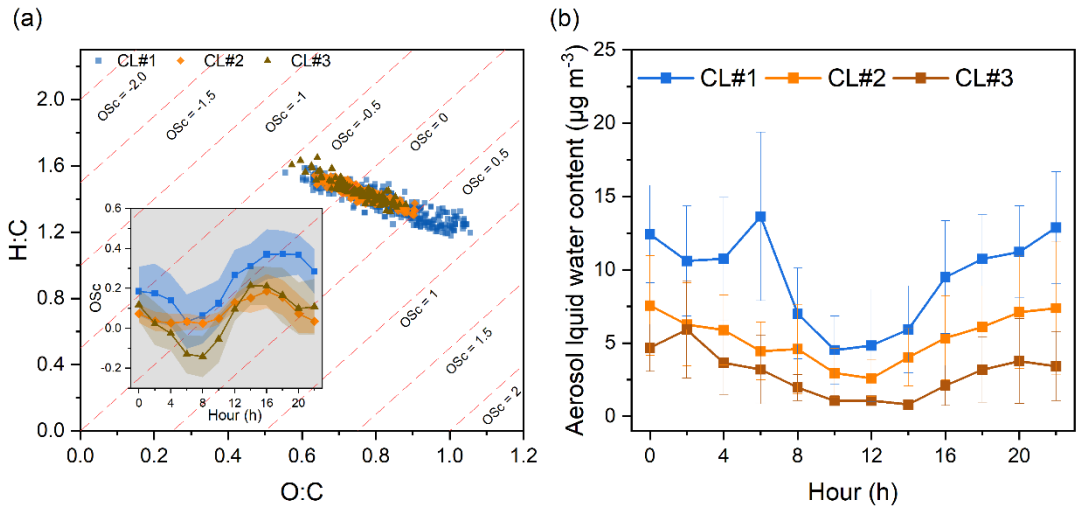

Figure 4. 2. (a) van Krevelen diagram showing H: C and O: C ratios in three clusters, with the diurnal pattern of average carbon oxidation state presented in the inserted panel; (b) diurnal profile of aerosol liquid water content (ALWC) in three clusters.

Significant variations in SOA markers, including those derived from aromatics, isoprene and monoterpenes, were observed throughout the sampling period. Generally, the CL2 air featured the highest concentrations of all SOA markers (Table 4.1). This seemed not to be explained by the atmospheric oxidative capacity or OA aging degree, given the lower levels of O_3_corr and $\overline{OS}_C$ than those in the CL1. Instead, the elevated concentrations of primary air pollutants in the CL2 implied that the upwind urban areas provided abundant precursors for SOA formation, which is further discussed below. Additionally, the higher concentration of SO_2 in CL2 may promote the formation of sulfate, with the concomitant nucleation and acid-catalyzed reactions favoring SOA production (Zhao et al., 2018). Most of the SOA tracers peaked during the day in all types of air masses (Figure 4.3). Thus, photochemical processes played an important role in the formation of these SOA tracers, even though the other processes could not be excluded. However, as the isoprene SOA tracer formed in low-NO_x environments, the 2-MTs were an exception, which had the highest concentrations at night. Besides, the highest levels of C_5-alkenetriols in the CL1 were observed in the morning. It is

noteworthy that the nighttime enhancement of 2-MTs was repeatedly observed in HK, enabled by the higher-than-before temporal resolution of TAG measurements. The possible reasons for this phenomenon are discussed below.

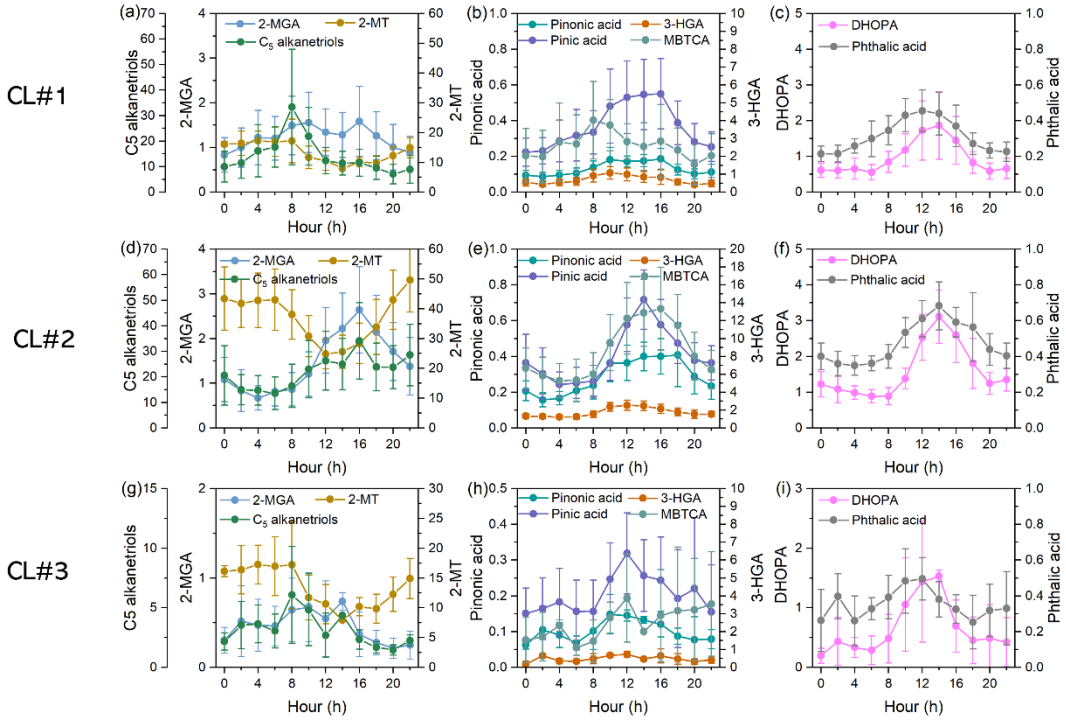

Figure 4. 3. Diurnal patterns of SOA markers in the three clusters for isoprene-derived tracers (a,d,g), monoterpene-derived tracers (b,e,h), and anthropogenic-related SOA tracers (c,f,i). The error bar represents a 95% confidence interval (CI).

4.3 Characteristics and formation processes of speciated OA markers

4.3.1 Anthropogenic SOA tracers

Two ASOA tracers were observed in this study, i.e., *o*-phthalic acid and DHOPA. It has been documented that *o*-phthalic acid is generated from the oxidation of naphthalene and 1-methylnaphthalene (Kleindienst et al., 2012), and DHOPA is an oxidation product

of BTEX (i.e., toluene, benzene, ethylbenzene and xylenes) (Al-Naiema and Stone, 2017). However, studies also indicated primary emissions of *o*-phthalic acid (Zhang and Hatakeyama, 2016, Kawamura and Kaplan, 1987b). Here, the average concentration of DHOPA (1.3 ± 0.1 ng m^{-3}) was slightly higher than that of *o*-phthalic acid (0.4 ± 0.02 ng m^{-3}). The DHOPA levels we observed were close to those reported in the PRD region (e.g., 1.51-1.80 ng m^{-3}) (Yang et al., 2023, Yuan et al., 2018), and Hong Kong (e.g., 0.26-1.17 ng m^{-3}) (Wang et al., 2022b). However, the concentrations of *o*-phthalic acid were lower than those reported elsewhere, e.g., 7.9-22.6 ng m^{-3} (He et al., 2018b). Although the intense anthropogenic emissions that elevate precursor levels in the PRD region (Zhong et al., 2018), our measurement still has a discrepancy compared to the results from another rural site in Hong Kong (e.g., 12.4-15.3 ng m^{-3}) (Wang et al., 2022b). Therefore, we will mainly focus on the trend of *o*-phthalic acid and refrain from comparing the concentration in the following discussion. The CL2 air contained the highest concentrations of DHOPA (1.6 ± 0.2 ng m^{-3}), followed by the CL1 (1.0 ± 0.2 ng m^{-3}) and CL3 (0.6 ± 0.2 ng m^{-3}). A similar pattern was also observed for *o*-phthalic acid (Table 4.1). It has been documented that the formation of DHOPA and *o*-phthalic acid is closely related to OH radicals (He et al., 2018b, Wang et al., 2007). Using O_3_corr as a proxy for OH, we examined the correlation of ASOA tracers with O_3_corr and identified a moderate correlation in both the CL2 and the CL3, but not in the CL1 indicating that atmospheric oxidants were an important factor influencing the formation of both ASOA tracers in the continental air. As the potential precursors of DHOPA, the BTEX exhibited significantly higher concentrations in the CL2 (1.9 ± 0.06 ppb) than in the CL1 (0.9 ± 0.1 ppb) and in the CL3 (1.0 ± 0.2 ppb), which at least partially explained the highest levels of DHOPA in the CL2. Despite its low concentrations in the CL3, the mass fraction of DHOPA in all the detected SOA tracers was not low (Figure 4.4a). Furthermore, the correlation of DHOPA with PM_1-OM was the best in the CL3 (Figure 4.4b), implying that the contribution of aromatics SOA to

the PM_1-OM might be higher than that in the other two types of air. Therefore, the low concentrations of DHOPA in the CL3 were likely a result of atmospheric mixing, dispersion and removal during the long-range transport.

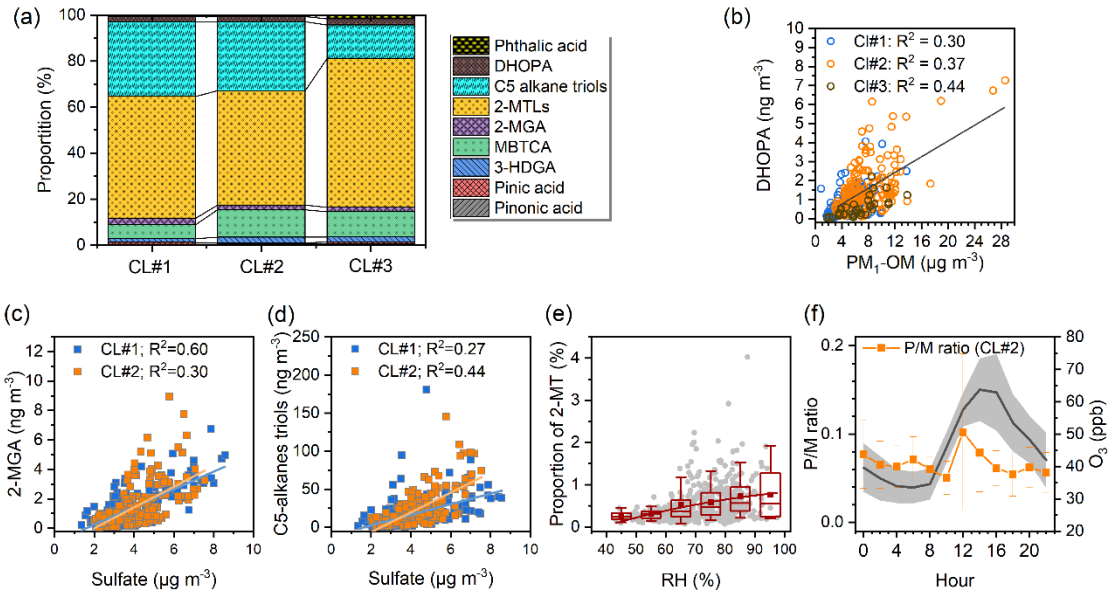

Figure 4. 4. Characterization of speciated OA. (a) Mass fraction of nine speciated SOA markers in different clusters: coastal (CL1), short-range continental (CL2) and long-range continental (CL3). (b) Correlation of DHOPA with PM_1-OM (R^2=0.31). (c) Comparison of 2-MGA levels with sulfate in CL1 and CL2. (d) Comparison of C_5-alkanestriols levels with sulfate in CL1 and CL2. (e) Relationship between the proportion of 2-MTs in the total mass of SOA derived from AMS (sum of MO-OOA, LO-OOA1 and LO-OOA2) at nighttime (22:00-06:00). Data are binned according to RH, with each bin showing the median (middle horizontal line), mean (solid squares), 25th and 75th percentiles (lower and upper boxes), and 10th and 90th percentiles (lower and upper whiskers) for each bin. (f) Diurnal pattern of pinic acid/MBTCA ratio and O_3 in CL2 (shown in grey line). The error bar represents 95% CI.

4.3.2 Biogenic SOA tracers

A previous study detected five biogenic SOA (BSOA) tracers at this site using the same TAG (Lyu et al., 2020). Through optimizing the instrument, we quantified the concentrations of ten BSOA tracers. Consistent with DHOPA, the concentrations of all BSOA tracers were also significantly higher in the CL2 than in the other two types of air (Table 4.1). The CL2 air was richest in biogenic precursors, e.g., isoprene and monoterpenes, probably due to the dense vegetation along the trajectory path, especially in Jiangxi and Fujian province in South China. Despite the highest temperature, the CL1 air did not contain proportionately high concentrations of BVOCs (Figure 4.4a). The ratio of the sum of methyl vinyl ketone (MVK) and methacrolein (MACR) to isoprene was calculated to indicate the degree of isoprene oxidation. The ratio turned out to be the lowest in the CL1 and highest in the CL2 (Table 4.1). As such, it was not the chemical consumption that dominated the distribution of BVOCs in different air masses. The vegetation cover on the air transport path seemed to have played a more important role. Nonetheless, it is important to note that there is a minimal variation in BVOCs levels among the three air masses (e.g., 0.1 ppb in CL1&3 *v.s* 0.2 ppb in CL2). However, the concentrations of SOA markers derived from these precursors are significantly higher, suggesting that the formation processes are amplified (Xu et al., 2015).

It has been demonstrated that the formation of isoprene SOA (iSOA) is closely related to NO_x (Carlton et al., 2009). Among the iSOA tracers detected, the 2-MTs (sum of 2-methylthreitol and 2-methylerythritol) had the highest concentration (27.6 ± 1.9 ng m^{-3}), followed by C_5-alkenetriols including *cis*-2-methyl-1,3,4-trihydroxy-1-butene, 3-methyl-2,3,4-trihydroxy-1-butene and *trans*-2-methy-1,3,4-trihydroxy-1-butene (15.9 ± 1.8 ng m^{-3}) and 2-MGA (1.2 ± 0.1 ng m^{-3}). The concentration of HMML-derived tracers (high-NO_x pathway) was more than one order of magnitude lower than that of

the IEPOX-derived tracers (low-NO_x pathway). A similar result was observed in the heavily polluted PRD and YRD regions, where the average mixing ratios of NO_x exceeded 80 ppb and 25 ppb, respectively (He et al., 2018a, Zhu et al., 2018). Moreover, we identified a positive correlation between 2-MGA and C_5-alkenetriols tracers and sulfate in the CL1 and CL2 air while there existed a weak correlation between 2-MTs and sulfate. However, no significant correlation was found in the long-range air cluster (CL3: $R^2 < 0.1$). More specifically, the 2-MGA correlated better with sulfate with the R^2 of 0.6 in the CL1, higher than that in the CL2 ($R^2 = 0.3$) (Figure 4.4c). Our previous work showed that sulfate in the coastal air with high RH and ALWC was mainly formed through aqueous processes (Huo et al., 2024a). The high aerosol liquid water content makes HMML more likely to form ring-open products from key gas-phase intermediates at the aerosol surface compared to IEPOX, as suggested by kinetic model simulations (Worton et al., 2013). Besides, the much smaller Henry's Law constant of HMML epoxide (7.5×106 M atm^{-1}), compared to IEPOX epoxide (1.3×108 M atm^{-1}), also favored the gas-to-particle partitioning (Eddingsaas et al., 2010). Therefore, the better correlation of 2-MGA with sulfate in the CL1 was likely related to the higher RH and ALWC in the coastal air. In contrast, the correlation between C_5-alkenetriols and sulfate was better in the CL2, with an R^2 of 0.48 (Figure 4.4d). Unlike CL1, CL2 is characterized by higher levels of SO_2. Previous chamber experiments indicated that new particle formation and growth occurred in the BVOCs ozonolysis reaction system when SO_2 was present (Stangl et al., 2019). The growth of particles increases their surface area, enhancing the uptake process of IEPOX (Xu et al., 2016, Budisulistiorini et al., 2015), which in turn leads to the observed correlation between C_5-alkenetriols and sulfate.

2-MTs are also the iSOA tracer derived from the IEPOX pathway. A weak correlation was observed between 2-MTs and air pollutants with well-defined formation

mechanisms (e.g., sulfate and nitrate) among all clusters. Moreover, a relatively high proportion of 2-MTs was found in CL3, suggesting that these compounds can travel long distances without significant degradation or removal. The online measurements revealed that higher levels of 2-MTs occurred during 22:00-06:00, in contrast to the rise during the day for the other iSOA tracers (Figure 4.3). To understand the reasons, we examined the relationships between 2-MTs in PM-bound organics and environmental factors (e.g., temperature, RH and wind field). It was found that the concentrations of 2-MTs increased with RH, and the variations were larger in the zone of higher RH (Figure 4.4e). Earlier laboratory work has elucidated the formation of 2-MTs from acid-catalyzed aqueous-phase reactions (Wong et al., 2015). In field measurements, the ratio of 2-methylerythritol to the total of 2-methylerythritol and 2-methylthreitol can indicate aqueous-phase oxidation when the ratio is approximately 0.9 (Nozière et al., 2011). However, in our results, this ratio is around 0.7 across three clusters, which can be attributed to NO_x-rich photooxidation processes. Furthermore, the relationship between 2-MTs and RH is not linear, suggesting that while aqueous-phase reactions significantly influence 2-MTs levels, they do not solely account for the increase. This is due to the complexity of atmospheric conditions and the variability of SOA chemistry across different environments.

The SOA tracers of monoterpenes (mSOA) we observed included earlier-generation products pinonic acid (PNA) and pinic acid (PA) and later-generation products 3-hydroxyglutaric acid (3-HGA) and 3-methyl-1,2,3-butane-tricarboxylic acid (MBTCA). Compared to a previous online measurement conducted in Hong Kong (Wang et al., 2022b), the concentrations of two earlier-generation products are slightly lower, while the levels of two later-generation products remain similar. This difference may suggest that the air masses reaching the HT site are more aged than those at the other sites in Hong Kong. A higher proportion of mSOA was found in the two types of continental

air (Figure 4.4a), which could be attributed to the terrestrial emissions of monoterpenes. As pinic acid is generated from α-pinene oxidation and subsequently converted to MBTCA (Szmigielski et al., 2007), the ratio of pinic acid to MBTCA (hereinafter referred to as P/M ratio) was used to reflect the aging degree of mSOA, with lower P/M ratios indicating more aged mSOA (Ding et al., 2014). The average P/M ratios were 0.31 ± 0.04, 0.07 ± 0.01, and 0.14 ± 0.04 for CL1, CL2, and CL3, respectively. These findings indicate that the mSOA was more aged in the short-ranged continental air, where O_3 levels were the lowest among the three clusters. Figure 4.4f illustrates the diurnal variation of the P/M ratio in CL2, revealing a distinct afternoon peak that sets it apart from the other two clusters. Additionally, the diurnal pattern of O_3 in CL2 differs from those in the other clusters. Previous studies (Müller et al., 2012, Claeys et al., 2007) have shown that PNA and PA can be further transformed into MBTCA through photochemical processes. Furthermore, PNA is significantly influenced by gas-particle partitioning, and lower temperatures can increase the particle fraction of PNA (Booth et al., 2011). This explains why the highest P/M ratios were observed in CL2: active photochemical O_3 production may enhance the ozonolysis of monoterpenes, while the lower temperatures in this air mass could further facilitate the partitioning of PNA into the particle phase, leading to the formation of aged products.

4.3.3 Effects of anthropogenic emissions on SOA formation

Previous laboratory and field studies have demonstrated that anthropogenic emissions (e.g., NO_x and SO_2) can influence SOA formation through atmospheric multiphase chemistry (Shrivastava et al., 2019, Jaoui et al., 2008, Edney et al., 2005). The above discussion on speciated SOA tracers underscores the significant role of sulfate and atmospheric oxidant levels in SOA chemistry. However, further exploration is needed to understand the influence of anthropogenic emissions on SOA formation. Firstly, our

focus was limited to specific SOA formation pathways, without considering how the overall quality of SOA was affected. Secondly, sulfate and atmospheric oxidants are generated through complex atmospheric reactions involving gaseous precursors (e.g., SO_2, NO_x, and VOCs), and the above discussion did not address how the levels of these precursors impact SOA formation. To address this shortcoming, we combined the measurements from AMS to apportion the bulk SOA in this work, complementing observations from TAG. Details of the AMS data and source apportionment in this campaign can be found in a separate paper (Huo et al., 2024b). In short, four OA sources were resolved by the AMS-based PMF model, including one primary OA factor (0.69 ± 0.02 μg m^{-3}) and three SOA factors (6.0 ± 0.18 μg m^{-3}). The correlation coefficients between source-specific OA markers versus AMS-derived SOA factors were calculated to determine the potential origin of bulk SOA (Table 4.2). The results indicated that, among the four factors, the less oxidized oxygenated organic aerosol (LO-OOA1) showed a stronger correlation with anthropogenic SOA markers, while the more oxidized oxygenated organic aerosol (MO-OOA) was more closely associated with those derived from biogenic sources. Figure 4.5 presents the average percentage of NR-PM_1 components in three air masses. The results indicate that the highest concentration of MO-OOA and LO-OOA1 was observed in CL2, which is characterized by the highest levels of NO_x and SO_2. To elucidate the impact of anthropogenic emissions on SOA formation from various sources, scatter plots of anthropogenic and biogenic SOA concentrations colored by the concentrations of NO_x, SO_2, and O_3 were presented (Figure 4.6). Given the complex sources and reactions of VOCs in the atmosphere, here we use ozone levels as an indicator of VOC oxidation and their contribution to atmospheric oxidizing capacity. Significant positive correlations between MO-OOA and LO-OOA1 were observed across all cluster types, suggesting a simultaneous correlation of ambient SOA production from different sources. In CL1, biogenic SOA levels exceed those from anthropogenic sources, and this disparity increases

progressively with rising SO_2 levels (Figure 4.6a). The presence of SO_2 in coastal air is likely linked to ship emissions, which have been shown to enhance high-polar SOA formation in previous studies conducted in Hong Kong (Lyu et al., 2020). Laboratory experiments have also demonstrated that SO_2 can enhance biogenic SOA formation through acid-catalyzed reactions (Nakayama et al., 2015, Jaoui et al., 2008). Note that the trajectory of the coastal air masses did not pass through areas with high biogenic emissions, indicating that the efficiency of biogenic SOA production was enhanced by anthropogenically emitted SO_2. Additionally, the ozone level also played a role in promoting this process in coastal air. MO-OOA and LO-OOA1 levels are mostly similar in the short-range continental clusters, except for some extremely high LO-OOA1 values. As shown in Figure 4.6, the extreme LO-OOA1 values are closely related to high levels of SO_2, NO_x, and O_3, suggesting they may result from strong anthropogenic emissions and high atmospheric oxidant levels. Excluding these high values, LO-OOA1 levels in CL2 showed greater sensitivity to O_3 levels rather than SO_2 and NO_x levels. The trajectories of CL2 passed through areas rich in both anthropogenic and biogenic VOCs emissions, with some regions exhibiting significantly higher concentrations of anthropogenic VOCs compared to biogenic ones (Yin et al., 2015, Zheng et al., 2009). High concentrations of anthropogenic precursors can lead to increased SOA formation, and anthropogenic SOA formation can also be enhanced during ozone generation (Hoyle et al., 2011). The influence of anthropogenic sources on SOA formation is not evident in CL3, likely due to deposition during long-distance transport. Overall, the observational evidence revealed that the interaction of various anthropogenic factors influencing SOA levels can vary under different atmospheric conditions.

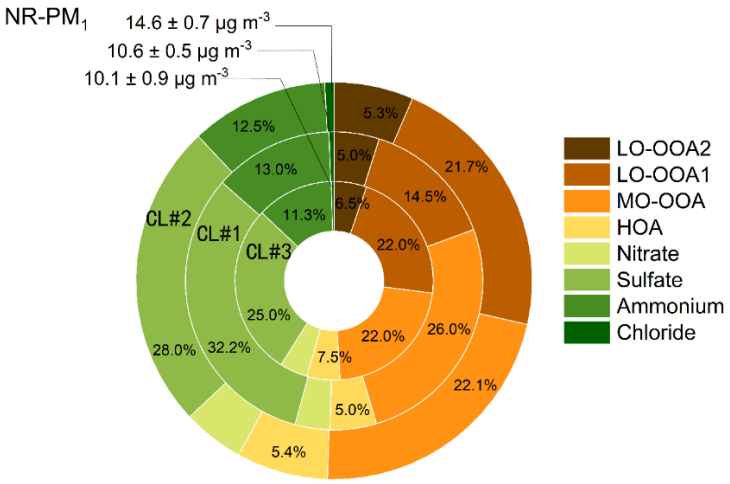

Figure 4. 5. Average percentage of NR-PM_1 components in the three air masses. Fractions below 5% are not indicated in the figure.

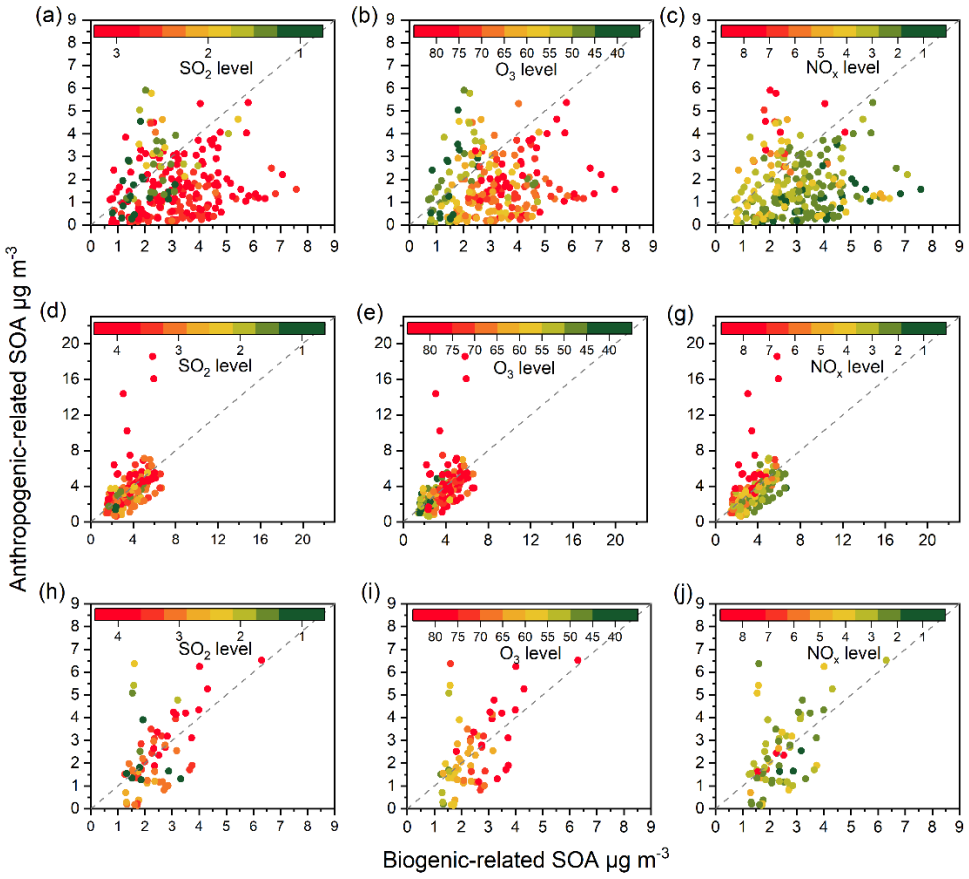

Figure 4. 6. Scatter plots illustrating the relationship between biogenic-related SOA and anthropogenic-related SOA across different clusters: (a, b, c) coastal cluster (CL1), (d,

e, f) short-range continental cluster (CL2), and (h, i, j) long-range continental cluster. Each subplot is color-coded to indicate levels of SO_2 (a, d, h), O_3 (b, e, i), and NO_x (c, f, j). The dashed grey diagonal line represents the 1:1 ratio.

Table 4. 2. Summary of coefficient of determination (R^2) for the correlations between bulk SOA masses resolved by AMS and selected tracer species detected by TAG. R^2 values below 0.1 are omitted. *P* values are calculated for correlations with R^2 >0.3.

	LO-OOA1	LO-OOA2	MO-OOA
Isoprene-derived SOA tracers			
2-MGA	0.14	0.04	**0.55****
2-MTs	0.04	0.02	0.05
C_5-alkenetriols	0.07	N.A.	0.26
Monoterpene-derived SOA tracers			
PA	0.06	N.A.	**0.54****
PNA	**0.47***	0.28	**0.30***
3-HDGA	0.10	0.02	0.13
MBTCA	0.13	0.04.	0.16
Anthropogenic SOA tracers			
DHOPA	0.26	N.A.	0.26
Phthalic acid	**0.44***	0.10	0.10
Dicarboxylic acids			
Adipic acid	**0.63****	0.23	0.19
Azelaic acid	**0.32***	0.10	0.04
Hydrobenzoic acids			

3-hydrobenzoic acid	**0.34***	**0.35**	0.05
4-hydrobenzoic acid	**0.46****	**0.41**	0.03

* p <0.05, * p <0.1.

4.4 High levels of particulate OHDCA in Hong Kong

As listed in Table 4.3, the average concentration of individual OHDCA species was 197.2 ± 18.6 ng m^{-3} for a tartaric acid isomer, 186.2 ± 14.3 ng m^{-3} for another tartaric acid isomer, 84.9 ± 6.8 ng m^{-3} for malic acid, 45.6 ± 3.9 ng m^{-3} for 2-hydroxyglutaric acid, and 8.3 ± 0.7 ng m^{-3} for citramalic acid in descending order. Except for citramalic acid, the concentrations of OHDCA species were significantly higher than those of the other OA markers we detected. The total concentration of the five OHDCA species varied from 9 to 3290 ng m^{-3} with an average (±95% Confidence Interval, CI) of 521 ± 43 ng m^{-3}. This value was even higher than the concentration of oxalic acid averaged over five Chinese megacities in summer 2018 (413 ng m^{-3}, Xu et al., 2022) and that measured at an urban site in Guangzhou, a megacity in South China and ~120 km to the northwest of Hong Kong, in autumn 2018 (475 ng m^{-3}, (Liu et al., 2021). These OHDCA species were also observed with high concentrations of PM_1 at the same site in a previous study (Lyu et al., 2020), and dominated over many other OA markers measured in South China (Liao and Yu, 2020, Wang et al., 2017b).

Table 4. 3. Detailed information about the 43 OA compounds that are quantified. Bolded compounds are OHDCA. * Authentic standards used.

No.	**Compound name**	**Quantification ion (m/z)**	**Retention time (s)**	**Internal standard**	**Surrogate standard**	**R^2 of calibration curve**	**Average concentration (ng m^{-3})**
1	**Citramalic acid**	247	667.21	Pentaerythritol-13C	*	0.9605	8.3 ± 0.7
2	**Malic acid**	233	676.51	Pentaerythritol-13C	*	0.9621	84.9 ± 6.8
3	**2-hydroxyglutaric acid (2-HGA)**	349	722.91	Pentaerythritol-13C	Citramalic acid	0.9605	45.6 ± 3.9
4	**Tartaric acid isomer 1**	292	732.12	Pentaerythritol-13C	*	0.9439	186.2 ± 14.3

5	**Tartaric acid isomer 2**	292	763.22	Pentaerythritol-13C	*	0.9439	197.2 ± 18.6
6	2-methylglyceric acid (2-MGA)	219	569.81	Pentaerythritol-13C	Citramalic acid	0.9605	1.2 ± 0.1
7	*cis*-2-methyl-1,3,4-trihydroxy-1-butene (C_5 alkenetriol-1)	231	602.51	Pentaerythritol-13C	Citramalic acid	0.9605	0.8 ± 0.09
8	3-methyl-2,3,4-trihydroxy-1-butene (C_5 alkanetriol-2)	231	617.51	Pentaerythritol-13C	Citramalic acid	0.9605	1.3 ± 0.2
9	*trans*-2-methy-1,3,4-trihydroxy-1-butene (C_5 alkanetriol-3)	231	622.21	Pentaerythritol-13C	Citramalic acid	0.9605	13.9 ± 1.5
10	2-methylthreitol (2-MT isomer 1)	219	704.31	Pentaerythritol-13C	Citramalic acid	0.9605	7.5 ± 0.5
11	2-methylerythritol (2-MT isomer 2)	219	714.91	Pentaerythritol-13C	Citramalic acid	0.9605	20.2 ± 0.4
12	Pinic acid	171	770.81	1-Dodecan-d25-ol	Pinonic acid	0.9789	0.4 ± 0.02
13	3-methyl-1,2,3-butanetricarboxylic acid (MBTCA)	405	810.82	Pentaerythritol-13C	Citramalic acid	0.9605	5.5 ± 0.6
14	2,3-dihydroxy-4-oxopentanoic acid (DHOPA)	321	693.31	Pentaerythritol-13C	Citramalic acid	0.9605	1.2 ± 0.1
15	Phthalic acid	295	790.81	D-phthalic acid	*	0.9623	0.4 ± 0.02
16	Levoglucosan	333	790.82	Pentaerythritol-13C	*	0.9719	32.2 ± 3.6
17	Mannosan	333	450.61	Pentaerythritol-13C	*	0.9815	0.39 ± 0.03
18	Glucose	204	912.52	Pentaerythritol-13C	*	0.9822	1.22 ± 0.13
19	Eicosane (n-C20)	57	907.02	Eicosane-d42	*	0.9818	0.20 ± 0.02
20	Heneicosane (n-C21)	57	946.02	Eicosane-d42	*	0.9791	0.08 ± 0.01
21	Docosane (n-C22)	57	982.72	Docosane-d46	*	0.9766	0.14 ± 0.01
22	Tricosane (n-C23)	57	1018.3	Docosane-d46	*	0.9722	0.14 ± 0.01
23	Tetracosane (n-C24)	57	1052.2	Tetracosane-d50	*	0.9765	0.18 ± 0.01
24	Pentacosane (n-C25)	57	1084.7	Tetracosane-d50	*	0.9748	0.26 ± 0.01
25	Hexacosane (n-C26)	57	1116.1	Hexacosane-d54	*	0.9768	0.33 ± 0.01
26	Heptacosane (n-C27)	57	1146.3	Hexacosane-d54	*	0.9691	0.41 ± 0.01
27	Octacosane (n-C28)	57	1175.4	Octacosane-d58	*	0.9675	0.49 ± 0.01
28	Nonacosane (n-C29)	57	1203.4	Octacosane-d58	*	0.9613	0.57 ± 0.02
29	Triacontane (n-C30)	57	1230.7	Triacontane-d62	*	0.9648	0.31 ± 0.01
30	Hentriacontane (n-C31)	57	1257.6	Triacontane-d62	*	0.9625	0.63 ± 0.03
31	Dotriacontane (n-C32)	57	1283.5	Dotriacontane-d66	*	0.9631	0.21 ± 0.01
32	Tritriacontane (n-C33)	57	1310.5	Dotriacontane-d66	*	0.9617	0.33 ± 0.02
33	Tetratriacontane (n-C34)	57	1337.4	Tetratriacontane-d70	*	0.9607	0.12 ± 0.01
34	Adipic acid	111	681.41	D-adipic acid	*	0.9713	1.50 ± 0.11
35	Azealic acid	317	825.118	D-Pentadecanol	*	0.9798	2.49 ± 0.12
36	Terephthalic acid	295	824.82	D-phthalic acid	*	0.9536	5.59 ± 0.24
37	Isophthalic acid	295	793.62	D-Pentadecanol	*	0.9591	2.28 ± 0.06
38	Phthalic acid	295	781.82	D-Pentadecanol	*	0.9623	0.40 ± 0.02
39	3-hydroxybenzoic acid (3-OHBA)	267	722.71	1-Dodecan-d25-ol	*	0.9820	0.49 ± 0.01

40	4-hydroxybenzoic acid (4-OHBA)	267	754.81	1-Dodecan-d25-ol	*	0.9850	0.35 ± 0.02
41	Palmitic acid (C16:0)	313	926.42	1-Octadeca-d37-nol	*	0.9745	0.13 ± 0.01
42	Stearic acid (C18:0)	341	999.52	Stearic-d35 acid	*	0.9781	0.06 ± 0.004
43	Oleic acid (C18:1)	339	999.62	Stearic-d35 acid	*	0.9735	3.15 ± 0.32

Figure 4.7 shows the time series of OHDCA species, along with the variations of PM_1 compositions, trace gases, and meteorological parameters over the sampling period. The time segments with different clusters and stages of air masses are labeled. Northeast winds dominated the whole sampling period, bringing the continental air or continental outflows along the coastline to the site, both of which were considered to be laden with various air pollutants. The average temperature and RH were 24.6°C and 75.1%, respectively. Both were noticeably higher than the national average temperature of 15.2°C and RH of 69.0% in autumn 2020 (National Bureau of Statistics of China, 2021). As expected for an autumn sampling campaign, the temperature and RH were higher in the earlier period, when higher levels of OHDCA were observed, especially before 7th Oct. This was in line with the temporal pattern of the 2018 measurements (Lyu et al., 2020). The total concentration of OHDCA correlated moderately with temperature (R^2=0.47), implying temperature dependence of the formation and/or precursor emissions. The temporal variations were consistent among all the OHDCA species. In this study, the PM_1-bound organic matter (PM_1-OM) was 6.1 ± 0.3 μg m^{-3}, which was 50 ± 3% of the total concentration of the nonrefractory composition. Due to the presence of other constituents, the $PM_{2.5}$, PM_1, and even PM_1-OM did not follow the variation of OHDCA. For example, in the afternoon of 6th Nov., affected by a typhoon off the east coast of Hong Kong, $PM_{2.5}$, PM_1, and PM_1-OM all increased drastically, while the increase in OHDCA was less significant. Such discrepancy indicated that the sources and chemistry of OHDCA differed from most PM components by mass. It is noteworthy that the highest levels of OHDCA were observed between the evening of 4th Oct. and the morning of 5th Oct., when a cold front approached. Meanwhile, the

RH, LWC and sulfate were elevated, as expected for warm moist air before a cold front, indicating the likelihood of enhanced aqueous processes. As the cold front passed, the OHDCA concentration decreased by 50% within 2 hr due to strong winds and rainfall.

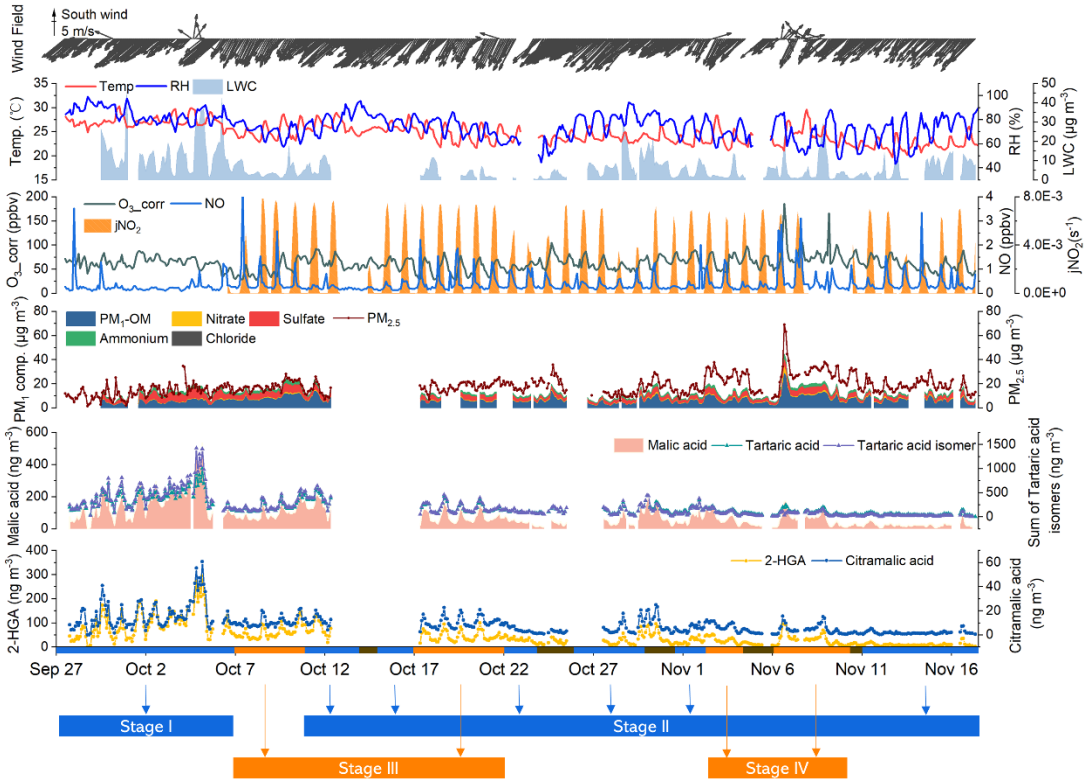

Figure 4. 7. Time series of OHDCA species, other selected air pollutants, and meteorological parameters during the observation period. The blue, orange, and brown bar on the bottom axis represents the period with CL1, CL2, and CL3 air masses, respectively. Segmentation of the CL1 and CL2 cases is illustrated in Chapter 3. Missing data are due to instrument maintenance.

By the category of air masses, we found that the coastal air (CL1) had the highest concentration of OHDCA (670.5 ± 86.0 ng m^{-3}), followed by the short-range continental air (CL2, 475.8 ± 40.8 ng m^{-3}), and the long-range continental air (CL3, 184.8 ± 30.6 ng m^{-3}). In fact, the concentrations of individual OHDCA species were not significantly different between CL1 and CL2, except for the two isomers of tartaric acid (450.9 ±

55.3 ng m^{-3} in CL1 vs. 336.3 ± 30.8 ng m^{-3} in CL2). Tartaric acid, with the same carbon skeleton as malic acid and one more OH group, has a higher oxidation state than malic acid. To compare the chemical age of air masses, we calculated the ratio of xylenes to ethylbenzene (X/E) that signifies more aged air with lower ratio (Monod et al., 2001). It turned out to be 0.87 in CL1 and 1.22 in CL2. Besides, the oxygen to carbon (O/C) ratio of PM_1-OM measured by AMS was higher in CL1 (0.81) than that in CL2 (0.76), reiterating that the CL1 air was more aged. Studies have demonstrated the importance of chlorine chemistry in coastal areas (Peng et al., 2022, Xue et al., 2015). However, chlorine-initiated oxidations of unsaturated aliphatic VOCs including isoprene may not lead to OHDCA formation due to the addition of chlorine atom(s) into the main products (Guo et al., 2020, Wang et al., 2022a). The ratio of toluene to benzene (T/B) was calculated to examine this effect, as the reaction between benzene and chlorine is very slow (Xue et al., 2015). The difference in T/B ratio between CL1 (1.83) and CL2 (2.23) corroborated the different aging degrees of the two types of air masses, which however was no more significant than the difference in X/E ratio. In fact, we would expect a lower T/B ratio in CL1, assuming that the proportional difference in T/B ratio between the CL1 and CL2 was consistent with that in the X/E ratio. This was still an overestimation, because the reaction rate constant of toluene with OH was ~4.7 times that of benzene with OH, while the difference between xylenes and ethylbenzene was less than a factor of 2. Thus, the chlorine-initiated oxidation of VOCs did not appear to be more significant in CL1 than in CL2. This is not surprising given the presence of large sources of chlorine in the continental air that has been confirmed at this site, such as nitryl chloride photolysis and oxidation of chloride by aqueous OH radical generated from particulate nitrate photolysis (Peng et al., 2022, Xue et al., 2015). Therefore, the higher levels of OHDCA in CL1, especially tartaric acid, were likely a result of higher degree of chemical aging that allowed OHDCA formation.

Of the OHDCA species we detected, malic acid was the most commonly studied, and its bihourly concentration reached up to 533 ng m^{-3} in this study. Here, we integrate the literature data and examine the world distribution of malic acid (Figure 4.8 and Table 4.4). Since both biogenic and anthropogenic VOCs could be the precursors of malic acid, the annual average emissions of isoprene, monoterpenes, and anthropogenic non-methane VOCs (NMVOCs) in 2020 (year of field measurement in this study) are also plotted to provide background information for interpreting the malic acid distribution. However, completely matching the timing of VOCs emissions and malic acid measurements is impossible, because the latter spanned decades. Thus, the VOCs emissions can only be used as a rough reference. It should also be noted that the differences in sampling time, analytical methods, site categories, and particle size complicate the comparison of malic acid concentrations between studies. We try to minimize these interferences in the discussions below. For example, the high concentrations of malic acid in Hong Kong are evidenced by not only the TAG data but also the traditional gas chromatography-mass spectrometry analysis results.

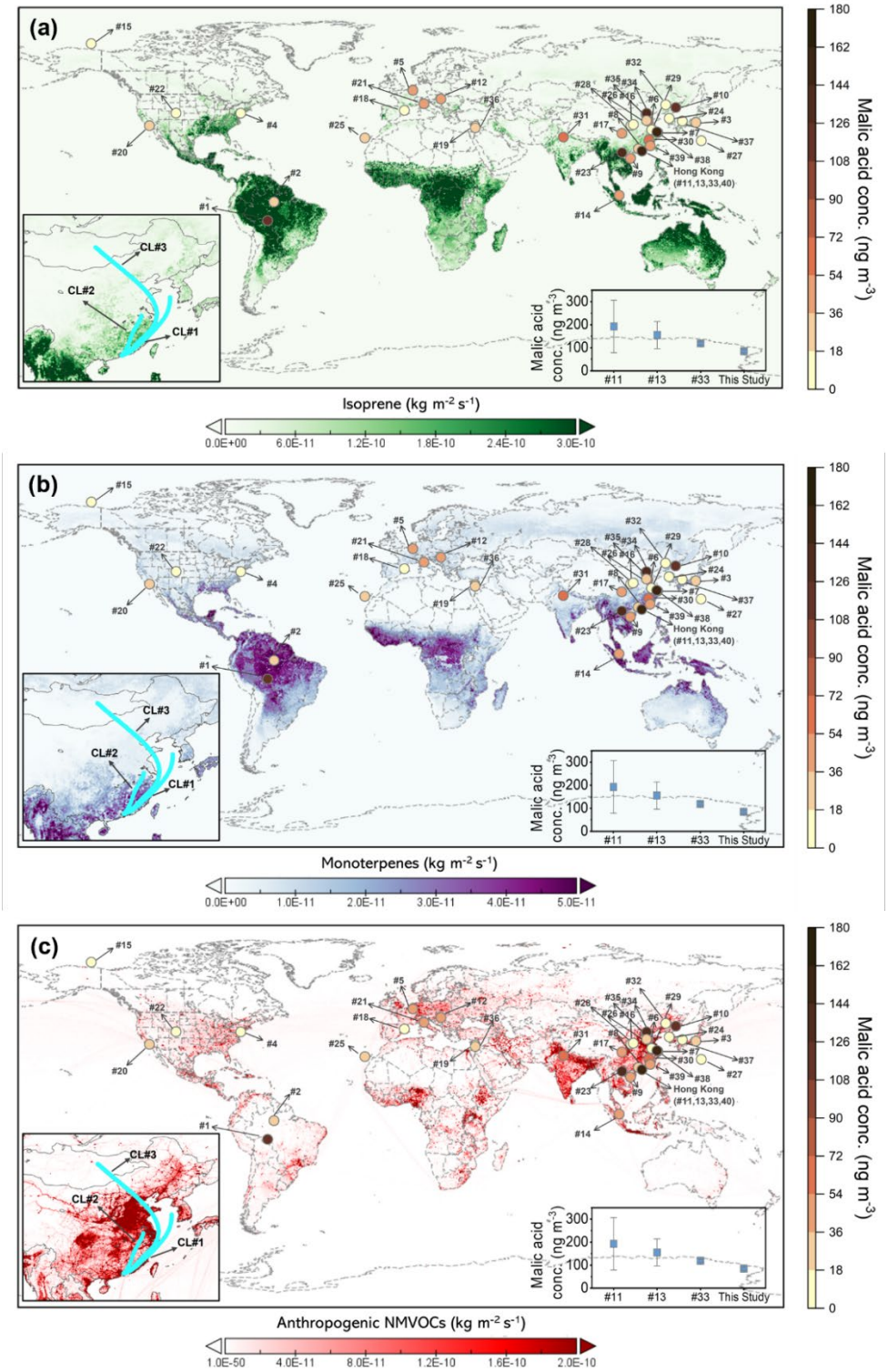

Figure 4. 8. Global distribution of malic acid concentrations on the map of annual average emissions of isoprene (a), monoterpenes (sum of α-pinene and β-pinene) (b), and anthropogenic NMVOCs (c) in 2020 (year of field measurement in this study). The

data for Hong Kong is a mean value of malic acid concentrations reported in several studies, which are shown in the inset. The VOC emission fluxes are downloaded from the Emissions of atmospheric Compounds and Compilation of Ancillary Data available at https://eccad.sedoo.fr/ (Granier et al., 2019; Sindelarova et al., 2022). Average 72-hr backward trajectories of the three clusters are shown in the lower left inset. The studies are numbered chronologically according to publication or sampling time. A detailed description of the data is summarized in Table 4.4.

Table 4. 4. Sampling and analytical details about the data of malic acid concentration presented in Figure 4.8. * Average concentration of malic acid in $PM_{2.5}$ unless otherwise specified. # TSP: Total Suspended Particles. † Samples collected on filters and analyzed by offline Gas Chromatography coupled with Mass Spectrometry (GC-MS).

No.	Site location	Site category	Sampling period	Sample collection & analysis methods	Concentration (ng m^{-3}) *	Reference
1	Rondonia, Brazil	Pasture	Oct. 1999	Filter & GC-MS †	115	Graham et al. (2002)
2	Balbina, Brazil	Forest site	Jul. 2001	†	32	Claeys et al. (2004)
3	Tokyo, Japan	Rural site	Jun. 1989	†	27.3 (TSP) #	Kawamura et al. (2005)
4	Philadelphia, PA, USA	Urban site	Jul. – Aug. 2000	†	16.2 (PM_{10}) ^	Li et al. (2006)
5	Julich, Germany	Forest site	Jul. 2003	†	39	Kourtchev et al. (2008)
6	Mt.Tai, China	Mountain site	May. – Jun. 2006	†	68.2 (TSP)	Fu et al. (2008)
7	Chongming Island, China	Forest site	Jun. 2006	†	79	Wang et al. (2008)
8	Dinghu Mt., China	Forest site	Aug. 2006	†	29	Wang et al. (2008)
9	Jiangfenglin, China	Forest site	Nov. 2006	†	46	Wang et al. (2008)
10	Changbai Mt., China	Forest site	Jul. 2007	†	109	Wang et al. (2008)
11	Hong Kong, China	Urban site	Jul. – Aug. 2006	†	209	Hu et al. (2008)
12	K-puszta, Hungary	Forest site	Jun. – Jul. 2003	†	40	Kourtchev et al. (2009)
13	Hong Kong, China	Urban site	Nov. 2007 – Jan.2008	†	155	Hu and Yu (2013)
14	Singapore	Suburban site	Sep. – Oct. 2008	†	40.9	Yang et al. (2013)

15	Beaufort Sea	Marine area	Aug. 2009	†	0.95 (TSP)	Fu et al. (2013)
16	Mt.Hua, China	Mountain site	Jul. – Aug. 2009	†	7.3 (PM_{10})	Li et al. (2013a)
17	Sichuan, China	Forest site	Jul. 2010	†	53.1	Li et al. (2013b)
18	Barcelona, Spain	Urban site	Sep. – Oct. 2010	†	14.2	Alier et al. (2013)
19	Beirut, Lebanon	Suburban site	Jan. – Feb. 2012	†	12.7	Waked et al. (2013)
20	Los Angeles, U.S.A.	Suburban site	Sep. – Oct. 2010	†	19.4	Alier et al. (2014)
21	Bologna, Italy	Urban background site	Nov. – Dec. 2011	†	40.9	Pietrogrande et al. (2014)
22	Colorado, U.S.A.	Mountain site	Oct. 2010 – Apr. 2012	†	2.14 (TSP)	Xie et al. (2016)
23	Sonla, Vietnam	Suburban site	Mar. 2013	†	128	Nguyen et al. (2016)
24	Seoul, Korea	Suburban site	Oct. 2012 – Sep. 2013	†	13.11	Kim et al. (2016)
25	Tenerife, Spain	Mountain site	Aug. 2013	†	32.21 (TSP)	Garcia et al. (2017)
26	Shanxi, China	Rural site	Jun. – Jul. 2015	†	18.9	Li et al. (2017)
27	Chichijima Island, Japan	Remote site	Dec. 2010 – Nov. 2011	†	6.50	Gowda et al. (2018)
28	Xi'an, China	Urban site	Mar. 2013	†	17 (TSP)	Ren et al. (2019)
29	Nanjing, China	Urban site	Dec. 2014 – Jan. 2015	†	1.19	Haque et al. (2019)
30	Fujian, China	Mountain site	Nov. 2015 – Feb. 2016	†	68	Hong et al. (2019)
31	Delhi, India	Urban site	Dec. 2011	†	56.16 (TSP)	Agarwal et al. (2020)
32	Jilin, China	Rural site	Oct. – Nov. 2016	†	0.7	Wu et al. (2020)
33	Hong Kong, China	Urban background site	Nov. – Dec. 2018	TAG	119 (PM_1)	Lyu et al. (2020)
34	Hebei, China	Suburban site	10 Jul. – 10 Aug. 2015	†	58.7	Li et al. (2021)
35	Beijing, Chnia	Urban site	Jul. 2017	†	132.4	Yu et al. (2021)
36	Limassol, Greece	Urban site	Jun. – Aug. 2018	†	22.3	Kanellopoulos et al. (2021)
37	Oki Islands, Japan	Remote site	Mar. – Apr. 2019	†	13.2	Ikemori et al. (2021)
38	Shanghai, China	Urban site	Nov. 2019 – Jan. 2020	TAG	156	Zhu et al. (2023)
39	Fujian, China	Coastal site	Jul. 2020	†	37.6	Hong et al. (2022)
40	Hong Kong, China	Urban background site	Sep. – Nov. 2020	TAG	84.9	This study

Bearing the uncertainties in mind, we noticed that the concentration of malic acid varied

by more than two orders of magnitude at these sites and was much higher in Asia. Moreover, eight of the top 10 concentrations were reported in China, including the highest of all 201 ng m^{-3} measured at a suburban site in Hong Kong in Jul-Aug 2006 (Hu et al., 2008). The subsequent studies have repeatedly confirmed the elevated levels of malic acid at several locations in Hong Kong (Lyu et al., 2020, Hu and Yu, 2013). High concentrations of malic acid were also observed in Shanghai and Beijing (Yu et al., 2021, Zhu et al., 2023), where the biogenic emissions were expected to be lower. In particular, the measurement in Shanghai was conducted at an urban site in a cold season (Nov-Jan), reducing the likelihood of high biogenic contributions to malic acid in that study period. In contrast, at a forest site on Changbai mountain with sparse anthropogenic emissions, the average concentration of malic acid was as high as 109 ng m^{-3} (Wang et al., 2008). Similarly, an average of 115 ng m^{-3} of malic acid was observed in a Brazilian pasture (Graham et al., 2002). Both evidence implied that biogenic emissions could also be the precursors of malic acid. However, not all the forest or mountainous sites featured elevated concentrations of malic acid, same for the sites with potentially strong anthropogenic emissions, as shown in Table 4.4. This might be because the distribution of malic acid was also regulated by other factors, such as atmospheric oxidation capacity. Ground-level measurement and modeling indicated serious O_3 pollution in eastern China (Gaudel et al., 2018, Lyu et al., 2023). Although O_3 is not necessarily a main oxidant involved in malic acid formation, it to some extent reflects the abundance of many other oxidants, for example, OH radical. Therefore, it is likely that the high levels of malic acid in several Chinese cities were partially attributable to the strong atmospheric oxidation capacity.

Besides, biomass burning was found to increase malic acid concentration, such as that observed at a suburban site in Vietnam, that is, 128 ng m^{-3} (Nguyen et al., 2016). Nevertheless, it was rare in Hong Kong, and we did not find any relationship between

malic acid and biomass burning tracers (e.g., levoglucosan) in the OHDCA-rich CL1 and CL2 air. Meteorological conditions play a critical role in regulating SOA formation. Water-soluble organics, such as oxalic acid, were found to increase under high relative humidity (Wang et al., 2017a, Xu et al., 2022). As a subtropical coastal city, Hong Kong's autumn is warm and humid, which might have also favored OHDCA formation, especially for the case of CL1. Thus, there may be multiple factors underpinning the high levels of malic acid in Hong Kong. Moreover, the effects of all the influencing factors were blended during the transport of air masses to this background site, and the observed OHDCA might be partially attributed to emissions and chemistry in the whole region or even further afield. As an effort to unravel this mystery, we next explore the formation mechanisms of OHDCA by types of air masses.

4.4.1 Different factors dominating OHDCA formation

The OHDCA species correlated strongly with each other (R^2=0.80-0.96) and exhibited bell-shaped diurnal patterns with afternoon peaks at 14:00-16:00, implying the secondary formation origin (Figure 4.9). In the coastal air (CL1), the baseline level (lowest value in the average diurnal cycle) of OHDCA was relatively high, with the minimum to maximum ratio of 0.84. This might be due to the retention of aged air masses in the coastal area, where OHDCA could be formed through oxidation of the precursors in continental outflows.

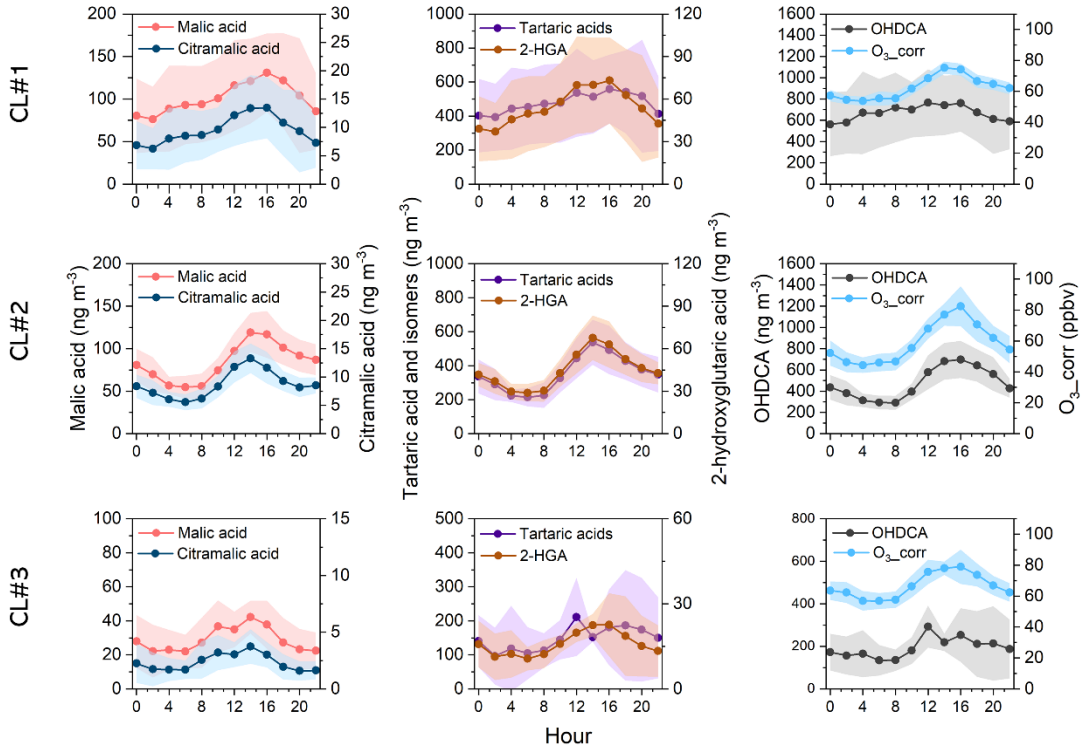

Figure 4. 9. Diurnal variations of OHDCA species and O_3_corr in separate clusters. Shaded areas denote 95% confidence intervals.

To explore the formation mechanisms of OHDCA, we first examined the correlations between OHDCA and some secondary air pollutants, as listed in Table 4.5. The OHDCA species correlated well with sulfate when the coastal air reached the site (R^2=0.53-0.67). Similar correlation was also reported for oxalic acid and considered as an evidence of in-cloud formation processes (Yu et al., 2005, Zhou et al., 2015b). It has been documented that sulfate formed through aqueous reactions (e.g., in-cloud and fog processes) tends to be distributed in droplet mode (0.56-1 μm), compared to that formed from gas-phase oxidation in condensation mode (0.32-0.56 μm) (Liu et al., 2021, Wang et al., 2016, Yu et al., 2005, Meng and Seinfeld, 1994). In the CL1 air masses, sulfate distribution was in a droplet mode with the mass modal diameter (d, diameter size at which the highest concentration occurs) of 0.62 μm in the earlier period (Stage I) when the RH and ALWC were higher (Figure 4.10). The distribution shifted to a condensation

mode (d=0.36 μm) in the later period with CL1 air (Stage II). As expected for the aqueous formation of sulfate, the sulfur oxidation ratio (molar ratio of sulfate to the sum of sulfate and SO_2) was higher in Stage I (Figure 4.11). Most importantly, higher concentrations of OHDCA and a better correlation of OHDCA with sulfate were observed in Stage I (Figure 4.10b). Overall, the evidence points to aqueous formation of OHDCA in the coastal air with high ALWC. Nevertheless, the OHDCA concentration was higher in daytime, opposite to the diurnal pattern of LWC (Figure 4.12). Thus, it was photochemical rather than dark (nocturnal) aqueous reactions that dominated the OHDCA formation.

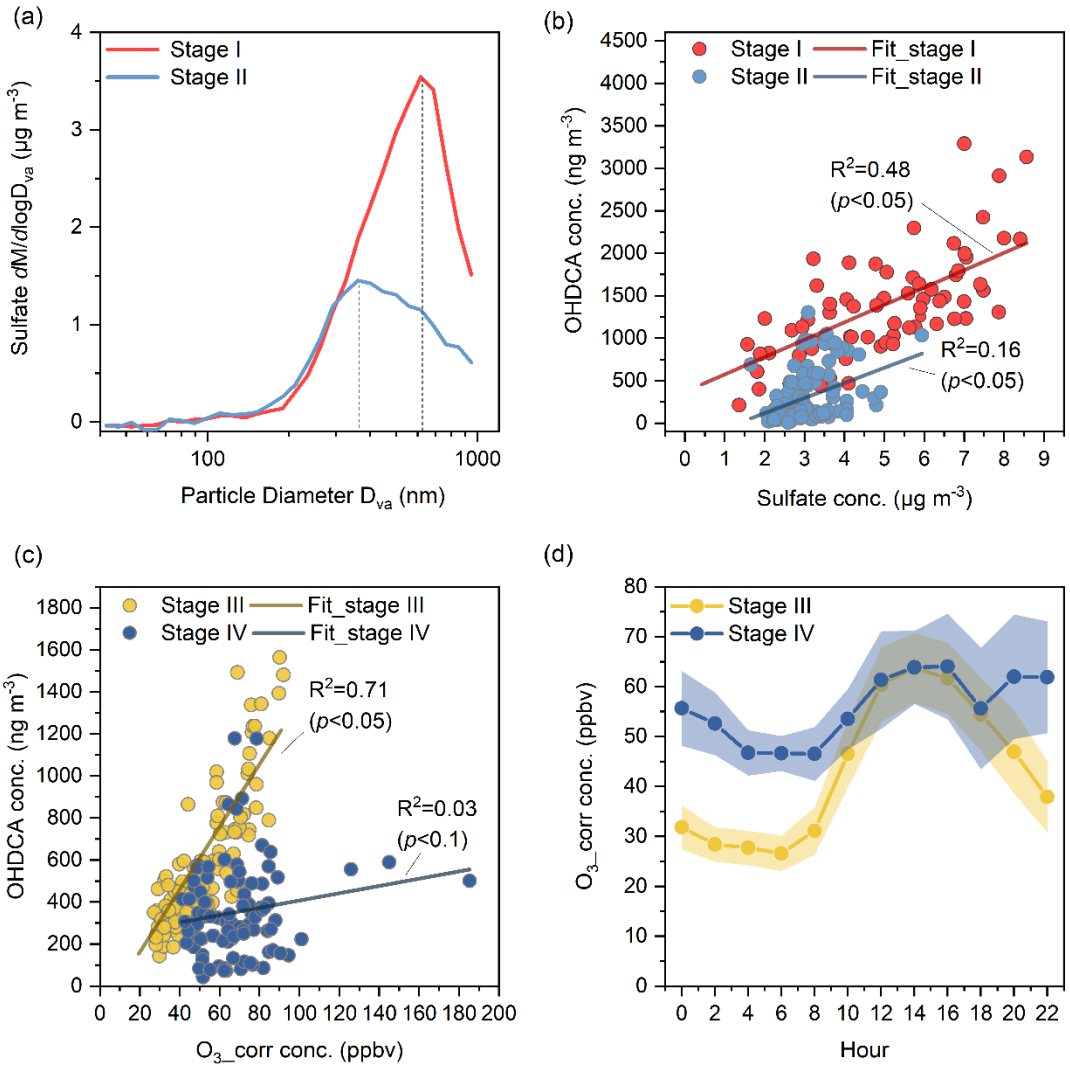

Figure 4. 10. Size distribution of sulfate in the range of <1 μm measured by AMS in Stage I and Stage II (a); Correlation between OHDCA and sulfate in Stage I and Stage II (b); Correlation between OHDCA and O_3_corr in Stage III and Stage IV (c); and Average diurnal cycles of O_3_corr in Stage III and Stage IV (d). Mass modal diameter of sulfate distribution is shown with the dotted line in (a).

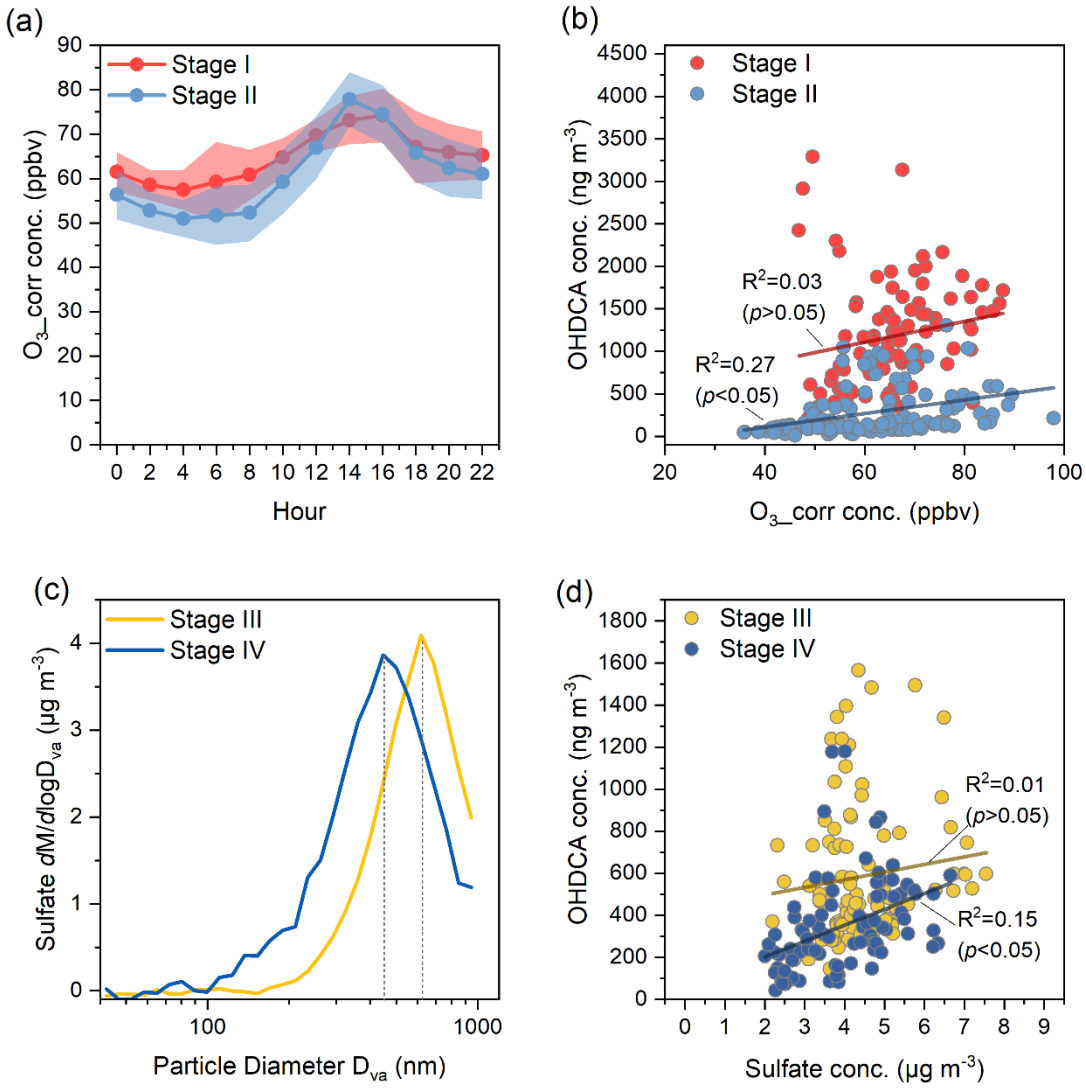

Figure 4. 11. Average diurnal variations of O_3_corr in Stage I and Stage II (a); Correlation between OHDCA and O_3_corr in Stage I and Stage II (b); Size distribution of sulfate in the range of < 1 μm in Stage III and Stage IV (c); and Correlation between OHDCA and sulfate in Stage III and Stage IV (d).

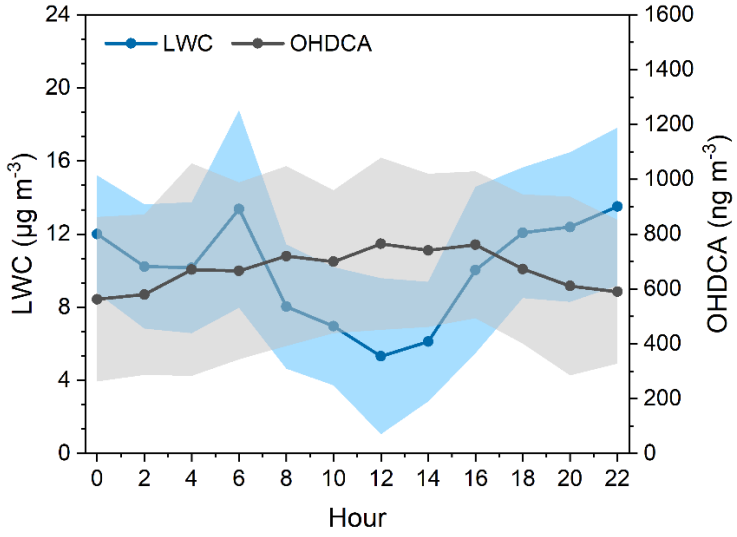

Figure 4. 12. Average diurnal patterns of OHDCA and LWC in the CL1 air.

Table 4. 5. Summary of R^2 for the correlations between speciated OHDCA and selected tracer species. R^2 values of <0.25 are omitted. *P* values are calculated for correlations with $R^2 > 0.3$.

		Secondary inorganic ions		Oxidant	Isoprene SOA tracers			Monoterpenes SOA tracers		Anthropogenic SOA tracers	
		Sulfate	Nitrate	O_3_corr	2-MGA	2-MTs	C_5 alkenetriols	Pinic acid	MBTCA	DHOPA	Phthalic acid
CL#1	**Malic acid**	0.67**	<0.10	0.10	0.70**	0.22	0.41**	0.43**	0.33	0.11	<0.10
	Citramalic acid	0.53**	<0.10	0.10	0.58**	0.22	0.41**	0.58**	0.37	0.27	<0.10
	Tartaric acid	0.58**	<0.10	0.10	0.64**	0.19	0.39**	0.40**	0.30	0.10	<0.10
	2-HGA	0.65**	<0.10	0.10	0.68**	0.20	0.40**	0.51**	0.31	0.15	<0.10
CL#2	**Malic acid**	0.18	<0.10	0.20	0.66**	<0.10	0.40**	0.62**	0.40	0.48**	0.31*
	Citramalic acid	0.11	<0.10	<0.10	0.34*	<0.10	0.28	0.67**	0.40	0.63**	0.35*
	Tartaric acid	<0.10	<0.10	<0.10	0.41*	<0.10	0.27	0.51**	0.35	0.31*	0.12
	2-HGA	0.18	<0.10	0.12	0.54**	<0.10	0.38**	0.56**	0.52	0.53**	0.36*
CL#3	**Malic acid**	0.37*	0.39	0.44	0.13	<0.10	0.19	0.72**	<0.10	0.68**	0.31*
	Citramalic acid	0.48**	0.45	0.41	0.16	<0.10	0.24	0.68**	<0.10	0.79**	0.41**
	Tartaric acid	0.19	0.13	0.32	<0.10	<0.10	<0.10	0.68**	0.35*	0.18	0.14
	2-HGA	0.34*	0.34	0.53	<0.10	<0.10	<0.10	0.77**	0.48*	0.33*	0.29

** p <0.05, * p <0.1.

In contrast, OHDCA experienced a more pronounced increase from morning to afternoon in CL2, with a minimum to maximum ratio of 0.52 and net increment of 406

ng m^{-3} in the average diurnal cycle, compared to 202 ng m^{-3} in CL1 & 158 ng m^{-3} in CL3 (Figure 4.10). The same went for O_3_corr, which increased by 35.7 ppbv (77%) between the morning trough and the afternoon peak, compared to 19.9 ppbv (36%) for CL1 and 21.3 ppbv (37%) for CL3. Our previous work indicated a moderate correlation (R^2=0.50) between OHDCA and O_3_corr in continental air at the same site (Lyu et al., 2020). However, in this field campaign, OHDCA did not show concordance with O_3_corr ($R^2 < 0.20$) in CL2. This is somewhat counterintuitive, due to the synchronized diurnal patterns between them. Through investigating the day-to-day variations, we found that OHDCA correlated well with O_3_corr (R^2=0.71) in CL2 air in the earlier period (Stage III) when the jNO_2 was the highest throughout the sampling campaign (Table 4.6), but the correlation was significantly weakened in the later period (Stage IV), as shown in Figure 4.10c. While the maximum O_3_corr levels were comparable in both stages, the O_3_corr increment from morning to afternoon was markedly higher in Stage III (Figure 4.10d), indicating more intense photochemistry. Note that the OHDCA concentration was also noticeably higher on these days. Similar consistency was also reported for oxalic acid and O_3, which was taken as evidence that gas-phase precursors or O_3-initiated oxidations mediate oxalic acid formation (Cheng et al., 2017, Yang et al., 2022). Unlike Stage I of CL1, OHDCA showed no correlation with sulfate in Stage III of CL2. The SO_2 concentration and sulfur oxidation ratio were comparable between the two periods, although the sulfate concentration in Stage III was slightly lower (Table 4.6). Moreover, we noticed a droplet-mode distribution of sulfate in Stage III (Figure 4.11). Therefore, it was plausible that sulfate in the sampled air was also formed via aqueous or in-cloud processes, while the RH and LWC were much lower (Table 4.6). The poor correlation of OHDCA with sulfate in Stage III suggested that the dominant factors in OHDCA formation were different from those in Stage I. Gas-phase precursors formed in photochemical reactions or O_3-initiated oxidations might be the primary factor regulating OHDCA formation, as indicated by the good correlation between

OHDCA and O_3_corr. It is noteworthy that this conclusion does not necessarily exclude the involvement of aqueous processes in OHDCA formation in Stage III, which might occur after the precursors were partitioned into the aqueous phase.

Table 4. 6. Comparison of selected air pollutants and meteorological conditions between the stages. Photolysis frequencies are not measured in Stage I.

	Stage I	**Stage II**	**Stage III**	**Stage IV**
OHDCA (ng m^{-3})	1150.8 ± 130.4	281.3 ± 52.0	575.6 ± 58.0	353.4 ± 40.2
O_3_corr (ppbv)	64.8 ± 1.9	61.3 ± 1.8	51.1 ± 3.0	68.2 ± 3.9
Daytime increment of O_3_corr (ppbv)	16.7 ± 2.4	26.9 ± 3.8	37.2 ± 6.4	17.5 ± 4.6
SO_2 (ppbv)	2.7 ± 0.03	2.5 ± 0.1	2.7 ± 0.1	3.5 ± 0.2
Sulfate (μg m^{-3})	5.2 ± 0.4	2.9 ± 0.1	4.4 ± 0.2	4.1 ± 0.2
SOR	0.5 ± 0.03	0.5 ± 0.02	0.5 ± 0.02	0.4 ± 0.01
RH (%)	84.5 ± 1.2	77.8 ± 1.3	72.0 ± 1.2	67.7 ± 2.1
LWC (μg m^{-3})	14.2 ± 2.2	7.1 ± 0.9	4.7 ± 0.7	5.7 ± 1.4
jNO_2 (s^{-1})	N.A.	0.0019 ± 0.0004	0.0021 ± 0.0005	0.0017 ± 0.0005

The OHDCA concentrations in Stage II and Stage IV were relatively low (Table 4.6) and might represent background levels in the coastal air and short-range continental air, respectively. The relationships of OHDCA with O_3_corr and sulfate in the two periods appeared to reflect a mixed effect of the situations discussed above. Taken together, aqueous photooxidation was identified to be the main mechanism of OHDCA formation and was more discernible when the OHDCA concentrations were high. However, the dominant factors differed between the coastal Stage I and the continental Stage III under different atmospheric conditions. On one hand, our analysis based on observational data highlighted the importance of aqueous processes in OHDCA formation in the coastal air that were only proposed in chamber studies before (Gao et al., 2004, Sato et al.,

2007). On the other hand, the effects of photochemical production of gas-phase precursors or O_3-initiated oxidations on OHDCA formation were more pronounced in the short-range continental air.

As mentioned above, the CL3 air contained the lowest concentrations of OHDCA. In addition to moderate correlations with sulfate and O_3_corr, OHDCA in CL3 also correlated with several other compounds, including not only secondary (e.g., pinic acid and DHOPA) but also primary species (e.g., CO and levoglucosan) (Figure 4.13). This phenomenon implied their common dependence on atmospheric mixing and migration. Besides, some intertwined processes could not be ruled out. For example, biomass burning might enhance the emissions of OHDCA and/or the precursors (Wu et al., 2020b, Fu et al., 2012), resulting in a correlation between OHDCA and levoglucosan. Similar mechanisms were proposed to interpret the correlations between biogenic SOA species and biomass burning tracers (Ding et al., 2016).

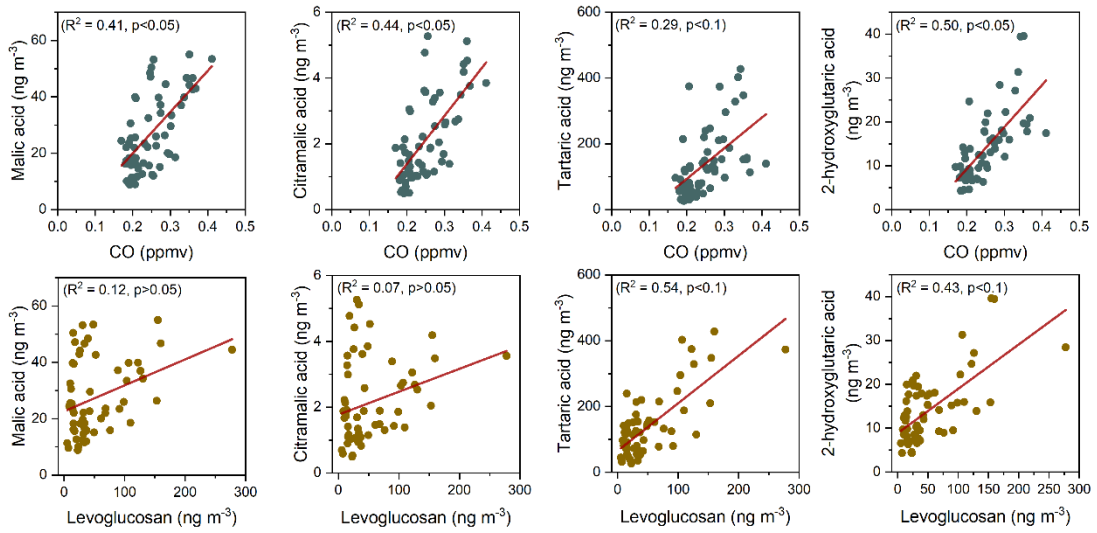

Figure 4. 13. Relationships of speciated OHDCA versus CO and levoglucosan in CL3.

4.4.2 Potential precursors of OHDCA

An important question after the above discussion is what the precursors of OHDCA were. We attempt to answer it by examining the relationships of OHDCA with a series of chemical signatures. In both CL1 and CL2 air, at least moderate correlations were identified between OHDCA species and 2-MGA (Figure 4.14 and Table 4.6), a tracer of isoprene SOA formed under high-NOx conditions (Kroll et al., 2006). Hu and Yu (2013) ever reported a strong correlation between malic acid and the sum of three isoprene SOA tracers, that is, 2-MGA and two isomers of 2-MTs, based on daily data in summer (R^2=0.89). However, the formation pathways and atmospheric behaviors of 2-MGA and 2-MTs were quite different, because the latter are oxidation products of isoprene in a low-NO_x environment (Claeys et al., 2004). Consistent with the 2018 measurement results at this site (Lyu et al., 2020), higher levels of 2-MTs were observed at night, opposite to the diurnal pattern of 2-MGA. This explained the little relationship between OHDCA and 2-MTs, and the worse correlation of OHDCA with C_5 alkenetriols (Table 4.6), which are also isoprene SOA tracers under low NO_x conditions (Claeys et al., 2004). In addition, OHDCA had a moderate to good correlation with pinic acid (R^2=0.39-0.67) and a weaker correlation with MBTCA, an earlier and later generation SOA product of monoterpenes, respectively (Mutzel et al., 2016). The results suggested that biogenic VOCs might be the precursors of OHDCA, but the specific transformation pathways over multiple generations remain to be revealed.

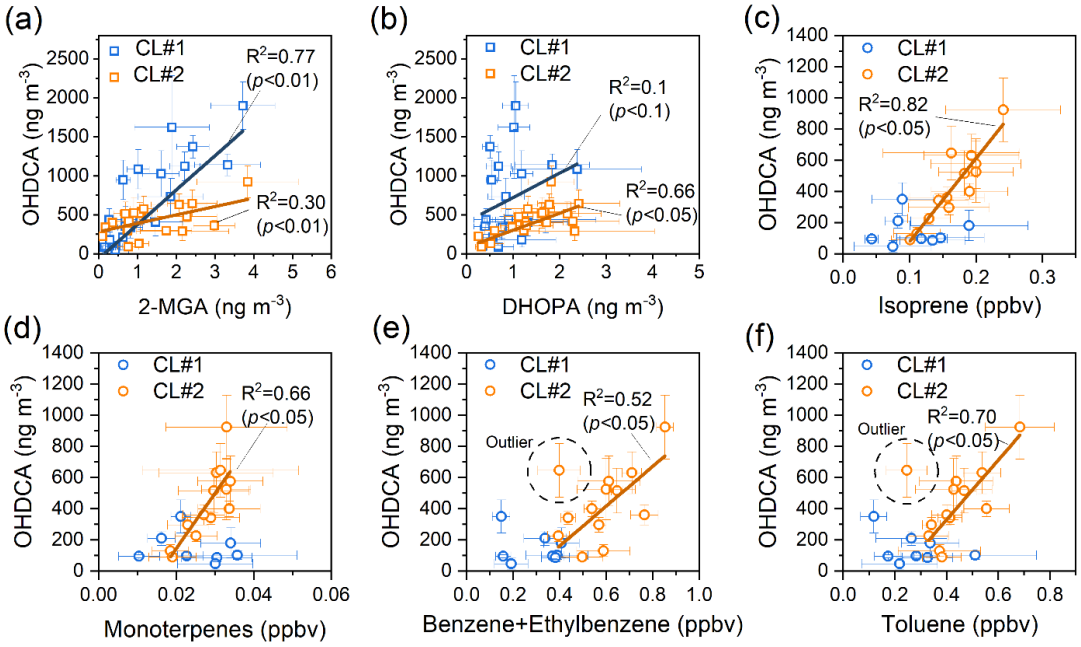

Figure 4. 14. Scatter plot of daily average concentration of OHDCA versus SOA tracers and VOC precursors, including 2-MGA (a), DHOPA (b), isoprene (c), monoterpenes (d), benzene and ethylbenzene (e), and toluene (f). Error bars represent 95% CIs. An outlier with much higher RH that may be influenced by aqueous processes is excluded from the regression for CL2 data points.

A notable phenomenon that differentiated CL2 from CL1 was the better correlations between OHDCA and anthropogenic SOA tracers derived from aromatics in CL2, that is, DHOPA and phthalic acid (Kleindienst et al., 2012, Kleindienst et al., 2004). As shown in Figure 4.15, both DHOPA and phthalic acid exhibited typical photochemical diurnal patterns. The correlation of phthalic acid with two common tracers of primary emissions, black carbon and carbon monoxide (R^2=0.28 and 0.12), was much worse than with DHOPA (R^2=0.65). Besides, terephthalic acid, an isomer of phthalic acid, is generally derived from primary emissions (Fu et al., 2010, Sheesley et al., 2010). Here, there was little consistency between the two isomers, with an R^2 of 0.03. The evidence indicated that the observed phthalic acid was more of secondary origin. Therefore,

anthropogenic VOCs, especially aromatic hydrocarbons, might have also contributed to OHDCA formation in the short-range continental air.

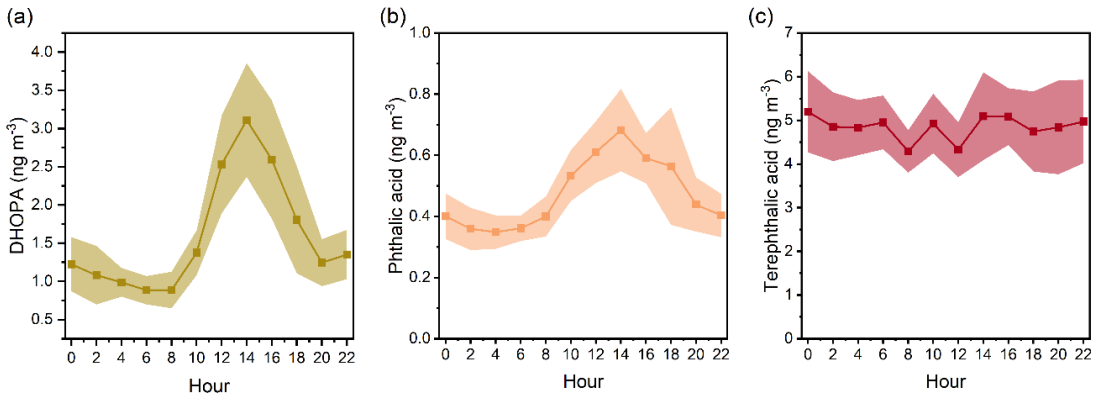

Figure 4. 15. Average diurnal cycles of DHOPA (a), phthalic acid (b), and terephthalic acid (c) in CL2.

Due to the time required for transformation of VOCs to OA compounds and its uncertainty, it was unrealistic to expect a correlation between OHDCA and VOCs at TAG's resolution. Thus, daily averages were adopted for the analysis, as shown in Figures 4.14 and 4.16. This method also eliminates the spurious correlations caused by similar diurnal variations unrelated to chemical linkages. No significant relationship was discerned between OHDCA and VOCs in CL1. On one hand, VOC data were only available for 8 days in coastal air, especially unavailable on days when high levels of OHDCA were observed. On the other hand, this might be due to the fact that the observed VOCs did not represent the oxidized fractions in the more aged coastal air, as indicated by the high O/C ratio and low X/E ratio (see Chapter 3.3). In contrast, there existed moderate to good correlations between OHDCA and biogenic OCs (isoprene and monoterpenes) and some anthropogenic VOCs (toluene, benzene and ethylbenzene, m/p-xylene, and cyclohexane) in the less aged CL2 air. This did not indicate the co-emissions of OHDCA and these VOCs, due to their different diurnal patterns and bad

correlations at a higher resolution (e.g., bihourly). Instead, it was plausible that these species and/or other undetected fractions that followed the same patterns as these species were the precursors of OHDCA in the short-range continental air. In particular, aromatics were highly suspected.

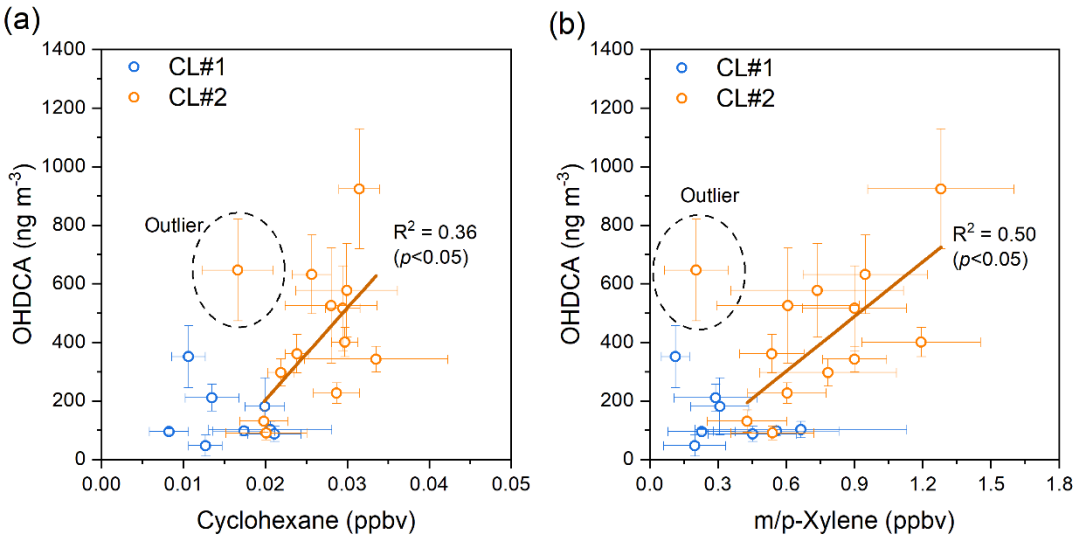

Figure 4. 16. Scatter plot of daily average concentration of OHDCA versus cyclohexane (a) and m/p-Xylene (b). An outlier with much higher RH that may be influenced by aqueous processes is excluded from the regression for CL2 data points.

A recent study elucidated the formation of oxalic acid (a typical dicarboxylic acid and an analog of OHDCA) at an inland site ~150 km northwest to HT using dual carbon isotope techniques (Xu et al., 2022). It indicated that oxalic acid in coastal air was mainly of biogenic origin, but more than half of it was derived from fossil sources in continental outflows. Therefore, the conclusions we drew from the chemical signatures, albeit not quantitative, are broadly in line with the carbon isotope-based analysis results for oxalic acid, the structurally simplest analog of OHDCA.

4.5 Concluding Remark

In this chapter, we conducted highly time-resolved measurements of bulk organics and

speciated OA markers at a regional background site in Hong Kong. The results revealed that the factors influencing aerosol aging vary with atmospheric conditions. In coastal air, the aqueous-phase reaction is important for high oxidation states of aerosol, whereas photochemical reaction dominated in continental air that has traveled through the PRD region. Molecular-level information further demonstrated that both anthropogenic and biogenic SOA markers exhibited the highest concentrations in the continental air. For anthropogenic SOA markers, the combination of high precursor levels and intense photochemical reactions resulted in the highest level of SOA. Additionally, anthropogenic SOA markers correlated better with total organics compared to biogenic markers, suggesting a greater impact of anthropogenic sources on particle-bound organics. For biogenic SOA, the high concentrations observed in continental air seem not to be driven by precursor levels, and the influence factors differ for the speciated SOA. The detailed analysis found that 2-MGA and sulfate were correlated in coastal air, indicating contributions from aqueous-phase reactions. In contrast, C_5-alkenetriols and sulfate exhibited a strong correlation in continental air, where sulfate formation is not dominated by aqueous reactions. Instead, the highest concentrations of sulfate precursors suggest that SO_2 presence promotes particle seed formation, increasing particle surface area and enhancing SOA formation. Among the measured iSOA markers, 2-MTs showed the highest concentration, with a diurnal variation that did not follow a clear photochemical pattern. Correlation analysis with environmental factors indicated that relative humidity contributed to the nighttime peak. The P/M ratio was used to analyze the aging process of monoterpenes under different atmospheric conditions. Results indicated that monoterpene SOA was more aged in continental air due to intense photochemical processes and lower temperatures, which favor the partitioning of fresh oxidation products into the condensed phase. Moreover, we correlated AMS-resolved factors with speciated SOA markers to estimate the total mass of biogenic and anthropogenic SOA. The influence of NO_x, SO_2, and atmospheric

oxidation levels on SOA formation was also investigated. Results showed that NO_x had an insignificant impact on SOA formation across all clusters. In coastal air, we found that SO_2 levels could promote BSOA formation, but this effect is not evident in continental air. In continental air, high atmospheric oxidation conditions could enhance the formation of anthropogenic SOA under elevated precursor levels.

Low molecular weight dicarboxylic acids and their oxygenated analogs in atmospheric PM have significant impacts on air quality and climate, due to their high concentrations and hygroscopicity. While numerous studies have focused on oxalic acid, the current understanding of OHDCA is markedly insufficient. Our interest in OHDCA stemmed from the discovery of their high concentrations in the Hong Kong atmosphere based on both offline and in situ measurements. The mass loadings of some individual OHDCA species were in the same order of magnitude as oxalic acid, while the total concentration of OHDCA was even higher (maximum to 3290 ng m^{-3}). Through observational evidence, we unraveled the aqueous photochemical formation of OHDCA and the varying dominant factors between different types of air. The precursors of OHDCA were also explored by examining the relationships with chemical fingerprints. Based on the findings, the high levels of OHDCA in Hong Kong were interpretable, albeit not quantitative. First, there were plenty of anthropogenic and biogenic air pollutants in South China and the site received continental outflows from further inland with even higher anthropogenic emissions. Second, the aging of air pollutants led to an increase in atmospheric oxidative capacity, as indicated by high levels of O_3_corr (61.2 ppbv). Third, the subtropical climate, especially the warm and humid weather, was favorable for OHDCA formation through aqueous photochemical reactions.

Overall, this study provided observational insights into the formation mechanisms of SOA, corroborating and complementing a handful of chamber studies with controllable variables. It also formed cross-validation with other field observational research, such

as a recent radiocarbon-based study of oxalic acid in the same region. The findings of this study will help improve the representation of SOA chemistry in air quality and climate models and reduce modeling uncertainties. They may also apply to other places with similar emissions and meteorological characteristics. We acknowledge the lack of more direct evidence for the formation mechanisms and quantitative evaluation of pathway/precursor contributions to some speciated SOA (e.g., OHDCA). Therefore, more research is needed to figure out the chemical kinetics under atmospherically relevant conditions and to establish the quantitative relationships between formation processes and influencing factors.

Chapter 5 Real-time molecular characterization of air pollutants in a Hong Kong residence: bringing atmospheric chemistry homes

5.1 Introduction

People spend approximately 80%-90% of their time indoors (Klepeis et al., 2001). The premature deaths associated with indoor air pollution continuously increase, especially in developing countries (Smith and Mehta, 2003). Fine particulate matter ($PM_{2.5}$) has been identified as a big threat to human health by causing respiratory and cardiovascular diseases (Li et al., 2003, Pope et al., 1995). Organics account for significant fractions of $PM_{2.5}$ indoors (Rivas et al., 2014) and lead to adverse health outcomes as indicated by epidemiological and toxicological studies (Breitner et al., 2011). Moreover, the toxicities of particulate organics differ among species and are not necessarily mass-dependent (Jin et al., 2019). Molecular information helps to identify the sources and chemical evolution of PM-bound organics (Lyu et al., 2021, Zeng et al., 2020), which eventually enhances the traceability of indoor air toxicity. Therefore, studies on speciated organics provide a fundamental insight on indoor air quality.

Indoor sources including occupant-related activities generate a large number of organics spanning a wide range of volatility, with considerable fractions in PM (Wu et al., 2018, Wei et al., 2016). While studies shed some light on the composition of indoor PM-bound organics, the conventional filter-based and long-time-span sampling failed to recognize the emissions of individual sources from convolved chemical information (Lai et al., 2020, Loupa et al., 2016). Chamber experiments are capable of measuring and even quantifying emissions from individual indoor sources (Manoukian et al., 2013, Lee and Wang, 2006, Lee and Wang, 2004). However, many factors in real indoor

environments, such as ventilation conditions and concentrations of oxidants which may influence the diffusion and chemical aging of air pollutants, are difficult to be reproduced in chambers (Morrison et al., 2019, Vu and Harrison, 2019). In addition, with filter-based measurements or chamber experiments, it is almost impossible to examine the evolution of organics in real indoor environments, due to the low time resolution or incomparable settings. AMS partly overcomes the deficiencies of traditional filter-based method and is increasingly used in analysis of indoor PM-bound organics in recent years (Li et al., 2021, Avery et al., 2019, Johnson et al., 2017). Nevertheless, it measures total and fragmented organics instead of specific molecules, which impedes identification of definite sources and related toxicity.

TAG coupled with mass spectrometry is an emerging technique tailored for in situ analysis of speciated organics in PM, which has been extensively applied in atmospheric chemistry studies (Isaacman et al., 2014, Williams et al., 2006). In brief, it automates the processes of sample collection, transfer and detection and incorporates online derivatization and calibration with internal standards, enabling quantitative analysis of a wide range of both polar and non-polar organics (Lyu et al., 2020). Recently, a member in TAG family has been involved in studies on indoor PM-bound organics (Lunderberg et al., 2020, Kristensen et al., 2019, Lunderberg et al., 2019). The first deployment of a SV-TAG in a California residence revealed continuous emissions of SVOCs from static indoor sources, while the abundances of SVOCs were almost unaffected by the number of occupants (Kristensen et al., 2019). Based on the fast response data measured by SV-TAG, Lunderberg et al. (2019) indicated that indoor air temperature and particle loading were key factors that influenced the gas-particle partitioning of diethylhexyl phthalate indoors. Overall, the TAG technology has been proven robust for studying indoor PM-bound organics.

Hong Kong, one of the most densely populated metropolises in the world, is known for

its small living space per capital. The lifestyle in Hong Kong is a fusion of Eastern and Western ones. Typical examples are the supply of both Chinese and Western foods in many restaurants. With a subtropical climate, Hong Kong is warm and humid throughout the year, despite relatively lower temperature and moisture in cool seasons, leading to widespread and long-duration use of air conditioning systems. Outdoor air pollution resulting from local sources (e.g., vehicle exhausts) and regional transport in cool seasons is also significant (Chen et al., 2020, Yim et al., 2009). Previous studies in Hong Kong investigated the concentrations, emissions, and sources of criteria air pollutants and volatile organic compounds indoors, covering the prevalent housing types and common residential activities (Guo, 2011, Guo et al., 2009, Lee et al., 2002a). A handful of studies have focused on speciated PM-bound organics (Chen et al., 2020, Deng et al., 2016, Lui et al., 2016). However, the reported species were confined to several categories of organics with known health risks, such as PAHs and carbonyls. Moreover, the analysis was limited by the low time resolution of the data associated with long-time-span sampling methods.

In this chapter, we measured total and speciated PM-bound organics for ~1 month in a Hong Kong residence, where prescribed activities were carried out. The application of TAG and AMS significantly improved the resolution of the measurements in time and chemical information (distinguishable at the molecular level), compared to previous studies. With a special focus on PM-bound speciated organics, here we discussed their high level indoors and emissions from prescribed activities. The sources and airborne fate of indoor PM-bound organic matters (OM) were explored. Furthermore, we investigated the indoor evolution of cooking-emitted particles.

5.2 High levels of PM-bound organics indoors

In this study, we define the “disturbed period” as the time intervals during which indoor

activities occurred. Conversely, the "undisturbed period" refers to all other times when no such activities were taking place. The chemical compositions of indoor disturbed, undisturbed period and outdoor NR-PM_1 measured by AMS are shown in Figure 5.1 A. Noticeably, PM_1-OM dominated the compositions of both indoor and outdoor samples, accounting for 91.3 ± 41.4% of NR-PM_1 in the disturbed indoor samples, 65.0 ± 5.8% in the undisturbed indoor samples, and 57.6 ± 4.6% in the outdoor samples. The concentration of indoor PM_1-OM during the disturbed period (57.4 ± 21.8 μg m^{-3}) was also significantly higher than that during the undisturbed period (8.2 ± 0.1 μg m^{-3}) and the outdoor counterpart (10.3 ± 0.7 μg m^{-3}).

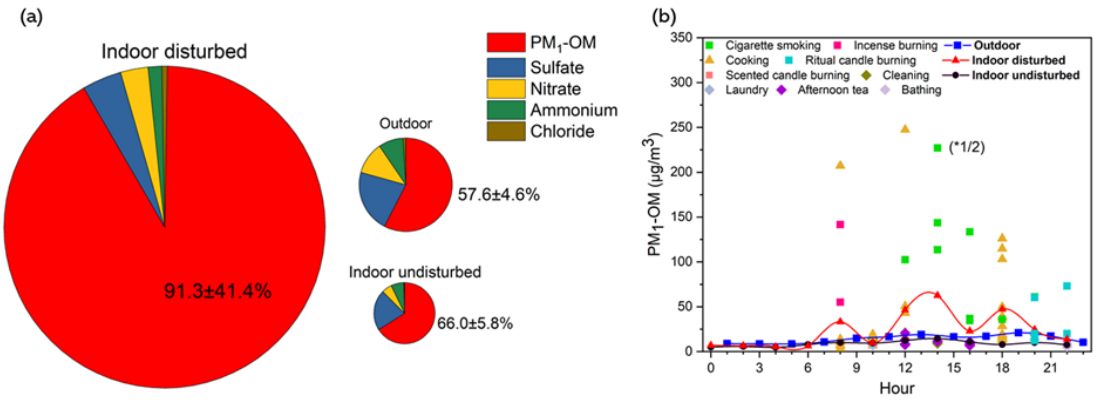

Figure 5. 1. (A) Compositions of indoor (disturbed and undisturbed period, separately) and outdoor NR-PM_1. Pie areas are proportional to PM_1 concentrations. (B) Average diurnal variations of PM_1-OM in different scenarios and PM_1-OM levels in the presence of individual indoor activity. (*1/2) represents that the real concentration is scaled by 1/2.

The lower levels of indoor PM_1-OM during the undisturbed period than the outdoor concentrations are discernable in Figure 5.1 B. The indoor-to-outdoor (I/O) ratio (0.89 ± 0.04) was roughly consistent with previous studies (Farmer et al., 2019; Ho et al., 2004) and was expectable in the cases that the PM_1-OM mainly came from outdoor air

infiltration. On one day when there was no occupant in the apartment, the variations of indoor and outdoor PM_1-OM over time followed the same pattern (Figure 5.2), which was an obvious sign of outdoor air infiltration. However, the OM fraction in PM_1 was lower for the outdoor samples than the indoor undisturbed samples. On one hand, the discrepancy could be due to the more efficient formation of secondary inorganic aerosol (SIA) species, including sulfate, nitrate, and ammonium, in outdoor atmosphere (Talbot et al., 2016, Lunden et al., 2003). The average SIA concentration was 7.6 ± 0.3 μg m^{-3} outdoors and 4.0 ± 0.2 μg m^{-3} for the indoor undisturbed samples. On the other hand, it indicated the indoor PM_1 could not be solely explained by infiltration of outdoor air during the undisturbed period. On activity-intensive days, the OM fraction in PM_1 indoors (61.7 ± 6.8%) was noticeably higher than that in the simultaneous outdoor samples (48.3 ± 6.8%) even during 0:00-7:00 when no activity was performed. Therefore, the possibility of carrying-over and/or re-emission of certain compounds in the apartment during the undisturbed period cannot be ruled out (Kristensen et al., 2019). Besides, the enhanced evaporation of volatile components in PM_1, for example, nitrate, also partially accounted for the higher fraction of OM indoors, which is discussed in Section 5.4.

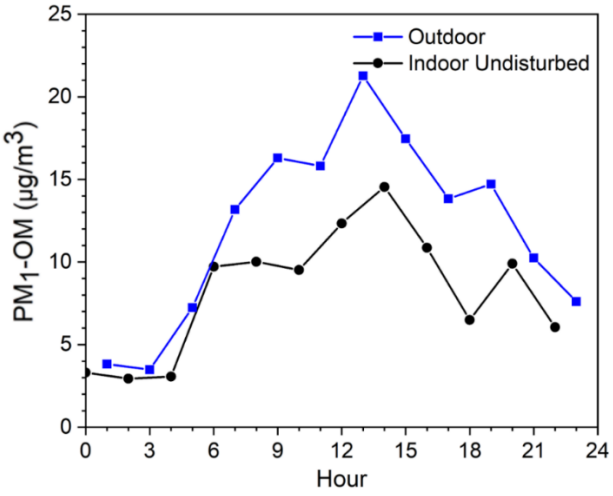

Figure 5. 2. Variations of indoor and outdoor PM_1-OM over time on an undisturbed day

(26 Nov).

The indoor PM_1-OM levels were substantially elevated by some activities (Figure 5.1B). For example, cigarette smoking at 14:00 on 1 Dec. led to the soaring of PM_1-OM up to 454.1 μg m^{-3}. We adopt the metrics of net increment (NIC) to stand for the concentration increase, which was calculated in the same way as that introduced in Lyu et al. (2021). On average, the NIC of PM_1-OM in the samples influenced by cigarette smoking, incense burning, cooking, and ritual candle burning was 115 ± 85.6, 93.0 ± 84.8, 38.0 ± 20.3, and 28.1 ± 20.8 μg m^{-3}, respectively. The variations of NIC for the same activities were mainly attributable to the differences in activity strengths, for example, simple breakfast *vs.* big dinner. It is interesting to note that the concentrations of PM_1-OM in the disturbed scenario decreased significantly at 10:00, 16:00, and 20:00, compared to the much higher concentrations 2 h earlier. Although it seemed to be explained by the dominance of low-emission activities (emission here specifically referred to emissions of PM-bound organics; same for the high-emission activities elsewhere) in these hours, such obvious reductions in the concentrations within 2 h indicated quick removal of PM_1-OM. At the same time, loss of condensed SVOCs could be enhanced with the reduction of PM loadings (Lunderberg et al., 2020), which further accelerated the decline in PM_1-OM concentration.

5.3 Indoor-to-outdoor ratios of PM compositions

Our previous work (Lyu et al., 2021) overviewed the I/O ratios of air pollutants including PM-bound organics collected in this sampling campaign, here the discussion on individual rather than lumped species with more metrics (not only mean values) gives a broader insight into the origins of specific compounds of interest. Moreover, the ratios are calculated for the disturbed and undisturbed periods separately. The species are classified into 3 groups: Group A species with both the median and mean I/O ratios

lower than 1 were of predominantly outdoor origins, Group B species with both the median and mean I/O ratios higher than 1 were of predominantly indoor origins; and Group C species with the median I/O ratio lower than 1 while the mean higher than 1 had mixed origins. Figure 5.3 shows the I/O ratios of speciated organics in $PM_{2.5}$ and NR-PM_1 compositions that are distinct from the majority of species in classification, and the ratios for the majority are presented in Figure 5.4. It was not surprising that most of the primary species were classified as Group B during the disturbed period. We further calculated the I/O ratios of individual PM compositions during specific types of high-emission activities. The ratio was as high as 21.7 for linoleic acid during cooking, 72.5 for a fructose isomer during smoking, 118 for *n*-Heneicosane during incense burning, and 31.7 for *n*-Pentatriacontane during ritual candle burning. Interestingly, some biogenic SOA and OHDCA that are considered to be secondarily formed (Lyu et al., 2020) are also in Group B. This might be attributed to the enhancement of gas-to-particle partitioning, when the indoor PM loadings were significantly increased (Lunderberg et al., 2020). SIA and a majority of SOA were the main compounds in Group A during the disturbed period (Figure 5.3 A). For these reasons, the generally higher oxidative capacity of ambient air is more favorable for the production of these secondary components. During specific activities, Group A also included some primary species. For example, two biomass burning tracers (e.g., levoglucosan and mannosan) presented higher outdoor concentrations during cooking, which was not discovered by examining the overall I/O ratio of saccharides (2.57 ± 2.11). This unexpected pattern for levoglucosan and mannosan was likely associated with the combustion of worship supplies made of paper and bamboo in nearby funeral parlors. According to our observations, the smoke was most intensive in early evening, overlapping the time for making dinner.

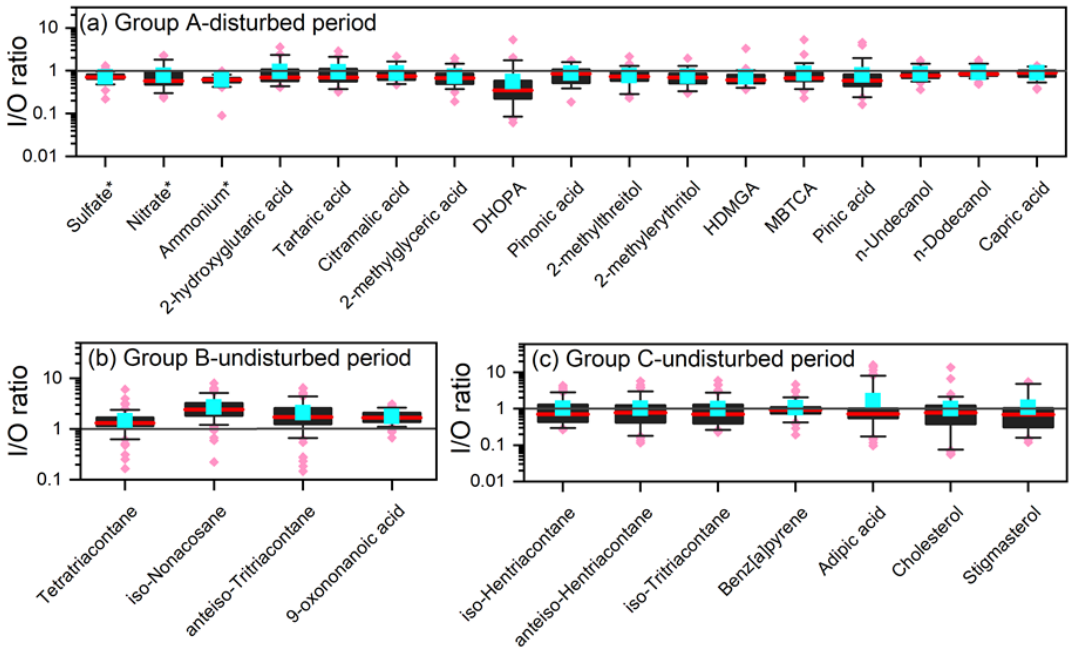

Figure 5. 3. Box and whisker plots of I/O ratios for some speciated organics and NR-PM_1 compositions (marked with asterisk). The top and bottom edges of the box are 75th and 25th percentiles, respectively, and the line in the center of the box represents the median. The tip of the top (bottom) whisker denotes 95th (5th) percentile. Blue squares stand for mean values of I/O ratios, and the pink diamonds are for values beyond the range of 5th-95th percentiles. Group B and Group C species during the disturbed period and Group A species during the undisturbed period (the majority species) are not presented.

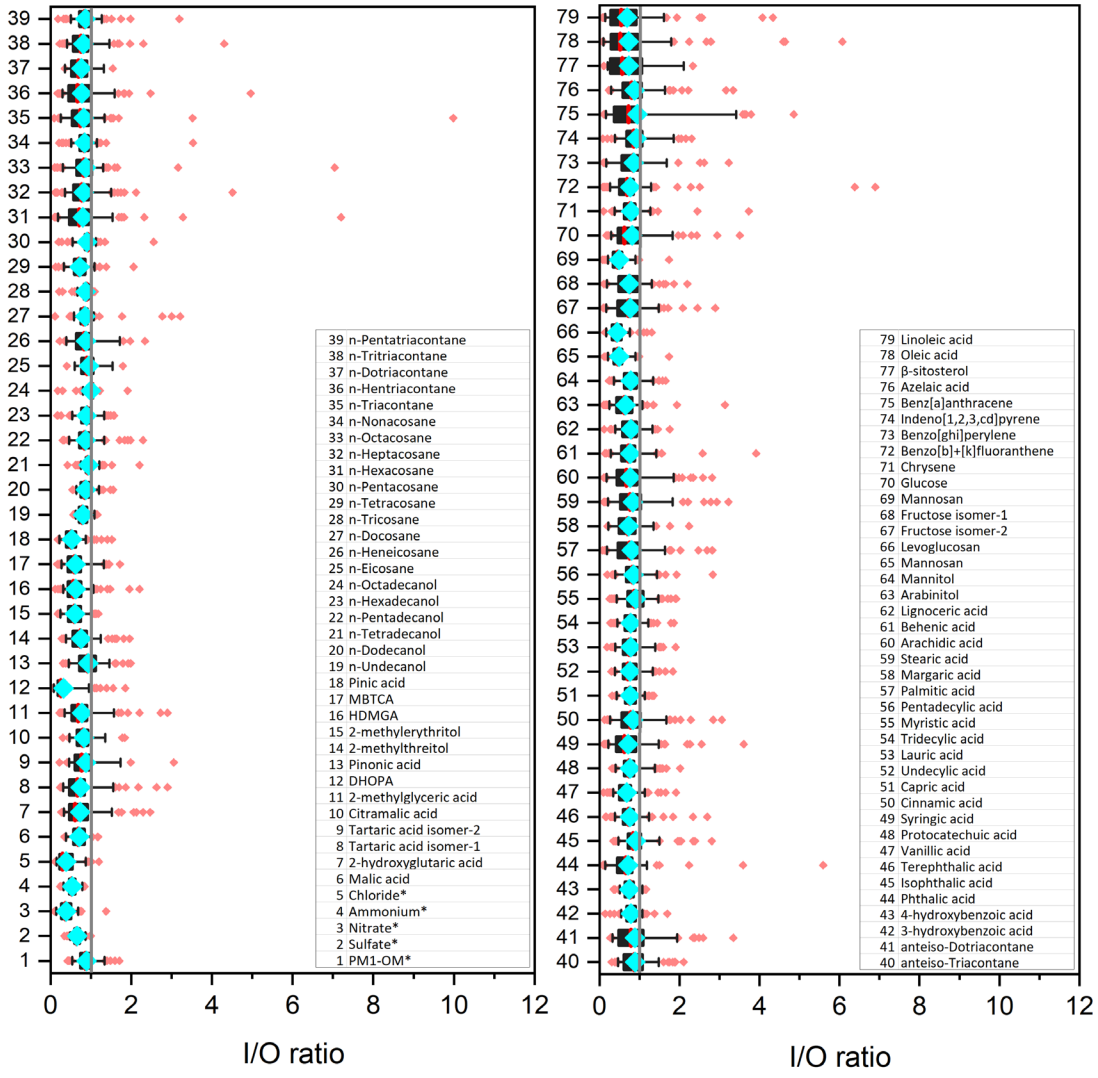

Figure 5. 4. Box and whisker plots of I/O ratios for PM compositions in Group A during the undisturbed period. The far right and far left of the box are 75th and 25th percentiles, respectively, and the line in the center of the box represents the median. The tip of the right (left) whisker denotes 95th (5th) percentile. Blue diamonds stand for mean values of I/O ratios, and the pink diamonds are for values beyond the range of 5th–95th percentiles. Numbers represent PM compositions listed in the insert tables. Species measured by AMS are marked with asterisks.

During the undisturbed period, most (~87%) of the species were in Group A, comprising SIA, many secondary organic aerosol (SOA) species and some POA species,

such as *n*-alkanes, fatty acids, *n*-alcohols, aromatic acids, biomass burning tracers, and PAHs (Figure 5.4). Group B contained tetratriacontane, *iso*-nonacosane, *anteiso*-tritriacontane, and 9-oxononanoic acid (Figure 5.3 B). As shown in Table 5.1, the high-emission activities (especially smoking) could bring the mean I/O ratios for *iso*-nonacosane and *anteiso*-tritriacontane to above 1. The mean and median I/O ratios of both species (tracers of tobacco combustion) were still higher than 1 during the undisturbed period. It was indicated that cigarette smoking particles could remain airborne for a long time (Hussein et al., 2006), which might explain the higher concentrations of the two compounds indoors in absence of activity. We speculate the same effect was applicable for tetratriacontane, which was greatly enhanced in ritual candle burning (I/O ratio: 30.3). It is unknown whether the effect was attributable to carrying-over, re-emission, or both. As an aging product of cooking emissions, 9-oxononanoic acid exhibited consistently higher levels indoors driven by heterogeneous processes, which will be discussed in Section 5.5. Some species were classified into Group C during the undisturbed period, including some branched alkanes, benz[a]pyrene, adipic acid, cholesterol, and β-sitosterol (Figure 5.3 C). It was likely that these compounds were also subject to carrying-over and/or re-emission, but the effects were weaker than those for Group B species excluding 9-oxononanoic acid.

Table 5. 1. Mean and median I/O ratios of PM compositions during the implementation of high-emission activities.

NO.	PM compositions	Cooking		Cigarette Smoking		Incense burning	Ritual candle burning	
		Mean ± 95% C.I.	Median	Mean ± 95% C.I.	Median	Mean/Median	Mean ± 95% C.I.	Median
1	PM_1-OM *	3.16 ± 1.74 $^{B\#}$	1.37	7.95 ± 4.01 ^{B}	7.27	4.35 ^{B}	3.52 ± 2.15 ^{B}	2.00
2	Sulfate *	0.71 ± 0.04 ^{A}	0.71	0.54 ± 0.13 ^{A}	0.63	0.67 ^{A}	0.94 ± 0.16 ^{A}	0.83
3	Nitrate *	0.66 ± 0.16 ^{A}	0.50	1.11 ± 0.43 ^{C}	0.88	1.22 ^{B}	0.82 ± 0.33 ^{A}	0.61
4	Ammonium *	0.62 ± 0.04 ^{A}	0.63	0.48 ± 0.12 ^{A}	0.50	0.64 ^{A}	0.68 ± 0.12 ^{A}	0.64
5	Chloride *	1.35 ± 1.19 ^{C}	0.57	3.13 ± 1.63 ^{B}	3.05	1.44 ^{B}	5.63 ± 3.84 ^{B}	4.12
6	Malic acid	0.71 ± 0.06 ^{A}	0.69	2.09 ± 0.86 ^{B}	1.57	13.5 ^{B}	0.92 ± 0.19 ^{A}	1.07
7	2-hydroxyglutaric acid	0.77 ± 0.13 ^{A}	0.64	1.09 ± 0.43 ^{C}	0.82	2.10 ^{B}	1.38 ± 0.74 ^{C}	0.87
8	Tartaric acid isomer-1	0.87 ± 0.20 ^{A}	0.69	0.73 ± 0.41 ^{A}	0.62	1.74 ^{B}	1.12 ± 0.29 ^{B}	1.04
9	Tartaric acid isomer-2	0.82 ± 0.19 ^{A}	0.71	1.45 ± 0.58 ^{B}	1.24	N.A.†	1.00 ± 0.56 ^{C}	0.92
10	Citramalic acid	0.72 ± 0.09 ^{A}	0.68	1.15 ± 0.46 ^{B}	1.00	N.A.	0.95 ± 0.48 ^{A}	0.84
11	2-methylglyceric acid	0.70 ± 0.10 ^{A}	0.63	0.66 ± 0.19 ^{A}	0.69	N.A.	0.78 ± 0.20 ^{A}	0.74
12	DHOPA	0.37 ± 0.11 ^{A}	0.33	0.42 ± 0.19 ^{A}	0.29	0.81 ^{A}	1.40 ± 1.16 ^{C}	0.76
13	Pinonic acid	0.79 ± 0.16 ^{A}	0.77	1.34 ± 0.79 ^{B}	1.34	N.A.	0.96 ± 0.40 ^{A}	1.07
14	2-methylthreitol	0.82 ± 0.12 ^{A}	0.74	0.40 ± 0.22 ^{A}	0.46	0.28 ^{A}	0.80 ± 0.12 ^{A}	0.85
15	2-methylerythritol	0.74 ± 0.10 ^{A}	0.74	0.58 ± 0.14 ^{A}	0.54	0.98 ^{A}	0.67 ± 0.15 ^{A}	0.64
16	HDMGA	0.73 ± 0.18 ^{A}	0.61	0.54 ± 0.04 ^{A}	0.53	N.A.	0.78 ± 0.14 ^{A}	0.82
17	MBTCA	0.68 ± 0.08 ^{A}	0.65	0.74 ± 0.16 ^{A}	0.74	N.A.	1.67 ± 1.10 ^{B}	1.00

18	Pinic acid	0.52 ± 0.06 [A]	0.53	1.96 ± 1.04 [B]	1.51	N.A.	0.80 ± 0.19 [A]	0.77
19	Undecanol	0.88 ± 0.08 [A]	0.80	0.60 ± 0.07 [A]	0.63	1.02 [B]	0.88 ± 0.15 [A]	0.82
20	Dodecanol	0.91 ± 0.07 [A]	0.86	0.74 ± 0.07 [A]	0.76	1.04 [B]	1.10 ± 0.26 [B]	1.01
21	Tetradecanol	1.51 ± 0.54 [B]	1.07	2.10 ± 0.70 [B]	1.94	1.50 [B]	9.46 ± 7.54 [B]	5.93
22	Pentadecanol	2.19 ± 1.75 [C]	0.97	N.A.	N.A.	0.89 [A]	10.3 ± 9.59 [B]	4.42
23	Hexadecanol	3.62 ± 3.79 [B]	1.12	5.05 ± 2.94 [B]	3.71	N.A.	25.0 ± 14.3 [B]	27.5
24	Octadecanol	1.91 ± 1.17 [B]	1.18	2.06 ± 0.57 [B]	2.00	1.15 [B]	6.99 ± 3.95 [B]	7.63
25	*n*-Eicosane	2.01 ± 0.84 [B]	1.73	5.60 ± 4.99 [B]	6.83	N.A.	20.9 ± 21.7 [B]	9.78
26	*n*-Heneicosane	2.28 ± 0.95 [B]	1.15	1.38 ± 1.05 [C]	0.86	118 [B]	2.82 ± 1.10 [B]	2.47
27	*n*-Docosane	0.98 ± 0.12 [A]	0.91	1.20 ± 0.27 [B]	1.25	1.16 [B]	10.8 ± 7.37 [B]	8.02
28	*n*-Tricosane	1.10 ± 0.17 [C]	0.95	1.90 ± 0.54 [B]	1.79	1.26 [B]	12.4 ± 9.61 [B]	7.59
29	*n*-Tetracosane	1.54 ± 0.49 [B]	1.05	3.47 ± 1.52 [B]	3.02	1.46 [B]	21.4 ± 16.4 [B]	12.5
30	*n*-Pentacosane	1.26 ± 0.20 [B]	1.01	5.35 ± 2.53 [B]	4.80	1.39 [B]	19.1 ± 14.2 [B]	12.0
31	*n*-Hexacosane	2.90 ± 1.51 [B]	1.59	5.48 ± 2.68 [B]	4.28	3.30 [B]	18.5 ± 10.9 [B]	12.9
32	*n*-Heptacosane	1.02 ± 0.21 [C]	0.88	16.0 ± 7.02 [B]	16.5	1.69 [B]	11.4 ± 8.09 [B]	7.07
33	*n*-Octacosane	1.28 ± 0.34 [B]	1.04	9.44 ± 4.06 [B]	8.64	2.54 [B]	17.7 ± 11.4 [B]	12.2
34	*n*-Nonacosane	1.96 ± 0.89 [C]	0.98	14.9 ± 7.01 [B]	14.7	1.72 [B]	10.4 ± 9.18 [B]	4.49
35	*n*-Triacontane	1.19 ± 0.38 [C]	0.94	19.2 ± 8.75 [B]	17.4	2.80 [B]	18.5 ± 14.3 [B]	10.4
36	*n*-Hentriacontane	1.40 ± 0.45 [C]	0.86	24.1 ± 8.70 [B]	25.7	1.52 [B]	9.27 ± 9.01 [B]	3.67
37	*n*-Dotriacontane	4.17 ± 2.16 [B]	2.87	45.8 ± 15.7 [B]	45.5	7.44 [B]	29.7 ± 23.7 [B]	18.0
38	*n*-Tritriacontane	1.02 ± 0.24 [C]	0.81	29.6 ± 11.6 [B]	34.3	1.53 [B]	16.8 ± 18.9 [B]	4.18
39	*n*-Tetratriacontane	1.58 ± 0.53 [B]	1.21	9.43 ± 5.55 [B]	6.93	2.41 [B]	30.3 ± 32.7 [B]	7.75

40	*n*-Pentatriacontane	0.95 ± 0.15 [A]	0.85	6.16 ± 3.82 [B]	3.56	1.53 [B]	31.7 ± 37.7 [B]	2.98
41	3-hydroxybenzoic acid	0.83 ± 0.12 [A]	0.78	13.0 ± 7.60 [B]	9.01	2.93 [B]	1.06 ± 0.32 [B]	1.06
42	4-hydroxybenzoic acid	0.78 ± 0.09 [A]	0.75	3.18 ± 1.20 [B]	3.18	7.89 [B]	1.27 ± 0.31 [B]	1.30
43	Phthalic acid	0.75 ± 0.24 [A]	0.60	1.18 ± 0.43 [C]	0.94	N.A.	2.13 ± 1.22 [B]	1.55
44	Isophthalic acid	2.71 ± 1.62 [B]	1.17	0.87 ± 0.17 [A]	0.83	0.85 [A]	1.07 ± 0.14 [B]	1.03
45	Terephthalic acid	0.93 ± 0.10 [A]	0.89	0.93 ± 0.51 [A]	0.74	3.22 [B]	1.29 ± 0.63 [C]	0.98
46	Vanillic acid	0.79 ± 0.14 [A]	0.71	3.83 ± 1.51 [B]	4.31	3.89 [B]	1.65 ± 0.56 [B]	1.57
47	Protocatechuic acid	0.86 ± 0.11 [A]	0.79	3.22 ± 0.68 [B]	3.14	2.52 [B]	0.90 ± 0.14 [A]	0.93
48	Sringic acid	0.96 ± 0.26 [A]	0.68	6.46 ± 11.1 [C]	0.72	4.71 [B]	1.06 ± 0.30 [C]	0.95
49	Cinnamic acid	5.01 ± 3.99 [B]	1.07	23.6 ± 19.3 [B]	14.2	11.0 [B]	1.05 ± 0.22 [B]	1.00
50	Capric acid	0.90 ± 0.06 [A]	0.90	0.81 ± 0.19 [A]	0.88	0.90 [A]	0.97 ± 0.17 [A]	0.98
51	Undecylic acid	0.90 ± 0.11 [A]	0.82	1.26 ± 0.39 [B]	1.02	1.20 [B]	1.51 ± 0.75 [B]	1.14
52	Lauric acid	1.06 ± 0.24 [C]	0.85	1.64 ± 0.41 [B]	1.85	2.18 [B]	2.31 ± 1.47 [B]	1.58
53	Tridecylic acid	1.07 ± 0.33 [C]	0.83	3.27 ± 1.38 [B]	3.31	0.77 [A]	3.24 ± 2.47 [B]	1.48
54	Myristic acid	2.73 ± 2.53 [B]	1.10	4.91 ± 2.93 [B]	3.36	2.27 [B]	7.60 ± 5.17 [B]	4.48
55	Pentadecylic acid	4.09 ± 4.94 [B]	1.05	7.90 ± 6.02 [B]	4.85	2.73 [B]	12.9 ± 9.84 [B]	7.81
56	Palmitic acid	2.75 ± 1.39 [B]	1.30	5.55 ± 5.47 [B]	3.07	1.15 [B]	3.48 ± 2.50 [B]	2.47
57	Margaric acid	4.66 ± 4.89 [B]	1.00	11.3 ± 12.1 [B]	5.94	2.32 [B]	6.00 ± 5.78 [B]	3.26
58	Stearic acid	2.83 ± 1.84 [B]	1.14	5.12 ± 4.68 [B]	2.93	0.64 [A]	3.06 ± 2.08 [B]	2.11
59	Arachidic acid	8.73 ± 8.76 [B]	1.88	16.1 ± 14.4 [B]	7.90	3.59 [B]	3.25 ± 2.83 [B]	2.11
60	Behenic acid	4.66 ± 3.02 [B]	1.76	9.82 ± 5.43 [B]	7.95	3.51 [B]	2.42 ± 1.65 [B]	1.42
61	Lignoceric acid	4.75 ± 3.79 [B]	1.63	10.8 ± 7.57 [B]	7.66	6.61 [B]	4.70 ± 5.17 [C]	0.90

62	Arabinitol	6.67 ± 4.98 [C]	0.76	8.96 ± 11.2 [B]	2.67	10.1 [B]	1.62 ± 0.58 [B]	1.66
63	Mannitol	3.52 ± 2.37 [C]	0.79	42.1 ± 74.9 [B]	3.48	5.15 [B]	1.28 ± 0.31 [B]	1.26
64	Mannosan	0.65 ± 0.14 [A]	0.58	2.31 ± 0.95 [B]	2.08	12.0 [B]	0.82 ± 0.21 [A]	0.79
65	Levoglucosan	0.58 ± 0.10 [A]	0.52	2.46 ± 1.53 [B]	1.45	3.87 [B]	1.03 ± 0.42 [C]	0.92
66	Fructose isomer-1	3.36 ± 1.78 [B]	1.02	72.5 ± 91.7 [B]	19.0	2.45 [B]	1.52 ± 0.58 [B]	1.57
67	Fructose isomer-2	4.30 ± 2.78 [B]	1.04	42.0 ± 49.6 [B]	18.3	3.23 [B]	1.59 ± 0.59 [B]	1.65
68	Mannosan	0.65 ± 0.14 [A]	0.58	2.31 ± 0.95 [B]	2.08	12.0 [B]	0.82 ± 0.21 [A]	0.79
69	Glucose	1.15 ± 0.32 [C]	0.86	32.7 ± 15.7 [B]	29.6	1.01 [B]	0.83 ± 0.49 [A]	0.71
70	Chrysene	0.93 ± 0.21 [A]	0.78	1.83 ± 0.72 [B]	1.74	2.54 [B]	1.66 ± 0.62 [B]	1.60
71	Benzo[k,b]fluoranthene	0.79 ± 0.14 [A]	0.71	3.05 ± 1.20 [B]	2.75	4.67 [B]	0.73 ± 0.40 [A]	0.49
72	Benzo[ghi]perylene	0.96 ± 0.22 [A]	0.87	2.20 ± 0.52 [B]	2.29	14.7 [B]	0.84 ± 0.32 [A]	0.78
73	Indeno[1,2,3,cd]pyrene	5.35 ± 4.86 [B]	1.55	6.10 ± 5.76 [B]	2.12	12.4 [B]	0.88 ± 0.27 [A]	0.85
74	Benz[a]anthracene	0.85 ± 0.28 [A]	0.67	1.84 ± 0.59 [B]	1.48	16.0 [B]	4.26 ± 2.63 [B]	3.38
75	Benz[a]pyrene	0.99 ± 0.24 [A]	0.87	1.01 ± 0.51 [B]	1.22	N.A.	1.44 ± 1.39 [C]	0.87
76	Adipic acid	0.95 ± 0.22 [A]	0.86	2.09 ± 2.24 [C]	0.96	2.27 [B]	1.70 ± 0.69 [B]	1.56
77	Azelaic acid	2.09 ± 1.60 [C]	0.97	1.78 ± 0.55 [B]	1.72	4.12 [B]	2.45 ± 0.94 [B]	2.25
78	Oleic acid	6.80 ± 5.83 [B]	1.69	7.08 ± 10.7 [B]	1.65	1.28 [B]	2.04 ± 1.46 [B]	1.53
79	Linoleic acid	21.7 ± 23.2 [B]	1.31	21.3 ± 28.7 [B]	7.18	2.24 [B]	1.49 ± 1.14 [B]	1.21
80	anteiso-Triacontane	1.20 ± 0.46 [C]	0.79	36.3 ±14.8 [B]	38.6	1.01 [B]	3.35 ± 3.04 [B]	1.18
81	anteiso-Dotriacontane	1.38 ± 0.59 [C]	0.76	35.6 ± 15.6 [B]	31.3	1.53 [B]	2.94 ± 2.74 [B]	1.14
82	iso-Nonacosane	3.70 ± 1.09 [B]	2.80	39.0 ± 16.8 [B]	42.2	5.52 [B]	12.1 ± 8.88 [B]	6.38
83	anteiso-Tritriacontane	4.14 ± 3.67 [B]	1.49	27.7 ± 13.0 [B]	28.5	1.58 [B]	19.9 ± 24.1 [B]	2.88

84	iso-Hentriacontane	1.07 ± 0.43 [C]	0.65	36.2 ± 15.8 [B]	35.3	0.84 [A]	3.49 ± 3.12 [B]	1.43
85	anteiso-Hentriacontane	2.98 ± 3.01 [B]	1.15	45.6 ± 35.0 [B]	33.2	2.28 [B]	10.2 ± 10.6 [B]	3.26
86	iso-Tritriacontane	0.95 ± 0.33 [A]	0.76	41.1 ± 18.6 [B]	43.9	1.48 [B]	5.58 ± 5.85 [B]	1.27
87	Cholesterol	16.1 ± 14.3 [B]	2.39	12.1 ± 9.70 [B]	6.38	1.38 [B]	2.59 ± 2.25 [B]	1.32
88	Stigmasterol	2.51 ± 1.66 [B]	1.05	54.3 ± 22.4 [B]	62.3	N.A.	2.15 ± 2.23 [B]	1.28
89	β-sitosterol	9.95 ± 6.86 [B]	2.00	26.2 ± 16.0 [B]	17.9	N.A.	3.71 ± 3.74 [B]	3.24
90	9-oxononanoic acid	1.44 ± 0.14 [B]	1.41	1.65 ± 0.31 [B]	1.53	1.47 [B]	1.39 ± 0.22 [B]	1.33

* PM_1 components measured by AMS (the others are speciated organics in $PM_{2.5}$ measured by TAG). # A, B and C are groups. † N.A.: not available.
DHOPA: 2,3-dihydroxy-4-oxopentanoic acid; HDMGA: 3-hydroxy-4-4 dimethylglutaric acid; MBTCA: 3-methyl-1,2,3-butanetricarboxylic acid.

Table 5. 2. NICs and ERs (values in the parentheses) for $PM_{2.5}$-bound speciated organics and NR-PM_1 compositions during individual indoor activities. Unit of NIC is ng/m^3 unless otherwise specified.

Compounds or NR-PM_1 components	**Indoor activities**			
	Cooking	Cigarette Smoking	Incense burning	Ritual candle burning
2-methylglyceric acid	0.03±0.02 (1.37±0.20)	0.02±0.06 (1.11±0.41)	0.08±0.21 (1.85±2.33)	-0.004±0.04 (0.96±0.33)
DHOPA	/	0.01±0.002 (1.02±0.04)	/	0.0001±0.0002 (1.00±0.004)
Pinonic acid	-0.40±0.17 (0.55±0.19)	-0.80±0.45 (0.34±0.38)	/	0.55±0.70 (1.76±0.96)
2-methylthreitol	0.006±0.01 (1.07±0.12)	-0.04±0.02 (0.66±0.19)	/	-0.01±0.03 (0.89±0.24)

2-methylerythritol	0.05±0.03 (1.29±0.18)	0.04±0.05 (1.19±0.22)	0.11±0.35 (1.53±1.71)	-0.02±0.06 (0.89±0.28)
HDMGA	0.002±0.003 (1.03±0.06)	/	/	/
MBTCA	0.15±0.07 (2.47±0.72)	0.12±0.16 (1.42±0.57)	0.26±0.60 (3.40±5.57)	0.02±0.08 (1.16±0.59)
Pinic acid	0.21±0.09 (1.60±0.27)	2.31±1.20 (5.95±2.55)	/	0.27±0.32 (1.55±0.65)
Malic acid	0.33±0.26 (1.16±0.13)	6.50±1.81 (3.75±0.77)	33.52±15.65 (16.30±7.14)	0.82±1.04 (1.38±0.48)
2-hydroxyglutaric acid	0.12±0.08 (1.62±0.39)	0.64±0.25 (3.59±1.00)	0.53±1.10 (3.28±4.74)	0.27±0.34 (2.22±1.55)
Citramalic acid	0.05±0.02 (1.75±0.29)	0.10±0.09 (1.95±0.85)	0.23±0.42 (3.73±4.91)	0.08±0.12 (1.86±1.30)
Tartaric acid isomer 1	0.12±0.12 (1.13±0.13)	1.23±0.63 (2.24±0.64)	0.71±1.67 (1.68±1.58)	0.10±0.47 (1.09±0.43)
Tartaric acid isomer 2	0.32±0.23 (1.34±0.24)	2.01±1.23 (2.91±1.17)	1.42±3.05 (2.34±2.88)	-0.14±0.20 (0.89±0.17)
n-Eicosane	0.04±0.02 (1.68±0.42)	0.09±0.14 (2.13±1.80)	0.01±0.02 (1.15±0.30)	1.68±1.60 (25.68±23.48)
n-Heneicosane	0.26±0.12 (5.50±2.10)	0.06±0.04 (1.92±0.63)	3.55±6.80 (60.20±113.34)	0.20±0.09 (4.28±1.51)
n-Docosane	0.04±0.04 (1.14±0.14)	0.26±0.08 (2.05±0.33)	0.23±0.19 (2.01±0.83)	5.74±4.29 (23.16±16.57)
n-Tricosane	0.25±0.10 (1.61±0.24)	0.80±0.43 (2.65±0.88)	0.46±0.48 (2.09±1.15)	10.93±9.06 (25.21±20.08)
n-Tetracosane	0.42±0.17 (4.00±1.19)	1.14±0.59 (6.65±2.91)	0.86±1.11 (6.89±7.61)	12.80±11.42 (77.00±67.82)
n-Pentacosane	0.26±0.09 (1.81±0.29)	2.23±1.35 (6.98±3.61)	1.34±2.06 (5.08±6.26)	15.66±14.51 (46.08±41.76)
n-Hexacosane	1.19±0.49 (9.97±3.63)	3.31±1.89 (15.15±8.05)	3.54±5.59 (26.79±40.74)	15.94±15.25 (94.59±89.54)

n-Heptacosane	0.39±0.15 (2.20±0.44)	16.32±8.53 (34.13±17.30)	2.77±3.99 (9.64±12.47)	20.42±20.73 (45.71±45.39)
n-Octacosane	0.21±0.08 (2.25±0.54)	3.85±2.22 (19.43±10.62)	2.09±2.93 (16.19±21.26)	17.57±18.93 (95.94±102.24)
n-Nonacosane	2.26±1.56 (3.83±1.94)	29.39±16.55 (29.74±16.18)	3.87±4.63 (5.82±5.76)	32.79±36.04 (36.44±38.96)
n-Triacontane	0.15±0.08 (3.07±1.01)	6.98±4.39 (62.89±38.87)	1.65±2.14 (24.07±29.97)	20.33±22.97 (162.51±182.45)
n-Hentriacontane	1.13±0.65 (5.41±2.53)	47.80±22.50 (112.61±52.53)	2.32±1.97 (10.70±8.27)	27.99±31.26 (58.15±63.83)
n-Dotriacontane	0.09±0.07 (3.33±1.86)	5.55±3.57 (139.86±89.33)	0.73±0.87 (19.34±21.63)	9.95±11.57 (180.59±208.87)
n-Tritriacontane	0.20±0.12 (2.37±0.85)	23.45±13.50 (121.27±69.26)	0.97±0.90 (8.00±6.47)	23.02±27.03 (106.79±124.24)
n-Tetratriacontane	0.04±0.06 (1.44±0.68)	1.18±0.89 (9.89±6.70)	0.58±0.64 (8.23±8.11)	20.73±24.85 (226.31±270.12)
n-Pentatriacontane	0.02±0.06 (1.12±0.34)	1.58±1.36 (9.95±7.71)	0.86±0.53 (6.67±3.48)	22.12±27.11 (141.51±172.29)
Chrysene	0.004±0.005 (1.17±0.19)	0.05±0.05 (2.79±1.86)	0.13±0.14 (7.35±7.02)	0.07±0.02 (3.73±0.90)
Benzo[k,b]fluoranthene	0.0007±0.0006 (1.15±0.1.9)	0.04±0.02 (7.08±3.79)	0.14±0.21 (33.36±48.74)	0.002±0.004 (1.48±0.88)
Benzo[g,h,i]perylene	0.006±0.006 (1.59±0.57)	0.06±0.03 (5.61±2.55)	0.11±0.18 (14.81±21.92)	0.001±0.004 (1.18±0.48)
Indeno[1,2,3,cd] pyrene	0.08±0.07 (3.76±2.56)	0.11±0.07 (5.61±2.94)	0.37±0.64 (17.89±29.48)	-0.003±0.009 (0.84±0.51)

Benzo[a]anthracene	0.0002±0.0007 (1.06±0.25)	0.01±0.005 (4.26±1.67)	0.02±0.01 (8.26±5.17)	0.008±0.004 (4.80±2.00)
Benz[a]pyrene	-0.001±0.0008 (0.82±0.14)	0.006±0.003 (1.14±0.71)	/	-0.002±0.002 (0.66±0.42)
3-hydroxybenzoic acid	0.14±0.04 (1.95±0.27)	6.39±4.13 (28.68±17.88)	1.98±2.21 (13.57±13.98)	0.23±0.09 (2.09±0.41)
4-hydroxybenzoic acid	0.19±0.07 (2.03±0.37)	1.68±1.03 (6.73±3.50)	5.71±4.24 (30.58±21.98)	0.33±0.11 (2.33±0.46)
Phthalic acid	1.00±0.47 (1.97±0.46)	3.56±2.72 (3.52±1.92)	0.72±2.68 (1.68±2.55)	0.75±1.30 (1.67±1.17)
Isophthalic acid	2.69±1.96 (4.78±2.76)	-0.13±0.21 (0.86±0.22)	0.37±0.42 (1.52±0.56)	0.69±0.67 (1.58±0.57)
Terephthalic acid	1.31±0.86 (1.40±0.25)	0.93±3.45 (1.23±0.87)	5.69±11.33 (2.60±3.19)	1.22±1.87 (1.30±0.45)
Vanillic acid	8.22±3.50 (2.42±0.59)	46.92±22.16 (6.53±2.61)	600.49±650.39 (108.10±116.00)	18.78±9.67 (4.16±1.62)
Protocatechuic acid	1.79±0.54 (2.66±0.50)	10.01±3.44 (5.51±1.55)	6.93±0.19 (8.11±0.20)	1.47±1.02 (1.80±0.55)
Syringic acid	2.06±1.27 (1.73±0.43)	7.84±15.34 (3.44±4.76)	184.98±22.67 (79.93±9.68)	2.05±1.47 (2.09±0.78)
Palmitic acid	24.09±9.94 (18.71±7.19)	23.44±16.38 (7.48±4.53)	4.92±1.43 (7.12±1.78)	16.09±5.19 (9.07±2.61)
Stearic acid	6.24±3.23 (11.66±5.46)	6.46±4.70 (6.13±3.73)	2.36±2.89 (9.28±10.14)	4.07±1.76 (6.68±2.46)
Oleic acid	115.77±61.27 (37.67±19.21)	21.53±13.79 (4.49±2.24)	32.71±34.30 (44.86±46.00)	13.76±4.76 (9.10±2.81)
Cholesterol	24.53±18.03 (96.84±70.25)	11.54±5.68 (24.87±11.76)	0.75±1.73 (4.55±8.17)	0.97±0.28 (3.99±0.86)
Azelaic acid	4.53±1.93 (7.44±2.70)	3.68±2.56 (3.24±1.37)	4.00±2.72 (7.35±4.32)	2.49±0.76 (4.24±0.98)

Adipic acid	0.76±0.40 (1.85±0.42)	1.04±0.63 (1.90±0.55)	0.51±1.03 (1.68±1.38)	1.06±1.07 (1.80±0.81)
Levoglucosan	2.48±1.91 (1.47±0.32)	35.65±29.10 (7.08±4.96)	55.37±1.49 (9.79±0.24)	8.81±5.15 (2.74±1.02)
Arabinitol	113.49±92.96 (51.04±40.98)	40.02±45.10 (16.72±17.72)	24.38±10.55 (12.26±4.87)	8.35±4.24 (3.98±1.52)
Fructose isomer-1	43.32±23.25 (17.65±8.85)	768.27±1057.75 (206.32±282.67)	6.75±2.41 (5.43±1.58)	9.51±5.29 (5.81±2.68)
Fructose isomer-2	48.12±25.35 (19.06±9.42)	456.57±511.05 (118.71±131.75)	7.50±3.60 (6.12±2.46)	12.21±10.67 (6.25±2.83)
Mannitol	14.76±12.07 (15.50±11.83)	55.58±92.36 (38.19±61.80)	10.07±11.54 (10.76±11.19)	2.27±1.15 (2.65±0.83)
Mannosan	0.22±0.13 (1.98±0.56)	0.96±0.52 (4.66±1.99)	15.58±2.79 (63.71±11.23)	0.34±0.38 (2.16±1.30)
PM_1-OM # ($\mu g/m^3$)	38.00±20.27 (6.79±3.09)	114.65±85.60 (13.31±9.17)	92.99±84.75 (18.40±15.86)	28.12±20.82 (6.00±3.70)
Sulfate # ($\mu g/m^3$)	0.15±0.23 (1.06±0.09)	-0.48±0.75 (0.81±0.30)	-1.42±2.42 (0.91±1.12)	0.56±0.72 (1.24±0.30)
Nitrate # ($\mu g/m^3$)	0.92±0.43 (2.85±0.86)	2.54±1.68 (4.51±2.32)	3.21±2.13 (8.05±4.68)	0.56±0.21 (1.99±0.38)
Chloride # ($\mu g/m^3$)	0.15±0.14 (4.70±3.54)	0.54±0.38 (14.49±9.41)	0.59±0.39 (17.12±10.80)	0.87±0.72 (20.78±16.52)
Ammonium # ($\mu g/m^3$)	0.17±0.08 (1.23±0.11)	-0.01±0.18 (0.99±0.22)	0.21±0.60 (1.32±0.92)	0.07±0.18 (1.09±0.24)
Capric acid *	(1.83±0.25)	(0.75±0.09)	(2.21±2.57)	(1.32±0.26)
Undecylic acid *	(1.98±0.27)	(1.46±0.26)	(4.63±4.94)	(2.46±0.84)
Lauric acid *	(3.48±0.77)	(3.01±0.65)	(5.86±3.30)	(5.14±2.92)
Tridecylic acid *	(3.85±1.04)	(6.95±3.36)	(6.10±7.07)	(7.43±5.57)

Myristic acid *	(8.68±5.57)	(7.62±3.09)	(5.94±4.01)	(18.94±14.51)
Pentadecylic acid *	(13.16±11.29)	(14.06±7.83)	(15.16±18.31)	(36.88±30.14)
Margaric acid *	(14.03±10.63)	(19.01±13.74)	(24.22±32.59)	(13.59±11.57)
Arachidic acid *	(58.14±40.49)	(41.30±32.72)	(19.68±27.02)	(7.63±5.81)
Behenic acid *	(26.58±21.87)	(21.34±14.98)	(12.85±16.17)	(4.43±2.05)
Lignoceric acid *	(12.89±11.03)	(19.53±18.46)	(22.25±34.41)	(4.90±4.95)
Undecanol *	(1.28±0.17)	(0.77±0.17)	(1.24±0.89)	(1.24±0.30)
Dodecanol *	(1.38±0.27)	(0.87±0.24)	(2.52±3.07)	(1.60±0.56)
Tetradecanol *	(2.91±0.96)	(2.37±0.63)	(6.22±2.46)	(21.50±20.43)
Pentadecanol *	(5.50±4.88)	/	/	(30.29±31.76)
Hexadecanol *	(11.27±12.82)	(6.50±2.59)	/	(85.37±64.28)
Octadecanol *	(2.09±1.34)	(1.96±0.50)	(1.54±0.86)	(10.65±4.87)
iso-Nonacosane *	(2.11±0.53)	(47.42±26.44)	(6.21±2.96)	(18.45±16.21)
anteiso-Triacontane *	(2.02±0.48)	(112.47±57.34)	(4.70±4.25)	(10.00±9.70)
iso-Hentriacontane *	(3.64±1.29)	(172.26±82.73)	(6.08±0.84)	(15.51±15.01)
anteiso-Hentriacontane *	(4.48±2.40)	(111.76±56.95)	(17.68±18.48)	(49.42±54.63)

anteiso-Dotriacontane *	(3.44±1.31)	(142.66±62.25)	(9.52±5.96)	(9.44±8.73)
iso-Tritriacontane *	(3.04±1.01)	(195.05±115.33)	(8.99±2.33)	(23.63±26.33)
anteiso-Tritriacontane *	(2.09±0.87)	(46.09±27.77)	(4.16±0.21)	(39.28±45.49)
Stigmasterol *	(27.05±13.69)	(269.43±125.05)	(105.44±33.87)	(2.87±1.79)
β-sitosterol *	(51.00±22.75)	(113.60±58.24)	(121.59±86.78)	(6.60±3.67)
Linoleic acid *	(116.22±79.73)	(31.70±23.75)	(90.05±119.33)	(6.08±4.91)
9-oxononanoic acid *	(1.39±0.35)	(1.09±0.32)	(0.49±0.13)	(0.56±0.15)
Cinnamic acid *	(32.11±32.10)	(48.78±41.50)	(11.12±2.05)	(2.08±0.50)
Mannose *	(4.96±1.16)	(93.52±102.01)	(14.31±14.18)	(2.24±0.81)
Glucose *	(3.68±0.93)	(119.30±91.19)	/	(1.75±0.98)

Components of NR-PM_1. Others are speciated organics detected in $PM_{2.5}$. * NICs are not computable for the unquantified species. / Peaks are not identifiable from respective TAG chromatograms. DHOPA: 2,3-dihydroxy-4-oxopentanoic acid; HDMGA: 3-hydroxy-4-4 dimethylglutaric acid; MBTCA: 3-methyl-1,2,3-butanetricarboxylic acid.

5.4 Emission characteristics and profiles

To further understand the emissions of speciated PM-bound organics, we calculated the NICs and enhancement ratios (ERs) for the organic species in $PM_{2.5}$ during individual indoor activities, as summarized in Table 5.2. The ERs were calculated as the ratios of average concentrations (or IS-scaled abundances for unquantified species) in presence of activity to those in absence of activity at the same time slots. The total NIC of quantified speciated organics followed the same order as NIC of PM_1-OM, that is, cigarette smoking (1776 ng m^{-3}) > incense burning (1131 ng m^{-3}) > cooking (463 ng m^{-3}) > ritual candle burning (396 ng m^{-3}). Marginal increases were observed for the concentrations of PM-bound organics during scented candle burning, for which the NICs were hardly computable. The other activities did not lead to significant changes in the concentrations (or IS-scaled abundances) of the speciated organics. Therefore, we only obtained the emission profiles of speciated organics for the high-emission activities, which are expressed as the fractions of compound-specific NICs in total NIC in Figure 5.5. The acquisition of the emission profiles was based on the assumption that all the organic species underwent the same rates of physical and chemical decay within <1 h after they were emitted.

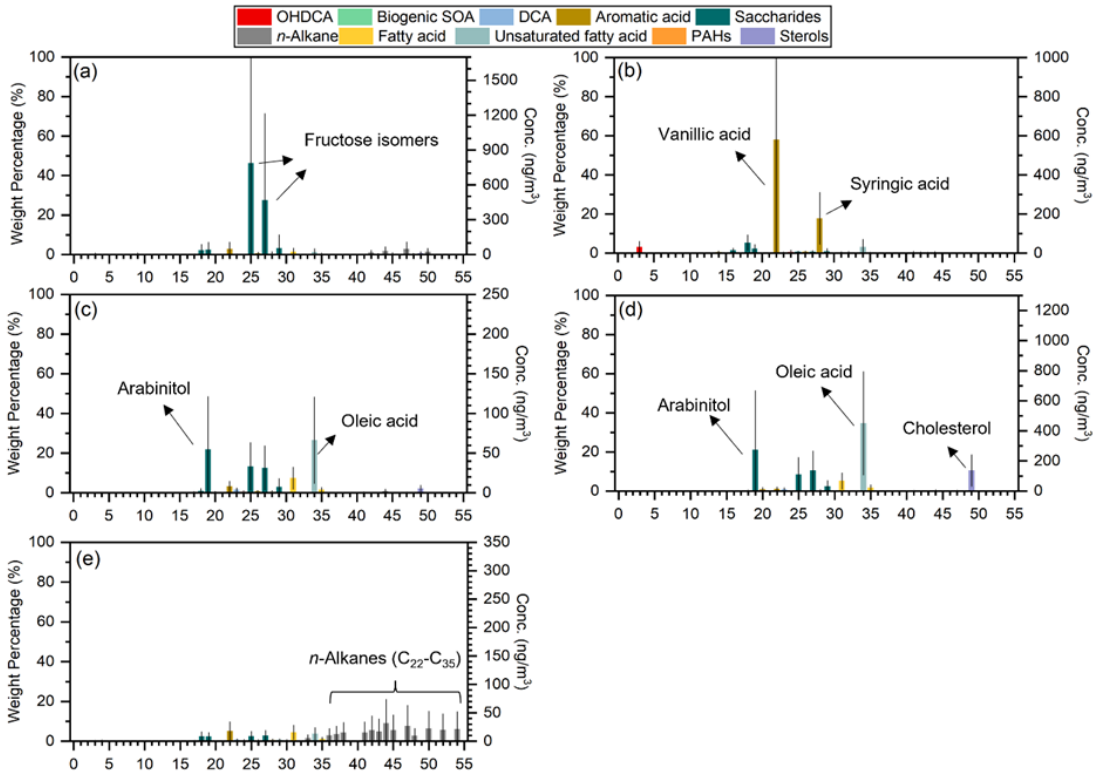

Figure 5. 5. Emission profiles of PM-bound organics for cigarette smoking (A), incense burning (B), cooking-1 (C), cooking-2 (D), and ritual candle burning (E). Error bars represent 95% confidence intervals. The compounds are sorted by chromatographic retention time in ascending order. Names of featured compounds are labeled.

Cigarette smoking was characterized by high emissions of fructose isomers. It was reported that saccharides, including fructose, were commonly emitted from burning of plant materials or fragments (Jansen et al., 2014, Pacini, 2000). The concentrations of odd *n*-alkanes in the carbon range of C_{27}-C_{33}, vanillic acid, levoglucosan, arabinitol, and mannitol were also enhanced during smoking. *Iso-/anteiso*-alkanes are usually regarded as tracers of cigarette burning because of their widespread presence in tobacco leaf waxes (Kavouras et al., 1998). In this study, they were identified from the TAG chromatograms but were not quantified due to the lack of standards. Indeed, the IS-scaled abundances of the C_{27}-C_{33} *iso-/anteiso*-alkanes were remarkably enhanced

during smoking, with the ERs of 46-195 (Table 5.2). The other unquantified organics with high ERs included stigmasterol, glucose, β-sitosterol, and mannose, some of which have been introduced in Lyu et al. (2021). Interestingly, a well-shaped peak of vitamin E was identified from the TAG chromatograms disturbed by smoking, which was not found during the undisturbed period, and thus, the ER was not computable. It is unclear whether the vitamin E was an additive specific to the cigarette used in this study or ubiquitously present in cigarettes.

With the application of AMS, previous studies (Ji et al., 2010, Li et al., 2012) detected the ion fragments of hydrocarbons, PAHs, and lignin-related compounds emitted from incense burning. However, the emissions of speciated organics were inadequately characterized, though a handful of studies (e.g., Lui et al. (2016)) focused on the species of health relevance, such as carbonyls, PAHs, and oxygenated PAHs. Here, we found that vanillic acid and syringic acid, two typical markers of lignin pyrolysis (Hyder and Jönsson, 2012, Simoneit et al., 1993), were the most distinguishable species in incense burning emissions, accounting for 58.1% and 17.9% of the total NIC, respectively. In spite of the lower NICs, levoglucosan, arabinitol, and oleic acid also experienced significant rise in concentrations during incense burning. Besides, β-sitosterol, stigmasterol, and linoleic acid, which were not quantified, had ER of 122, 105, and 90, respectively. The ERs were of the same magnitude as that for vanillic acid (108), indicating strong emissions of both plant sterols and linoleic acid (abundant in many plants, e.g., safflower, sunflower, and corn). It is noteworthy that incense burning also brought about the highest NICs and ERs for PAHs among all the activities (Table 5.2), indicating potential impacts of this ritual activity on health, which was demonstrated before (Zhou et al., 2015a).

Chinese cooking involves various ingredients and methods. As a result, cooking emissions contain a wide range of PM-bound organics, such as saturated and

unsaturated fatty acids, sterols, saccharides, and carbonyls (Robinson et al., 2006, Schauer et al., 2002, Zhao et al., 2007), and the emission profiles are not necessarily consistent. Among the 31 cooking activities carried out in this campaign, it was realistic to separate two types of emission profiles (Figure 5.5 C, D). Oleic acid, palmitic acid, arabinitol, and fructose isomers were the typical tracers in both profiles. The difference was that cholesterol constituted a considerable fraction (10.5%) of the total NIC of quantified organics in one profile (Figure 5.5 D), while it was almost negligible in the other one (Figure 5.5 C). The former with higher fractions of cholesterol represented emissions of PM-bound organics from cooking fishes and/or eggs, when elevated NICs were observed for cholesterol. In addition, some unquantified species were identified with high ERs during cooking, such as linoleic acid, arachidic acid, and β-sitosterol (Table 5.2). It is noteworthy that the IS-scaled abundances of linoleic acid were greatly enhanced during pan frying and deep frying, while frying vegetables caused slight enhancements of cinnamic acid. The representative species identified here were broadly in line with those reported in literature (Abbatt and Wang, 2020, Abdullahi et al., 2013, To et al., 2000, Fine et al., 1999). Here, discovering the different emission characteristics depending upon cooking ingredients and methods will contribute to a more comprehensive understanding of cooking emissions.

The emissions of ritual candle burning were recognizable due to the moderate to high NICs of C_{22}-C_{35} *n*-alkanes, accounting for ~30% of the total NIC (Figure 5.5 E). The NICs of individual *n*-alkanes correlated well with each other among the repeated 6 activities ($R^2 > 0.8$). In comparison with the emission factors of n-alkanes for burning of paraffin candles tested in a sealed chamber (Fine et al., 1999), the relative emission strengths were comparable for C_{22}-C_{28} *n*-alkanes between the two studies (Table 5.3). However, our measurements indicated higher proportions of C_{29}-C_{35} in the total emission of *n*-alkanes, which might be associated with the smoldering of the bamboo

stick inside the candle. Coincidently, the concentrations of some biomass burning tracers, such as vanillic acid and levoglucosan, were enhanced. Besides, palmitic acid, oleic acid, arabinitol, and fructose isomers also occupied large shares in the total NIC, likely resulting from the combination of emissions from the burning of paraffin and bamboo stick.

Table 5. 3. Emission factors (literature data) and NICs (this study) of C_{20}-C_{35} *n*-alkanes in paraffin candle burning.

Compound	Emission factors determined in a chamber study [a]		NICs determined from real indoor environment [b*]	
	Emission factor (mg/g)	Normalized to the value for *n*-hexacosane	NIC (ng m^{-3})	Normalized to the value for *n*-hexacosane
n-Eicosane	0.54	0.03	1.75 ± 1.60	0.11 ± 0.14
n-Heneicosane	1.68	0.10	0.25 ± 0.09	0.02 ± 0.02
n-Docosane	4.52	0.26	5.99 ± 4.30	0.37 ± 0.44
n-Tricosane	8.91	0.52	11.38 ± 9.06	0.71 ± 0.87
n-Tetracosane	13.56	0.79	12.97 ± 11.42	0.81 ± 1.04
n-Pentacosane	15.56	0.90	16.01 ± 14.51	0.99 ± 1.30
n-Hexacosane	17.21	1.00	16.11 ± 15.25	1.00 ± 1.34
n-Heptacosane	16.97	0.99	20.87 ± 20.73	1.30 ± 1.78
n-Octacosane	16.43	0.95	17.76 ± 18.93	1.10 ± 1.57
n-Nonacosane	15.08	0.88	33.71 ± 36.04	2.09 ± 2.99
n-Triacontane	13.38	0.78	20.46 ± 22.97	1.27 ± 1.87
n-Hentriacontane	10.71	0.62	28.78 ± 31.26	1.79 ± 2.57
n-Dotriacontane	7.89	0.46	10.00 ± 11.57	0.62 ± 0.93
n-Tritriacontane	6.41	0.37	23.23 ± 27.03	1.44 ± 2.16
n-Tetratriacontane	4.89	0.28	20.82 ± 24.85	1.29 ± 1.97

n-Pentatriacontane	3.34	0.19	22.28 ± 27.11	1.38 ± 2.13

[a] Fine et al. (1999); [b] this study; * The ritual candles used in this study were made of paraffin with a bamboo stick inside for supporting and holding purposes.

It is inevitable that any emission profile is dependent upon the number and species of compounds included. In this study, though some compounds with high ERs were not included in the profiles due to the unavailability of the NICs, the emission profiles, consisting of 55 organic compounds, are chemically comprehensive enough to guide source apportionment. Moreover, we emphasized the unquantified species with high ERs in the previous discussion. These species can also serve as references for source identification.

5.5 Sources and airborne fate of PM-bound organics

Since most activities were carried out individually, it is feasible to calculate the contributions of specific activities to PM_1-OM during the disturbed period. The average NIC for a single event ranked as follows: cigarette smoking > incense burning > cooking > ritual candle burning. However, when considering the frequency of these activities, cooking and cigarette smoking emerged as the largest sources of indoor PM_1-OM during the disturbed period, contributing 45.3% and 40.6%, respectively. These contributions significantly exceeded those from ritual candle burning (7.2%) and incense burning (7.0%). Although the activities were designed to mimic real daily life in both intensity and frequency, the quantitative results should be interpreted with caution. Previous studies have also highlighted that certain indoor activities, such as cooking, are significant primary sources of SOA indoors (Yang et al., 2024). The secondary evolution processes of these indoor activities will be further explored in the following sections.

Determining the indoor contributions to PM_1-OM during the undisturbed period is

particularly intriguing. As discussed in Section 5.2, the average OM fraction in PM_1 for the indoor undisturbed samples was 65.0%. This value fell between the 57.6% fraction observed in outdoor samples and the 91.3% fraction in indoor disturbed samples. To estimate the average indoor and outdoor contributions to indoor PM_1-OM during the undisturbed period, we employed an interpolation method by solving the following equations:

$$f_{undis} = g_{in}f_{dis} + g_{out}f_{out}$$

$$g_{in} + g_{out} = 1$$

where f_{undis}, f_{dis} and f_{out} are the fractions of OM in PM_1 for undisturbed indoor samples, disturbed indoor samples, and outdoor samples, respectively. g_{in} (g_{out}) represents the indoor (outdoor) percentage contribution. These equations are based on the principle of mass balance for PM_1-OM in indoor air, assuming that the OM fraction in PM_1 from indoor activities remained relatively stable over short intervals (generally a few hours) between activities. The major uncertainties in this estimation arise from f_{dis} and f_{out}. As discussed in Section 5.2, f_{dis} and f_{out} were averaged at 91.3% and 57.6%, respectively. To address uncertainties related to f_{out}, we applied corrections to volatile species in PM_1 using the I/O ratio of sulfate. By applying f_{dis} to the undisturbed period, we assume consistent decay rates for the main PM_1 components. The minor difference in room temperature between disturbed (24.9 °C) and undisturbed periods (24.1 °C) implied minor changes in gas-to-particle partitioning, supporting this assumption. However, potential re-emission of SVOCs could mean the OM fraction in indoor PM_1 during the undisturbed period might be higher than f_{dis} if there was no outdoor air exchange. Thus, during the undisturbed period, f_{dis} likely represents a lower estimate of the OM fraction in PM_1 from indoor activities, leading to a slight overestimation of g_{in}, since f_{undis} lies between f_{dis} and f_{out}. Nonetheless, this does not alter the conclusion that outdoor air infiltration is the dominant source of PM_1-OM

indoors in the absence of high-emission activities, as confirmed by low I/O ratios for most species during the undisturbed period (Section 5.3). Given the rough estimate, we calculated only the average contributions rather than dynamic contributions post-specific activities. Results showed that indoor and outdoor contributions to PM_1-OM in undisturbed indoor samples were 21.9% and 78.1%, respectively. However, the indoor temperature (24.1°C) was significantly higher than the outdoor temperature (18.8°C) during the undisturbed period, causing PM_1 components with higher volatilities to partition toward the gas phase upon entering the apartment. Indeed, the I/O ratios for nitrate (0.66), chloride (0.54), and ammonium (0.39) were notably lower than that of sulfate (0.89) during the undisturbed period. Using the I/O ratio of sulfate and outdoor concentrations of nitrate, chloride, and ammonium, and assuming no indoor sources for these species, we estimated their concentrations immediately after entering the apartment (lowest estimates). Consequently, the OM fraction in PM_1 prior to evaporation was determined to be no higher than 62.0% during the undisturbed period, aligning more closely with the 57.6% observed in outdoor samples. Through interpolation, we determined a much lower indoor contribution (≤13.1%) to PM_1-OM in the undisturbed samples.

The indoor contribution to PM_1-OM during the undisturbed period implied the carry-over and/or re-emission of PM_1-OM, including some specific compounds. Figure 5.6 demonstrates the concentration variations of certain organic tracers before, during, and after high-emission activities. Concentrations from a day without any indoor activity were adopted as background levels. Most tracers exhibited higher concentrations than these background levels 2 h after the activities. Notably, the concentrations of fructose and vanillic acid remained above background levels even 6 h later. However, post-activity concentrations generally did not exceed pre-activity levels, except for vanillic acid from incense burning. This could be attributed to outdoor air infiltration, as the background level was also variable. To account for this, we examined the variations in

I/O ratios, as depicted in Figure 5.7. Significant increases in I/O ratios above background values were observed for fructose and vanillic acid, while other tracers showed discernable enhancements within 6 h. Moreover, the I/O ratios of *iso*-nonacosane and *anteiso*-tritriacontane consistently exceeded 1 and those of sulfate (an indicator of outdoor air pollution), although they returned to background I/O ratios 2 h after smoking. This may be due to elevated levels of these species on the day without any indoor activity, likely from previous smoking. Overall, certain organic compounds from cigarette smoke and incense burning emissions appeared to be carried over and/or re-emitted indoors. These findings align with previous studies indicating the long airborne lifetimes of cigarette smoke particles (Hussein et al., 2006).

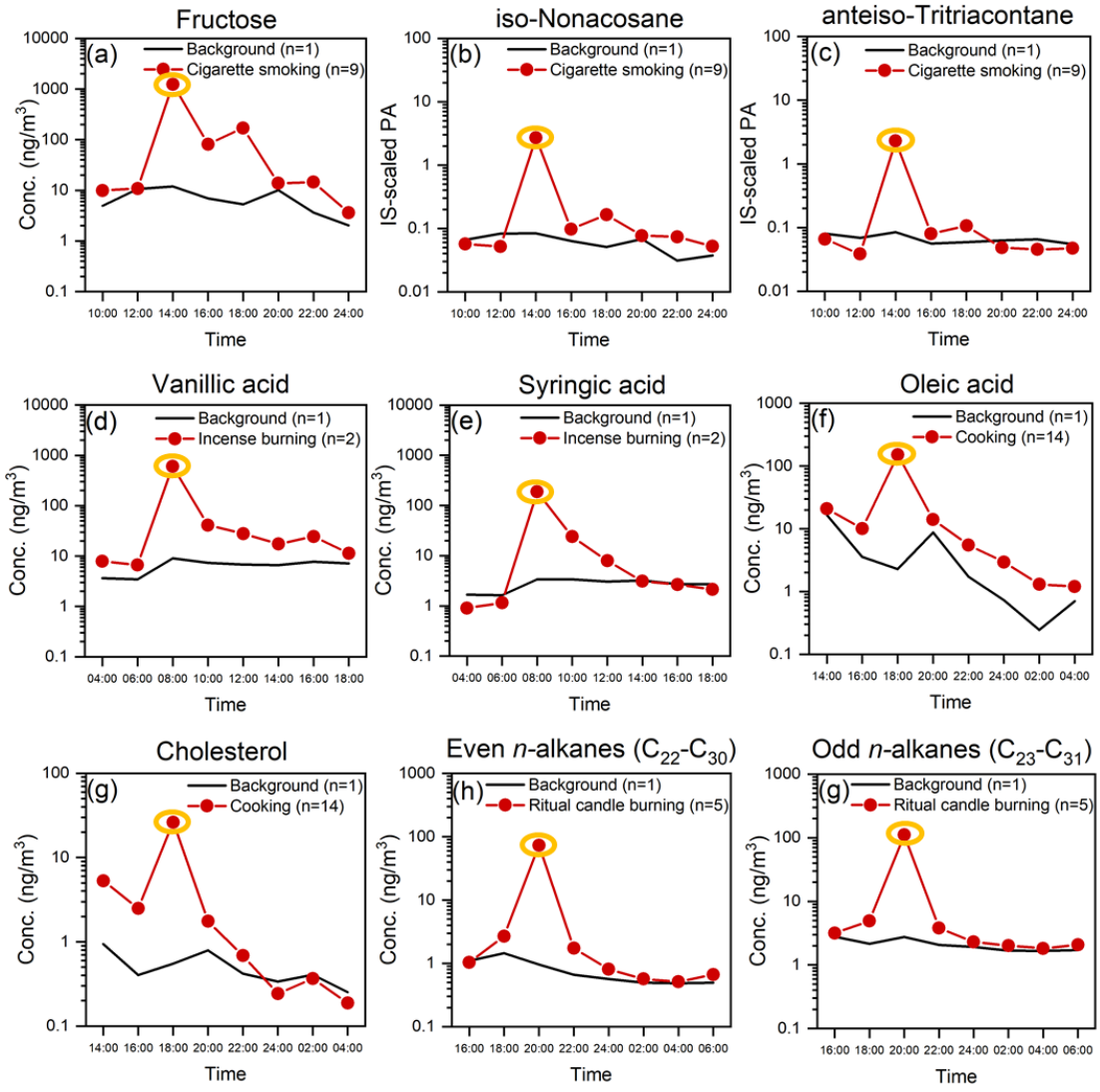

Figure 5. 6. Variations in the concentration or IS-scaled peak area (PA) of selected organic tracers before, during and after high-emission activities. Data points for activity samples are highlighted with orange circles. The IS-scaled PA refers to the peak area adjusted using an internal standard.

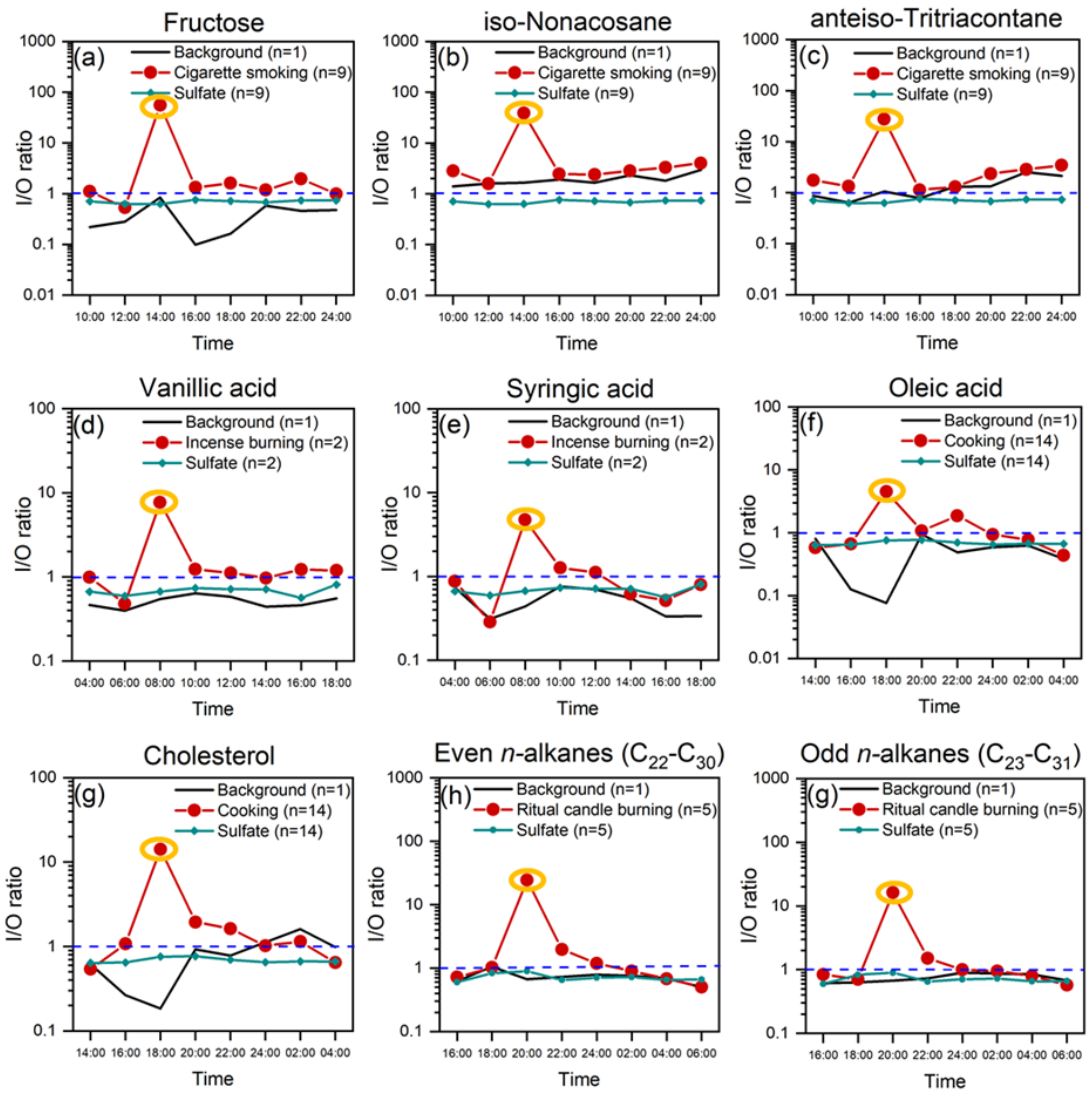

Figure 5. 7. Variations in the I/O ratios of selected organic tracers before, during, and after high-emission activities. The blue dashed line represents an I/O ratio of 1. Data points for activity samples are highlighted with orange circles.

Further, we examined the relationships between indoor concentrations of the specific tracers and room temperature during the undisturbed period, as shown in Figure 5.8. The concentrations of fructose, *iso*-nonacosane, vanillic acid, and *n*-alkanes showed a positive response ($p < 0.05$) to temperature increases, suggesting a re-emission process. However, the relatively weak correlations ($r \leq 0.5$) might be attributed to the influence of other factors on re-emission, such as the polarity of the surface reservoir (Abbatt and

Wang, 2020). To better understand the evolution of indoor air pollutants, we recommend conducting experiments with less intensive activities, measuring at higher time resolutions, and characterizing additional influential factors.

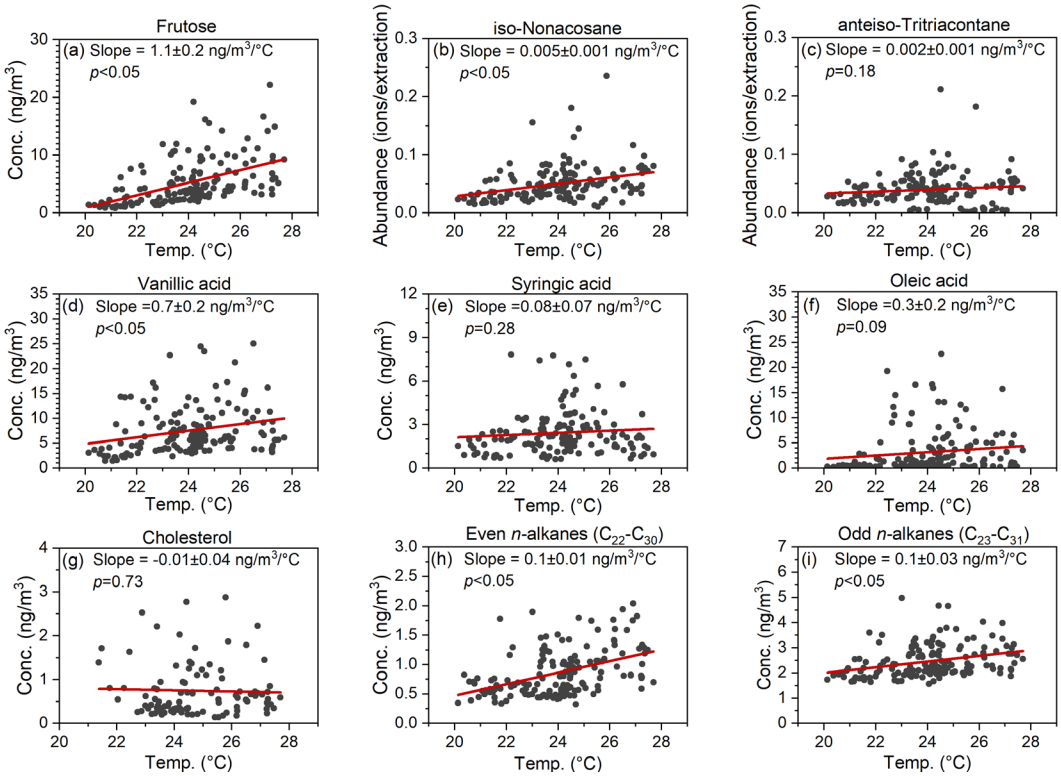

Figure 5. 8. Correlations between the concentrations of selected organic tracers and room temperature in undisturbed indoor samples.

Studying the chemical evolution of indoor air pollutants provides valuable insights into the fate and transformation of primary indoor emissions. Building upon previous research on outdoor OA, we investigated the aging of cooking emissions, uncovering a key aspect of indoor heterogeneous chemistry. Unsaturated fatty acids, such as oleic acid and linoleic acid, were found to undergo oxidation through heterogeneous reactions with O_3 and OH radicals (Nah et al., 2013, Zahardis and Petrucci, 2007). Known oxidation products include nonanal, nonanoic acid, azelaic acid, and 9-oxononanoic acid (Vesna et al., 2009, Ziemann, 2005). In this study, the TAG successfully detected signals of azelaic acid and 9-oxononanoic acid. However,

simultaneous increases in azelaic acid and oleic acid during cooking suggest that azelaic acid may also be a primary emission, consistent with previous findings (He et al., 2004). Consequently, we selected 9-oxononanoic acid as a marker for the oxidation products of cooking emissions. Due to the absence of authentic standards, TAG measurements of 9-oxononanoic acid were not quantified in this campaign; instead, internal standard (IS)-scaled peak areas were used for analysis. We first examined the diurnal patterns of 9-oxononanoic acid and O_3 indoors and outdoors, as shown in Figure 5.9 A-B. Two peaks were observed in the diurnal variation of 9-oxononanoic acid for both indoor and outdoor samples, delayed by approximately one hour relative to typical cooking times in Hong Kong, suggesting a strong link to fresh cooking emissions. Additionally, the average indoor abundance of 9-oxononanoic acid was significantly higher than outdoors, indicating that the indoor environment is more conducive to generating cooking SOA. Furthermore, the daytime peak of 9-oxononanoic acid in both environments corresponded well with O_3 patterns. Based on outdoor atmospheric chemistry, indoor OH levels are expected to peak around noon, coinciding with the highest ambient OH levels and intense photolysis of HONO indoors, driven by elevated HONO concentrations during lunch preparation and strong sunlight (Zeng et al., 2020). Thus, the afternoon peak likely resulted from the ozonolysis of oleic acid emitted during cooking (Wang et al., 2020). However, the indoor O_3 mixing ratio was much lower than outdoors (16.7 ± 0.09 ppb *v.s.* 24.7 ± 0.13 ppb), which alone cannot explain the higher indoor levels of 9-oxononanoic acid. A plausible explanation is the abundance of indoor precursors, such as oleic acid, which was more prevalent indoors and peaked during dinner preparation, likely fueling the production of 9-oxononanoic acid in the evening. High indoor levels of 9-oxononanoic acid may also be partially attributed to OH-initiated oxidation, especially when HONO levels were elevated post-cooking. Further exploration of factors influencing 9-oxononanoic acid yields is warranted.

To gain deeper insights into the chemical evolution of indoor OAs, we analyzed 9-

oxononanoic acid and oleic acid levels in indoor samples collected during cooking and two hours afterward. The difference between 9-oxononanoic acid and oleic acid was not significant (p=0.29), while 9-oxononanoic acid increased markedly as oleic acid decreased ($p < 0.001$), as shown in Figure 5.9 C. Consequently, the ratio of 9-oxononanoic acid to oleic acid rose, while the ratio of oleic acid to stearic acid declined (Figure 5.9 D). Given that oleic acid is more reactive than stearic acid, the increased ratio of secondary products to precursors, alongside the decreased precursor ratio, strongly suggests the chemical aging of cooking emissions indoors. With no intensive emission activity occurring after dinner until the following morning, we focused on samples from this period to examine the chemical evolution of cooking emissions. As shown in Figure 5.9 E, the level of 9-oxononanoic acid gradually increased after cooking, while oleic acid decreased, reaching peak levels 4-8 hours later. Moreover, the rate of increase for 9-oxononanoic acid during the first 2 hours (9.4% hr^{-1}) was much lower than the decrease rate for oleic acid (45.8% hr^{-1}), likely due to the multistage oxidation of oleic acid (Zahardis and Petrucci, 2007). As shown in Figure 5.9 F, the ratio of 9-oxononanoic acid to oleic acid increased during the undisturbed period and then decreased at the onset of the next cooking event. A continuous decline in the oleic acid to stearic acid ratio was observed until the last 2 hours.

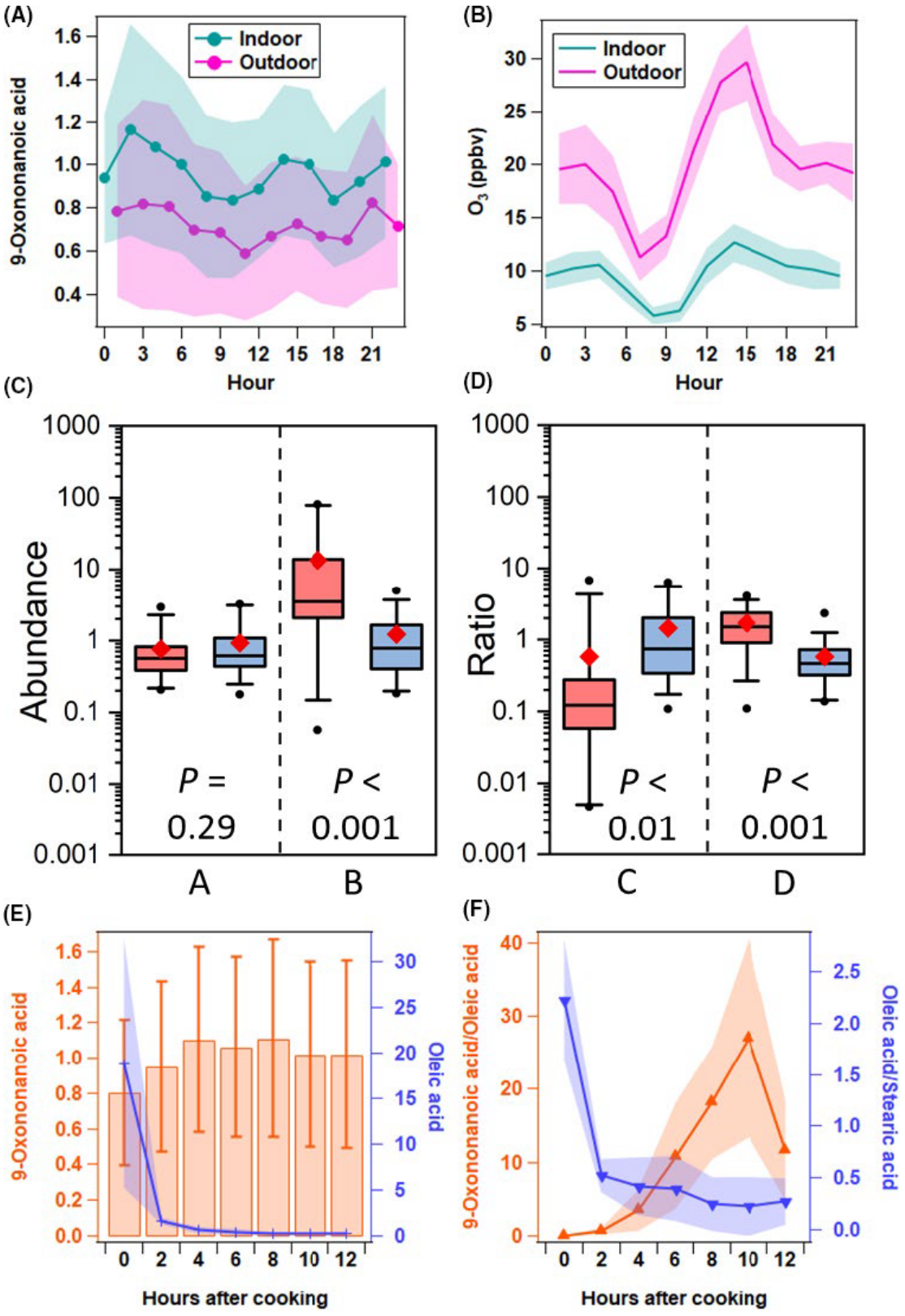

Figure 5. 9. Indoor chemical aging of cooking emissions. (a)-(b) Diurnal profiles of 9-oxononanoic acid (a) and O_3 (b). (c) IS-scaled peak areas of 9-oxononanoic acid (A)

and oleic acid (B) in cooking samples (Red box) and next indoor samples 2 hours later (Blue box). (d). Ratio of 9-oxononanoic acid to oleic acid (C) and oleic acid to stearic acid (D) in cooking samples (Red box) and next indoor samples 2 hours later (Blue box). (e)-(f) Variations of IS-scaled peak areas of 9-oxononanoic acid and oleic acid (e), and ratio of 9-oxononanoic acid to oleic acid and oleic acid to stearic acid (f) within 12 hours since making dinner.

We further calculated the effective rate constants and atmospheric lifetime of oleic acid in both indoor and outdoor environments, using the methodology proposed by Wang and Yu (2021). As illustrated in Figure 5.10, the fitting of nighttime samples demonstrates a clear decay of oleic acid in both settings. Indoor samples showed a significant drop during the first two hours post-cooking, whereas outdoor samples exhibited a gradual decline throughout the post-cooking hours. This discrepancy is likely due to differences in ventilation conditions, such as the use of a range hood during cooking. Consequently, we excluded the first sample from the indoor data fitting curve. Overall, the data from both environments fit well with an exponential function ($y = A \times e^{-kt}$), with a coefficient of determination exceeding 0.9. Although elevated levels of oleic acid and oxidants outdoors would typically suggest a higher decay rate for oleic acid oxidation, our results revealed the opposite: 0.13 h^{-1} outdoors compared to 0.20 h^{-1} indoors. This unexpected finding may be attributed to higher indoor temperatures, which could enhance heterogeneous reaction rates. Additionally, fresh OAs emitted from cooking predominantly consist of low-viscosity particles, which are more responsive to gas-phase ozone uptake (Shiraiwa et al., 2013, Krieger et al., 2012). We calculated the atmospheric lifetime ($\tau=1/k$) of oleic acid concerning its heterogeneous reaction with ozone. The estimated indoor lifetime of oleic acid is approximately 300 minutes at an ozone concentration of 10.0 ± 0.09 ppb, while the estimated outdoor lifetime is 462 minutes at an ozone concentration of 19.9 ± 0.17 ppb. The estimated outdoor lifetime is comparable to the study by Wang and Yu (2021). Interestingly, even

after excluding the first sample from the fitting, the estimated indoor lifetime of oleic acid approaches that of its outdoor counterpart, despite the outdoor ozone level being nearly double the indoor level. Furthermore, the estimated indoor lifetime is slightly longer than the corresponding outdoor lifetime reported by Wang and Yu (2021) under similar ozone conditions. Overall, the longer lifetime of cooking-emitted aerosols indoors suggested that they may undergo more chemical reactions with components in indoor air, potentially altering the chemical properties of the aerosols and impacting human health.

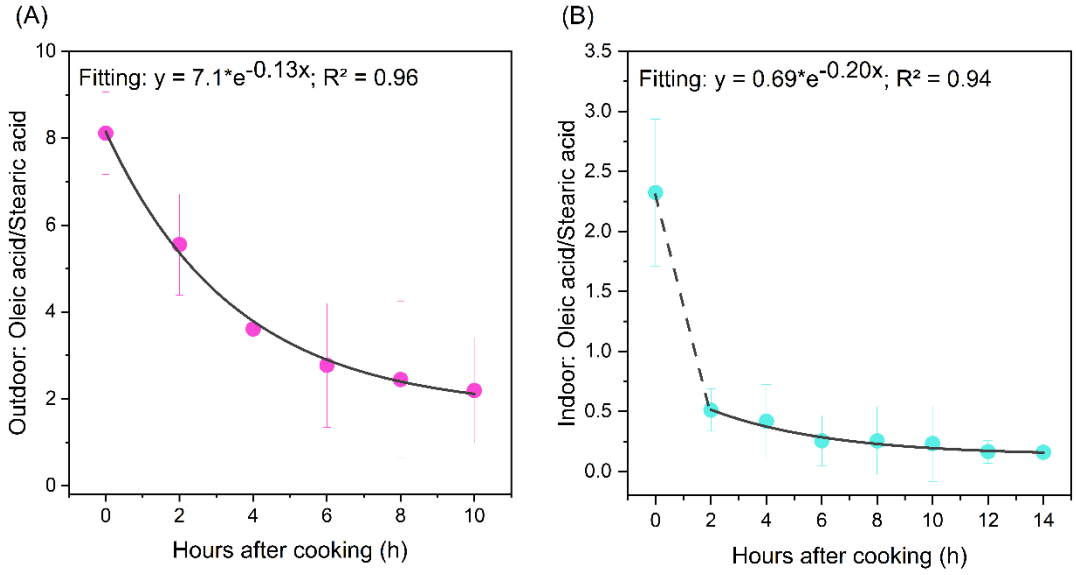

Figure 5. 10. Fitting curves of oleic acid normalized by stearic acid concentrations in outdoor (A) and indoor (B) environments. The dashed line represents the exponential fit, and the error bars indicate the 95% confidence interval.

5.6 Concluding Remark

Condensable organics are prevalent in nearly all indoor environments, with significant portions partitioning into fine PM. The chemical complexity and health impacts of indoor PM-bound organics essential. This study was conducted in a compact flat with

subdivided units in Hong Kong, typical of housing for low- and middle-income families. Despite activities like cooking, smoking, and burning worship supplies, indoor air pollution has not received as much attention as other hazards such as hygiene and fire safety. By employing novel analytical techniques originally developed for atmospheric chemistry, we measured total and speciated PM-bound organics in the flat with unprecedented temporal and chemical resolution. We found higher indoor levels of total PM-bound organics and numerous speciated compounds in $PM_{2.5}$ during high-emission indoor activities. The top contributors to PM-bound organic emissions were cigarette smoking, cooking, incense burning, and ritual candle burning. We developed comprehensive emission profiles for these activities, which corroborated and expanded upon previous laboratory findings. Specific tracers were identified, including but not limited to fructose isomers for cigarette smoking, vanillic acid for incense burning, oleic acid, cholesterol, and linoleic acid for cooking with different ingredients or methods. C_{22}-C_{35} alkanes were linked to ritual candle burning. During periods of high indoor activity, cooking and cigarette smoking were the primary sources of PM_1-OM. In the absence of such activities, outdoor air infiltration was the main source of PM_1-OM, although some compounds from cigarette smoking and incense burning persisted or were re-emitted indoors. Therefore, proper management of high-emission activities is crucial in enclosed spaces, especially for emissions that are persistent and toxic. The study also identified the chemical aging of cooking emissions indoors, with oleic acid and its oxidation products as indicators. Our findings indicate that cooking-emitted aerosols have a longer atmospheric lifetime indoors than outdoors. Further research is needed to understand indoor chemistry and its health effects on residents.

Chapter 6 Conclusions and Recommendations

6.1 Conclusions

This PhD thesis explored the characteristics and formation chemistry of OAs in both outdoor and indoor air in Hong Kong. By utilizing highly time-resolved measurements and molecular-level data, we clarified the interactions between anthropogenic and biogenic emissions in SOA formation and identified the factors influencing SOA formation under different atmospheric conditions. Moreover, this study provided a detailed analysis of indoor PM-bound organics, which have significant health implications in the densely populated living environments typical of Hong Kong. The key findings of this research are as follows:

1. As a land-sea transitional region, Hong Kong experiences varying influences on SOA formation depending on the origin of incoming air masses. In coastal air, aqueous-phase reactions significantly contribute to aerosol aging, whereas photochemical reactions are more prevalent in continental air masses that traverse the PRD region.

2. Molecular-level analysis revealed several factors influencing the formation of speciated SOA. For SOA derived from anthropogenic sources, significant formation occurred due to a combination of high precursor levels and intense photochemical activity. In biogenic SOA, a correlation between 2-MGA and sulfate in coastal air indicated contributions from aqueous-phase reactions. Conversely, in continental air, high levels of sulfate precursors promoted particle seed formation, enhancing SOA formation by increasing particle surface area. Additionally, monoterpene-derived SOA was more aged in continental air due to intense photochemical processes and lower temperatures,

which favored the partitioning of fresh oxidation products into the condensed phase.

3. This study examined the roles of NO_x, SO_2, and atmospheric oxidation levels in SOA formation in Hong Kong. It was found that SO_2 levels more effectively promoted biogenic SOA formation in coastal air compared to continental air. Additionally, high atmospheric oxidation conditions in continental air enhanced the formation of anthropogenic SOA, particularly when precursor levels were elevated.

4. The study explored the formation processes of high-level OHDCA in Hong Kong, uncovering significant implications for air quality and climate. Our findings highlighted the crucial role of aqueous photochemical reactions, particularly given Hong Kong's warm and humid subtropical climate.

5. By employing advanced analytical techniques initially developed for atmospheric chemistry, we measured both total and speciated organics in indoor particles. The results indicated that indoor levels of PM-bound organics frequently surpassed outdoor levels, especially during high-emission activities such as cigarette smoking, cooking, incense burning, and ritual candle burning.

6. Emission profiles for high-emission indoor activities were developed, identifying notable tracers: fructose isomers for cigarette smoking, vanillic acid for incense burning, oleic acid, cholesterol, and linoleic acid for various cooking methods, and C_{22}-C_{35} alkanes as markers for ritual candle burning.

7. Cooking and cigarette smoking were identified as the predominant contributors to indoor PM-bound organics during periods of high activity. In contrast, during times without high-emission activities, outdoor air infiltration became the dominant source. Additionally, certain compounds from cigarette smoking and

incense burning persisted indoors, either through carryover or re-emission processes.

8. The study examined the chemical aging of indoor cooking emissions. The evolution of oleic acid and its oxidation products suggested that the atmospheric lifetime of cooking-emitted aerosols is longer indoors than outdoors. This finding underscores the significance of indoor heterogeneous reactions, which merit further investigation.

6.2 Limitations of this study and future prospects

While this study offers a more comprehensive investigation into the characteristics and chemistry of OA in Hong Kong compared to previous research, it has certain limitations, particularly in quantifying the contribution of each influencing factor to SOA generation. The three main research directions in atmospheric chemistry include field observations, molecular-level studies through experimental investigations, and atmospheric modeling (Abbatt and Ravishankara, 2023). Below, the limitations of this study are briefly discussed from each of these perspectives.

1. In this study, highly time-resolved mass spectrometry was employed for the online measurement of total organics and speciated molecular markers in particulate matter, focusing on the factors influencing SOA formation. However, due to the lack of precursor data, we did not quantitatively explore the relationship between SOA and its precursors in-depth. The full characterization of organic carbon in field observations is hindered by its extreme chemical complexity, which is crucial for understanding the products and evolution of atmospheric organic carbon through multigenerational oxidation. Additionally, the evolution of organic carbon in the atmosphere involves complex multiphase reactions. Therefore, it is essential to simultaneously observe the physicochemical properties of particulates (e.g.,

viscosity, optical properties, cloud condensation nuclei (CCN)) especially in indoor studies where complex chemical processes are poorly understood. Future research could further explore how indoor sources, such as cooking, contribute to outdoor air pollution and affect ambient air quality. Moreover, considering the influence of meteorological conditions is essential, highlighting the need for long-term sampling campaigns to capture temporal variations and gain a deeper understanding of these dynamics. More comprehensive research should also link the concentration of organic aerosols with their health effects. Current epidemiological studies do not identify the specific molecules in particles, their formation pathways, or the mechanisms of toxicity leading to adverse health outcomes. We believe that high time-resolution data will provide new insights for the environmental health, medical, and toxicological communities.

2. Bridging fieldwork with laboratory studies is essential in atmospheric chemistry. Our findings provide several insights for future laboratory research: First, the mechanisms of OA formation under complex pollution conditions need further investigation, especially in systems where multiple inorganic pollutants coexist with anthropogenic and biogenic VOCs. Second, this study highlighted the influence of SO_2 on SOA formation in Hong Kong. While previous research suggests that sulfur-containing BSOA can form under the influence of SO_2, the detailed formation mechanisms remain unclear. Future laboratory work should conduct detailed molecular-level analyses of sulfur-containing SOA and investigate the formation mechanisms under atmospheric conditions. Third, although this study explored factors influencing SOA formation, the investigation of oxidants and intermediate products was limited by observational capabilities. Therefore, future laboratory work is needed to systematically study these formation processes. Fourth, aqueous-phase reactions may contribute to polar SOA formation in Hong Kong, but

their oxidation mechanisms are not fully understood. Future laboratory research should further investigate the formation mechanisms of polar SOA, considering the effects of ALWC, inorganic pollutants, particle acidity, and precursor levels.

3. Model simulations play a crucial role in quantitatively analyzing the contributions of various factors to the SOA formation process. The field observations of SOA concentrations and their temporal variations from this study can be used to validate and improve emission inventories and chemical mechanisms within these models. Furthermore, our investigation into the formation processes of climate-related SOA can be applied to climate models for better quantification of their potential effects. Beyond regional chemical transport models, there is a need to develop and refine models with explicit chemical mechanisms to further explore the contributions of different formation pathways and the impact of gas-particle partitioning during SOA formation. Moreover, our indoor study highlighted the complexity of indoor air, which current box models struggle to accurately predict. Future research could benefit from integrating explicit box models with computational fluid dynamics (CFD) modeling to simulate the formation and evolution of air pollutants indoors.

References

ABBATT, J. P. & RAVISHANKARA, A. R. 2023. Opinion: Atmospheric multiphase chemistry–past, present, and future. *Atmospheric Chemistry and Physics,* 23**,** 9765-9785.

ABBATT, J. P. & WANG, C. 2020. The atmospheric chemistry of indoor environments. *Environmental Science: Processes & Impacts,* 22**,** 25-48.

ABDULLAHI, K. L., DELGADO-SABORIT, J. M. & HARRISON, R. M. 2013. Emissions and indoor concentrations of particulate matter and its specific chemical components from cooking: A review. *Atmospheric Environment,* 71**,** 260-294.

AL-NAIEMA, I. M. & STONE, E. A. 2017. Evaluation of anthropogenic secondary organic aerosol tracers from aromatic hydrocarbons. *Atmospheric Chemistry and Physics,* 17**,** 2053-2065.

AMATO, F., PANDOLFI, M., ESCRIG, A., QUEROL, X., ALASTUEY, A., PEY, J., PéREZ, N. & HOPKE, P. K. 2009. Quantifying road dust resuspension in urban environment by multilinear engine: a comparison with PMF2. *Atmospheric Environment,* 43**,** 2770-2780.

AVERY, A. M., WARING, M. S. & DECARLO, P. F. 2019. Seasonal variation in aerosol composition and concentration upon transport from the outdoor to indoor environment. *Environmental Science: Processes & Impacts,* 21**,** 528-547.

BERTRAND, A., STEFENELLI, G., JEN, C. N., PIEBER, S. M., BRUNS, E. A., NI, H., TEMIME-ROUSSEL, B., SLOWIK, J. G., GOLDSTEIN, A. H. & EL HADDAD, I. 2018. Evolution of the chemical fingerprint of biomass burning organic aerosol during aging. *Atmospheric Chemistry and Physics,* 18**,** 7607-7624.

BOOTH, A., MONTAGUE, W., BARLEY, M., TOPPING, D., MCFIGGANS, G., GARFORTH, A. & PERCIVAL, C. 2011. Solid state and sub-cooled liquid vapour pressures of cyclic aliphatic dicarboxylic acids. *Atmospheric Chemistry and Physics,* 11**,** 655-665.

BRAUER, M., ROTH, G. A., ARAVKIN, A. Y., ZHENG, P., ABATE, K. H., ABATE, Y. H., ABBAFATI, C., ABBASGHOLIZADEH, R., ABBASI, M. A. & ABBASIAN, M. 2024. Global burden and strength of evidence for 88 risk factors in 204 countries and 811 subnational locations, 1990–2021: a systematic analysis for the Global Burden of Disease Study 2021. *The Lancet,* 403**,** 2162-2203.

BREITNER, S., LIU, L., CYRYS, J., BRüSKE, I., FRANCK, U., SCHLINK, U., LEITTE, A. M., HERBARTH, O., WIEDENSOHLER, A. & WEHNER, B. 2011. Sub-micrometer particulate air pollution and cardiovascular mortality in

Beijing, China. *Science of the Total Environment,* 409**,** 5196-5204.

BUDISULISTIORINI, S., LI, X., BAIRAI, S., RENFRO, J., LIU, Y., LIU, Y., MCKINNEY, K., MARTIN, S., MCNEILL, V. & PYE, H. 2015. Examining the effects of anthropogenic emissions on isoprene-derived secondary organic aerosol formation during the 2013 Southern Oxidant and Aerosol Study (SOAS) at the Look Rock, Tennessee ground site. *Atmospheric Chemistry and Physics,* 15**,** 8871-8888.

CAO, J., LEE, S., CHOW, J., CHENG, Y., HO, K., FUNG, K., LIU, S. & WATSON, J. 2005. Indoor/outdoor relationships for PM 2.5 and associated carbonaceous pollutants at residential homes in Hong Kong–case study. *Indoor air,* 15.

CAO, J., LEE, S., HO, K., ZHANG, X., ZOU, S., FUNG, K., CHOW, J. C. & WATSON, J. G. 2003. Characteristics of carbonaceous aerosol in Pearl River Delta Region, China during 2001 winter period. *Atmospheric Environment,* 37**,** 1451-1460.

CARLTON, A., WIEDINMYER, C. & KROLL, J. 2009. A review of Secondary Organic Aerosol (SOA) formation from isoprene. *Atmospheric Chemistry and Physics,* 9**,** 4987-5005.

CARLTON, A. G., TURPIN, B. J., ALTIERI, K. E., SEITZINGER, S., REFF, A., LIM, H.-J. & ERVENS, B. 2007. Atmospheric oxalic acid and SOA production from glyoxal: Results of aqueous photooxidation experiments. *Atmospheric Environment,* 41**,** 7588-7602.

CARTER, W. P. & ATKINSON, R. 1985. Atmospheric chemistry of alkanes. *Journal of atmospheric chemistry,* 3**,** 377-405.

CHAN, A., KREISBERG, N., HOHAUS, T., CAMPUZANO-JOST, P., ZHAO, Y., DAY, D., KASER, L., KARL, T., HANSEL, A. & TENG, A. 2016. Speciated measurements of semivolatile and intermediate volatility organic compounds (S/IVOCs) in a pine forest during BEACHON-RoMBAS 2011. *Atmospheric chemistry and physics,* 16**,** 1187-1205.

CHANG, T.-J., KAO, H.-M. & HSIEH, Y.-F. 2007. Numerical study of the effect of ventilation pattern on coarse, fine, and very fine particulate matter removal in partitioned indoor environment. *Journal of the air & waste management association,* 57**,** 179-189.

CHAO, C. Y. & WONG, K. K. 2002. Residential indoor PM10 and PM2. 5 in Hong Kong and the elemental composition. *Atmospheric Environment,* 36**,** 265-277.

CHARBOUILLOT, T., GORINI, S., VOYARD, G., PARAZOLS, M., BRIGANTE, M., DEGUILLAUME, L., DELORT, A.-M. & MAILHOT, G. 2012. Mechanism of carboxylic acid photooxidation in atmospheric aqueous phase: Formation, fate and reactivity. *Atmospheric environment,* 56**,** 1-8.

CHEN, X.-C., CHUANG, H.-C., WARD, T. J., TIAN, L., CAO, J.-J., HO, S. S.-H., LAU, N.-C., HSIAO, T.-C., YIM, S. H. & HO, K.-F. 2020. Indoor, outdoor, and personal exposure to PM2. 5 and their bioreactivity among healthy residents of

Hong Kong. *Environmental Research,* 188**,** 109780.
CHENG, C., LI, M., CHAN, C. K., TONG, H., CHEN, C., CHEN, D., WU, D., LI, L., WU, C. & CHENG, P. 2017. Mixing state of oxalic acid containing particles in the rural area of Pearl River Delta, China: implications for the formation mechanism of oxalic acid. *Atmospheric Chemistry and Physics,* 17**,** 9519-9533.
CHENG, Y., MA, Y. & HU, D. 2021. Tracer-based source apportioning of atmospheric organic carbon and the influence of anthropogenic emissions on secondary organic aerosol formation in Hong Kong. *Atmospheric Chemistry and Physics,* 21**,** 10589-10608.
CHOW, W. S., LIAO, K., HUANG, X., LEUNG, K. F., LAU, A. K. & YU, J. Z. 2022. Measurement report: The 10-year trend of PM 2.5 major components and source tracers from 2008 to 2017 in an urban site of Hong Kong, China. *Atmospheric Chemistry and Physics,* 22**,** 11557-11577.
CLAEYS, M., GRAHAM, B., VAS, G., WANG, W., VERMEYLEN, R., PASHYNSKA, V., CAFMEYER, J., GUYON, P., ANDREAE, M. O. & ARTAXO, P. 2004. Formation of secondary organic aerosols through photooxidation of isoprene. *Science,* 303**,** 1173-1176.
CLAEYS, M., SZMIGIELSKI, R., KOURTCHEV, I., VAN DER VEKEN, P., VERMEYLEN, R., MAENHAUT, W., JAOUI, M., KLEINDIENST, T. E., LEWANDOWSKI, M. & OFFENBERG, J. H. 2007. Hydroxydicarboxylic acids: Markers for secondary organic aerosol from the photooxidation of α-pinene. *Environmental Science & Technology,* 41**,** 1628-1634.
DE Sá, S. S., PALM, B. B., CAMPUZANO-JOST, P., DAY, D. A., NEWBURN, M. K., HU, W., ISAACMAN-VANWERTZ, G., YEE, L. D., THALMAN, R. & BRITO, J. 2017. Influence of urban pollution on the production of organic particulate matter from isoprene epoxydiols in central Amazonia. *Atmospheric Chemistry and Physics,* 17**,** 6611-6629.
DECARLO, P. F., KIMMEL, J. R., TRIMBORN, A., NORTHWAY, M. J., JAYNE, J. T., AIKEN, A. C., GONIN, M., FUHRER, K., HORVATH, T. & DOCHERTY, K. S. 2006. Field-deployable, high-resolution, time-of-flight aerosol mass spectrometer. *Analytical chemistry,* 78**,** 8281-8289.
DENG, W.-J., ZHENG, H.-L., TSUI, A. K. & CHEN, X.-W. 2016. Measurement and health risk assessment of PM2. 5, flame retardants, carbonyls and black carbon in indoor and outdoor air in kindergartens in Hong Kong. *Environment international,* 96**,** 65-74.
DING, X., HE, Q.-F., SHEN, R.-Q., YU, Q.-Q., ZHANG, Y.-Q., XIN, J.-Y., WEN, T.-X. & WANG, X.-M. 2016. Spatial and seasonal variations of isoprene secondary organic aerosol in China: Significant impact of biomass burning during winter. *Scientific reports,* 6**,** 20411.
DING, X., HE, Q. F., SHEN, R. Q., YU, Q. Q. & WANG, X. M. 2014. Spatial

distributions of secondary organic aerosols from isoprene, monoterpenes, β-caryophyllene, and aromatics over China during summer. *Journal of Geophysical Research: Atmospheres,* 119**,** 11,877-11,891.

DING, X., YE, P., ZHANG, Y., CHEN, D., LI, J., ZHANG, T., WANG, J., CHENG, Q., JIANG, H. & SONG, W. Impact of anthropogenic emissions on biogenic secondary organic aerosol: Observation in the Pearl River Delta, South China. AGU Fall Meeting Abstracts, 2019. A31B-06.

EDDINGSAAS, N. C., VANDERVELDE, D. G. & WENNBERG, P. O. 2010. Kinetics and products of the acid-catalyzed ring-opening of atmospherically relevant butyl epoxy alcohols. *The Journal of Physical Chemistry A,* 114**,** 8106-8113.

EDNEY, E., KLEINDIENST, T., JAOUI, M., LEWANDOWSKI, M., OFFENBERG, J., WANG, W. & CLAEYS, M. 2005. Formation of 2-methyl tetrols and 2-methylglyceric acid in secondary organic aerosol from laboratory irradiated isoprene/NOx/SO2/air mixtures and their detection in ambient PM2. 5 samples collected in the eastern United States. *Atmospheric Environment,* 39**,** 5281-5289.

EDWARDS, P., AIKIN, K., DUBE, W., FRY, J., GILMAN, J., DE GOUW, J., GRAUS, M., HANISCO, T., HOLLOWAY, J. & HUBLER, G. 2017. Transition from high-to low-NOx control of night-time oxidation in the southeastern US, Nat. Geosci., 10, 490–495.

ENGLERT, N. 2004. Fine particles and human health—a review of epidemiological studies. *Toxicology letters,* 149**,** 235-242.

ERVENS, B., FEINGOLD, G., FROST, G. J. & KREIDENWEIS, S. M. 2004. A modeling study of aqueous production of dicarboxylic acids: 1. Chemical pathways and speciated organic mass production. *Journal of Geophysical Research: Atmospheres,* 109.

ERVENS, B., TURPIN, B. & WEBER, R. 2011. Secondary organic aerosol formation in cloud droplets and aqueous particles (aqSOA): a review of laboratory, field and model studies. *Atmospheric Chemistry and Physics,* 11**,** 11069-11102.

FENG, S., GAO, D., LIAO, F., ZHOU, F. & WANG, X. 2016. The health effects of ambient PM2. 5 and potential mechanisms. *Ecotoxicology and environmental safety,* 128**,** 67-74.

FINE, P. M., CASS, G. R. & SIMONEIT, B. R. 1999. Characterization of fine particle emissions from burning church candles. *Environmental science & technology,* 33**,** 2352-2362.

FINLAYSON-PITTS, B. J. & PITTS JR, J. N. 1999. *Chemistry of the upper and lower atmosphere: theory, experiments, and applications*, Elsevier.

FORTENBERRY, C. F., WALKER, M. J., ZHANG, Y., MITROO, D., BRUNE, W. H. & WILLIAMS, B. J. 2018. Bulk and molecular-level characterization of laboratory-aged biomass burning organic aerosol from oak leaf and heartwood fuels. *Atmos. Chem. Phys,* 18**,** 2199-2224.

FU, P., KAWAMURA, K., CHEN, J., LI, J., SUN, Y., LIU, Y., TACHIBANA, E., AGGARWAL, S., OKUZAWA, K. & TANIMOTO, H. 2012. Diurnal variations of organic molecular tracers and stable carbon isotopic composition in atmospheric aerosols over Mt. Tai in the North China Plain: an influence of biomass burning. *Atmospheric Chemistry and Physics,* 12**,** 8359-8375.

FU, P., KAWAMURA, K., PAVULURI, C., SWAMINATHAN, T. & CHEN, J. 2010. Molecular characterization of urban organic aerosol in tropical India: contributions of primary emissions and secondary photooxidation. *Atmospheric Chemistry and Physics,* 10**,** 2663-2689.

GAO, S., KEYWOOD, M., NG, N. L., SURRATT, J., VARUTBANGKUL, V., BAHREINI, R., FLAGAN, R. C. & SEINFELD, J. H. 2004. Low-molecular-weight and oligomeric components in secondary organic aerosol from the ozonolysis of cycloalkenes and α-pinene. *The Journal of Physical Chemistry A,* 108**,** 10147-10164.

GAUDEL, A., COOPER, O. R., ANCELLET, G., BARRET, B., BOYNARD, A., BURROWS, J. P., CLERBAUX, C., COHEUR, P.-F., CUESTA, J. & CUEVAS, E. 2018. Tropospheric Ozone Assessment Report: Present-day distribution and trends of tropospheric ozone relevant to climate and global atmospheric chemistry model evaluation. *Elem Sci Anth,* 6**,** 39.

GOLDSTEIN, A. H. & GALBALLY, I. E. 2007. Known and unexplored organic constituents in the earth's atmosphere. *Environmental science & technology,* 41**,** 1514-1521.

GOLDSTEIN, A. H., KOVEN, C. D., HEALD, C. L. & FUNG, I. Y. 2009. Biogenic carbon and anthropogenic pollutants combine to form a cooling haze over the southeastern United States. *Proceedings of the National Academy of Sciences,* 106**,** 8835-8840.

GOLDSTEIN, A. H., WORTON, D. R., WILLIAMS, B. J., HERING, S. V., KREISBERG, N. M., PANIĆ, O. & GÓRECKI, T. 2008. Thermal desorption comprehensive two-dimensional gas chromatography for in-situ measurements of organic aerosols. *Journal of Chromatography a,* 1186**,** 340-347.

GRAHAM, B., MAYOL-BRACERO, O. L., GUYON, P., ROBERTS, G. C., DECESARI, S., FACCHINI, M. C., ARTAXO, P., MAENHAUT, W., KöLL, P. & ANDREAE, M. O. 2002. Water-soluble organic compounds in biomass burning aerosols over Amazonia 1. Characterization by NMR and GC-MS. *Journal of Geophysical Research: Atmospheres,* 107**,** LBA 14-1-LBA 14-16.

GRIFFIN, R. J., COCKER III, D. R., FLAGAN, R. C. & SEINFELD, J. H. 1999. Organic aerosol formation from the oxidation of biogenic hydrocarbons. *Journal of Geophysical Research: Atmospheres,* 104**,** 3555-3567.

GUENTHER, A., HEWITT, C. N., ERICKSON, D., FALL, R., GERON, C., GRAEDEL, T., HARLEY, P., KLINGER, L., LERDAU, M. & MCKAY, W.

1995. A global model of natural volatile organic compound emissions. *Journal of Geophysical Research: Atmospheres,* 100**,** 8873-8892.

GUO, H. 2011. Source apportionment of volatile organic compounds in Hong Kong homes. *Building and environment,* 46**,** 2280-2286.

GUO, H., KWOK, N., CHENG, H., LEE, S., HUNG, W. & LI, Y. S. 2009. Formaldehyde and volatile organic compounds in Hong Kong homes: concentrations and impact factors. *Indoor air,* 19.

GUO, X., MA, F., LIU, C., NIU, J., HE, N., CHEN, J. & XIE, H.-B. 2020. Atmospheric oxidation mechanism and kinetics of isoprene initiated by chlorine radicals: A computational study. *Science of the Total Environment,* 712**,** 136330.

HALLQUIST, M., WENGER, J. C., BALTENSPERGER, U., RUDICH, Y., SIMPSON, D., CLAEYS, M., DOMMEN, J., DONAHUE, N., GEORGE, C. & GOLDSTEIN, A. 2009. The formation, properties and impact of secondary organic aerosol: current and emerging issues. *Atmospheric chemistry and physics,* 9**,** 5155-5236.

HE, L.-Y., HU, M., HUANG, X.-F., YU, B.-D., ZHANG, Y.-H. & LIU, D.-Q. 2004. Measurement of emissions of fine particulate organic matter from Chinese cooking. *Atmospheric Environment,* 38**,** 6557-6564.

HE, L. Y., HUANG, X. F., XUE, L., HU, M., LIN, Y., ZHENG, J., ZHANG, R. & ZHANG, Y. H. 2011. Submicron aerosol analysis and organic source apportionment in an urban atmosphere in Pearl River Delta of China using high-resolution aerosol mass spectrometry. *Journal of Geophysical Research: Atmospheres,* 116.

HE, Q. F., DING, X., FU, X. X., ZHANG, Y. Q., WANG, J. Q., LIU, Y. X., TANG, M. J., WANG, X. M. & RUDICH, Y. 2018a. Secondary Organic Aerosol Formation From Isoprene Epoxides in the Pearl River Delta, South China: IEPOX-and HMML-Derived Tracers. *Journal of Geophysical Research: Atmospheres,* 123**,** 6999-7012.

HE, X., HUANG, X. H., CHOW, K. S., WANG, Q., ZHANG, T., WU, D. & YU, J. Z. 2018b. Abundance and sources of phthalic acids, benzene-tricarboxylic acids, and phenolic acids in PM2. 5 at urban and suburban sites in Southern China. *ACS Earth and Space Chemistry,* 2**,** 147-158.

HE, X., WANG, Q., HUANG, X. H., HUANG, D. D., ZHOU, M., QIAO, L., ZHU, S., MA, Y.-G., WANG, H.-L. & LI, L. 2020. Hourly measurements of organic molecular markers in urban Shanghai, China: Observation of enhanced formation of secondary organic aerosol during particulate matter episodic periods. *Atmospheric Environment,* 240**,** 117807.

HEALD, C., HENZE, D., HOROWITZ, L., FEDDEMA, J., LAMARQUE, J. F., GUENTHER, A., HESS, P., VITT, F., SEINFELD, J. & GOLDSTEIN, A. 2008. Predicted change in global secondary organic aerosol concentrations in response

to future climate, emissions, and land use change. *Journal of Geophysical Research: Atmospheres,* 113.

HEALD, C. L., JACOB, D. J., PARK, R. J., RUSSELL, L. M., HUEBERT, B. J., SEINFELD, J. H., LIAO, H. & WEBER, R. J. 2005. A large organic aerosol source in the free troposphere missing from current models. *Geophysical Research Letters,* 32.

HEO, J.-B., HOPKE, P. & YI, S.-M. 2009. Source apportionment of PM 2.5 in Seoul, Korea. *Atmospheric Chemistry and Physics,* 9**,** 4957-4971.

HO, K., LEE, S., CHAN, C. K., JIMMY, C. Y., CHOW, J. C. & YAO, X. 2003. Characterization of chemical species in PM2. 5 and PM10 aerosols in Hong Kong. *Atmospheric Environment,* 37**,** 31-39.

HODZIC, A., JIMENEZ, J. L., MADRONICH, S., CANAGARATNA, M., DECARLO, P. F., KLEINMAN, L. & FAST, J. 2010. Modeling organic aerosols in a megacity: potential contribution of semi-volatile and intermediate volatility primary organic compounds to secondary organic aerosol formation. *Atmospheric Chemistry and Physics,* 10**,** 5491-5514.

HOFFMANN, T., ODUM, J. R., BOWMAN, F., COLLINS, D., KLOCKOW, D., FLAGAN, R. C. & SEINFELD, J. H. 1997. Formation of organic aerosols from the oxidation of biogenic hydrocarbons. *Journal of Atmospheric Chemistry,* 26**,** 189-222.

HOPKE, P. K. 2003. Recent developments in receptor modeling. *Journal of Chemometrics: A Journal of the Chemometrics Society,* 17**,** 255-265.

HOYLE, C. R., BOY, M., DONAHUE, N. M., FRY, J. L., GLASIUS, M., GUENTHER, A., HALLAR, A. G., HUFF HARTZ, K., PETTERS, M. D. & PETäJä, T. 2011. A review of the anthropogenic influence on biogenic secondary organic aerosol. *Atmospheric Chemistry and Physics,* 11**,** 321-343.

HU, D., BIAN, Q., LAU, A. K. & YU, J. Z. 2010. Source apportioning of primary and secondary organic carbon in summer PM2. 5 in Hong Kong using positive matrix factorization of secondary and primary organic tracer data. *Journal of Geophysical Research: Atmospheres,* 115.

HU, D., BIAN, Q., LI, T. W., LAU, A. K. & YU, J. Z. 2008. Contributions of isoprene, monoterpenes, β-caryophyllene, and toluene to secondary organic aerosols in Hong Kong during the summer of 2006. *Journal of Geophysical Research: Atmospheres,* 113.

HU, D. & YU, J. Z. 2013. Secondary organic aerosol tracers and malic acid in Hong Kong: seasonal trends and origins. *Environmental Chemistry,* 10**,** 381-394.

HUANG, D. D., LI, Y. J., LEE, B. P. & CHAN, C. K. 2015a. Analysis of organic sulfur compounds in atmospheric aerosols at the HKUST supersite in Hong Kong using HR-ToF-AMS. *Environmental Science & Technology,* 49**,** 3672-3679.

HUANG, D. D., ZHU, S., AN, J., WANG, Q., QIAO, L., ZHOU, M., HE, X., MA, Y.,

SUN, Y. & HUANG, C. 2021. Comparative assessment of cooking emission contributions to urban organic aerosol using online molecular tracers and Aerosol Mass Spectrometry measurements. *Environmental Science & Technology,* 55**,** 14526-14535.

HUANG, R.-J., ZHANG, Y., BOZZETTI, C., HO, K.-F., CAO, J.-J., HAN, Y., DAELLENBACH, K. R., SLOWIK, J. G., PLATT, S. M. & CANONACO, F. 2014. High secondary aerosol contribution to particulate pollution during haze events in China. *Nature,* 514**,** 218-222.

HUANG, Y., LING, Z. H., LEE, S. C., HO, S. S. H., CAO, J. J., BLAKE, D. R., CHENG, Y., LAI, S. C., HO, K. F. & GAO, Y. 2015b. Characterization of volatile organic compounds at a roadside environment in Hong Kong: An investigation of influences after air pollution control strategies. *Atmospheric Environment,* 122**,** 809-818.

HUO, Y., LYU, X., YAO, D., ZHOU, B., YUAN, Q., LEE, S. C. & GUO, H. 2024a. Exploring the formation of high levels of hydroxyl dicarboxylic acids at an urban background site in South China. *Journal of Geophysical Research: Atmospheres,* 129**,** e2023JD040096.

HUO, Y., YAO, D. & GUO, H. 2024b. Differences in aerosol chemistry at a regional background site in Hong Kong before and during the COVID-19 pandemic. *Science of the Total Environment,* 926**,** 171990.

HUSSEIN, T., GLYTSOS, T., ONDRáČEK, J., DOHáNYOSOVá, P., ŽDíMAL, V., HäMERI, K., LAZARIDIS, M., SMOLíK, J. & KULMALA, M. 2006. Particle size characterization and emission rates during indoor activities in a house. *Atmospheric Environment,* 40**,** 4285-4307.

HYDER, M. & JöNSSON, J. Å. 2012. Hollow-fiber liquid phase microextraction for lignin pyrolysis acids in aerosol samples and gas chromatography–mass spectrometry analysis. *Journal of Chromatography A,* 1249**,** 48-53.

IINUMA, Y., BöGE, O., GRäFE, R. & HERRMANN, H. 2010. Methyl-nitrocatechols: atmospheric tracer compounds for biomass burning secondary organic aerosols. *Environmental science & technology,* 44**,** 8453-8459.

ISAACMAN-VANWERTZ, G., YEE, L. D., KREISBERG, N. M., WERNIS, R., MOSS, J. A., HERING, S. V., DE SÁ, S. S., MARTIN, S. T., ALEXANDER, M. L. & PALM, B. B. 2016. Ambient gas-particle partitioning of tracers for biogenic oxidation. *Environmental Science & Technology,* 50**,** 9952-9962.

ISAACMAN, G., KREISBERG, N., YEE, L., WORTON, D., CHAN, A., MOSS, J., HERING, S. & GOLDSTEIN, A. 2014. Online derivatization for hourly measurements of gas-and particle-phase semi-volatile oxygenated organic compounds by thermal desorption aerosol gas chromatography (SV-TAG). *Atmospheric Measurement Techniques,* 7**,** 4417-4429.

JANG, M., CZOSCHKE, N. M., LEE, S. & KAMENS, R. M. 2002. Heterogeneous

atmospheric aerosol production by acid-catalyzed particle-phase reactions. *Science,* 298**,** 814-817.

JANSEN, E., CREMERS, J., BORST, S. & TALHOUT, R. 2014. Simple determination of sugars in cigarettes. *Journal of Analytical & Bioanalytical Techniques,* 5**,** 1.

JAOUI, M., EDNEY, E. O., KLEINDIENST, T. E., LEWANDOWSKI, M., OFFENBERG, J. H., SURRATT, J. D. & SEINFELD, J. H. 2008. Formation of secondary organic aerosol from irradiated α-pinene/toluene/NOx mixtures and the effect of isoprene and sulfur dioxide. *Journal of Geophysical Research: Atmospheres,* 113.

JAYNE, J. T., LEARD, D. C., ZHANG, X., DAVIDOVITS, P., SMITH, K. A., KOLB, C. E. & WORSNOP, D. R. 2000. Development of an aerosol mass spectrometer for size and composition analysis of submicron particles. *Aerosol Science & Technology,* 33**,** 49-70.

JI, X., LE BIHAN, O., RAMALHO, O., MANDIN, C., D'ANNA, B., MARTINON, L., NICOLAS, M., BARD, D. & PAIRON, J. C. 2010. Characterization of particles emitted by incense burning in an experimental house. *Indoor Air,* 20**,** 147-158.

JIMENEZ, J. L., CANAGARATNA, M., DONAHUE, N., PREVOT, A., ZHANG, Q., KROLL, J. H., DECARLO, P. F., ALLAN, J. D., COE, H. & NG, N. 2009. Evolution of organic aerosols in the atmosphere. *science,* 326**,** 1525-1529.

JIN, L., XIE, J., WONG, C. K., CHAN, S. K., ABBASZADE, G. L., SCHNELLE-KREIS, J. R., ZIMMERMANN, R., LI, J., ZHANG, G. & FU, P. 2019. Contributions of city-specific fine particulate matter (PM2. 5) to differential in vitro oxidative stress and toxicity implications between Beijing and Guangzhou of China. *Environmental science & technology,* 53**,** 2881-2891.

JOHNSON, A. M., WARING, M. S. & DECARLO, P. F. 2017. Real-time transformation of outdoor aerosol components upon transport indoors measured with aerosol mass spectrometry. *Indoor Air,* 27**,** 230-240.

JURY, M. & WALKER, N. 1988. Marine boundary layer modification across the edge of the Agulhas Current. *Journal of Geophysical Research: Oceans,* 93**,** 647-654.

KAMENS, R., JANG, M., CHIEN, C.-J. & LEACH, K. 1999. Aerosol formation from the reaction of α-pinene and ozone using a gas-phase kinetics-aerosol partitioning model. *Environmental science & technology,* 33**,** 1430-1438.

KAMENS, R. & JAOUI, M. 2001. Modeling aerosol formation from α-pinene+ NO x in the presence of natural sunlight using gas-phase kinetics and gas-particle partitioning theory. *Environmental science & technology,* 35**,** 1394-1405.

KANAKIDOU, M., SEINFELD, J., PANDIS, S., BARNES, I., DENTENER, F. J., FACCHINI, M. C., VAN DINGENEN, R., ERVENS, B., NENES, A. & NIELSEN, C. 2005. Organic aerosol and global climate modelling: a review. *Atmospheric Chemistry and Physics,* 5**,** 1053-1123.

KATZ, E. F., LUNDERBERG, D. M., BROWN, W. L., DAY, D. A., JIMENEZ, J. L.,

NAZAROFF, W. W., GOLDSTEIN, A. H. & DECARLO, P. F. 2021. Large emissions of low-volatility siloxanes during residential oven use. *Environmental Science & Technology Letters,* 8**,** 519-524.

KAVOURAS, I. G., STRATIGAKIS, N. & STEPHANOU, E. G. 1998. Iso-and anteiso-alkanes: specific tracers of environmental tobacco smoke in indoor and outdoor particle-size distributed urban aerosols. *Environmental science & technology,* 32**,** 1369-1377.

KAWAMURA, K. & BIKKINA, S. 2016. A review of dicarboxylic acids and related compounds in atmospheric aerosols: Molecular distributions, sources and transformation. *Atmospheric Research,* 170**,** 140-160.

KAWAMURA, K. & IKUSHIMA, K. 1993. Seasonal changes in the distribution of dicarboxylic acids in the urban atmosphere. *Environmental Science & Technology,* 27**,** 2227-2235.

KAWAMURA, K. & KAPLAN, I. 1987a. Dicarboxylic acids generated by thermal alteration of kerogen and humic acids. *Geochimica et Cosmochimica Acta,* 51**,** 3201-3207.

KAWAMURA, K. & KAPLAN, I. R. 1987b. Motor exhaust emissions as a primary source for dicarboxylic acids in Los Angeles ambient air. *Environmental science & technology,* 21**,** 105-110.

KAWAMURA, K., KASUKABE, H. & BARRIE, L. A. 1996a. Source and reaction pathways of dicarboxylic acids, ketoacids and dicarbonyls in arctic aerosols: One year of observations. *Atmospheric Environment,* 30**,** 1709-1722.

KAWAMURA, K., SEMPERE, R., IMAI, Y., FUJII, Y. & HAYASHI, M. 1996b. Water soluble dicarboxylic acids and related compounds in Antarctic aerosols. *Journal of Geophysical Research: Atmospheres,* 101**,** 18721-18728.

KELLY, J. M., DOHERTY, R. M., O'CONNOR, F. M. & MANN, G. W. 2018. The impact of biogenic, anthropogenic, and biomass burning volatile organic compound emissions on regional and seasonal variations in secondary organic aerosol. *Atmospheric Chemistry and Physics,* 18**,** 7393-7422.

KLEINDIENST, T., CONVER, T., MCIVER, C. & EDNEY, E. 2004. Determination of secondary organic aerosol products from the photooxidation of toluene and their implications in ambient PM 2.5. *Journal of Atmospheric Chemistry,* 47**,** 79-100.

KLEINDIENST, T., JAOUI, M., LEWANDOWSKI, M., OFFENBERG, J. & DOCHERTY, K. 2012. The formation of SOA and chemical tracer compounds from the photooxidation of naphthalene and its methyl analogs in the presence and absence of nitrogen oxides. *Atmospheric Chemistry and Physics,* 12**,** 8711-8726.

KLEPEIS, N. E., NELSON, W. C., OTT, W. R., ROBINSON, J. P., TSANG, A. M., SWITZER, P., BEHAR, J. V., HERN, S. C. & ENGELMANN, W. H. 2001. The National Human Activity Pattern Survey (NHAPS): a resource for assessing

exposure to environmental pollutants. *Journal of Exposure Science & Environmental Epidemiology,* 11**,** 231-252.

KOURTCHEV, I., COPOLOVICI, L., CLAEYS, M. & MAENHAUT, W. 2009. Characterization of atmospheric aerosols at a forested site in Central Europe. *Environmental science & technology,* 43**,** 4665-4671.

KRIEGER, U. K., MARCOLLI, C. & REID, J. P. 2012. Exploring the complexity of aerosol particle properties and processes using single particle techniques. *Chemical Society Reviews,* 41**,** 6631-6662.

KRISTENSEN, K., LUNDERBERG, D. M., LIU, Y., MISZTAL, P. K., TIAN, Y., ARATA, C., NAZAROFF, W. W. & GOLDSTEIN, A. H. 2019. Sources and dynamics of semivolatile organic compounds in a single-family residence in northern California. *Indoor air,* 29**,** 645-655.

KROLL, J. H., NG, N. L., MURPHY, S. M., FLAGAN, R. C. & SEINFELD, J. H. 2005. Secondary organic aerosol formation from isoprene photooxidation under high-NOx conditions. *Geophysical Research Letters,* 32.

KROLL, J. H., NG, N. L., MURPHY, S. M., FLAGAN, R. C. & SEINFELD, J. H. 2006. Secondary organic aerosol formation from isoprene photooxidation. *Environmental science & technology,* 40**,** 1869-1877.

KROLL, J. H. & SEINFELD, J. H. 2008. Chemistry of secondary organic aerosol: Formation and evolution of low-volatility organics in the atmosphere. *Atmospheric Environment,* 42**,** 3593-3624.

KULMALA, M., PIRJOLA, L. & MäKELä, J. M. 2000. Stable sulphate clusters as a source of new atmospheric particles. *Nature,* 404**,** 66-69.

KUMAR, P., SINGH, A., ARORA, T., SINGH, S. & SINGH, R. 2023. Critical review on emerging health effects associated with the indoor air quality and its sustainable management. *Science of The Total Environment,* 872**,** 162163.

LAI, A. M., CLARK, S., CARTER, E., SHAN, M., NI, K., YANG, X., BAUMGARTNER, J. & SCHAUER, J. J. 2020. Impacts of stove/fuel use and outdoor air pollution on chemical composition of household particulate matter. *Indoor Air,* 30**,** 294-305.

LAMBE, A. T., MIRACOLO, M. A., HENNIGAN, C. J., ROBINSON, A. L. & DONAHUE, N. M. 2009. Effective rate constants and uptake coefficients for the reactions of organic molecular markers (n-alkanes, hopanes, and steranes) in motor oil and diesel primary organic aerosols with hydroxyl radicals. *Environmental Science & Technology,* 43**,** 8794-8800.

LANE, T. E., DONAHUE, N. M. & PANDIS, S. N. 2008. Simulating secondary organic aerosol formation using the volatility basis-set approach in a chemical transport model. *Atmospheric Environment,* 42**,** 7439-7451.

LANZ, V., ALFARRA, M., BALTENSPERGER, U., BUCHMANN, B., HUEGLIN, C. & PRéVôT, A. S. 2007. Source apportionment of submicron organic aerosols at

an urban site by factor analytical modelling of aerosol mass spectra. *Atmospheric Chemistry and Physics,* 7**,** 1503-1522.

LEAVEY, A., PATEL, S., MARTINEZ, R., MITROO, D., FORTENBERRY, C., WALKER, M., WILLIAMS, B. & BISWAS, P. 2017. Organic and inorganic speciation of particulate matter formed during different combustion phases in an improved cookstove. *Environmental research,* 158**,** 33-42.

LEE, B. P., LI, Y. J., YU, J. Z., LOUIE, P. K. & CHAN, C. K. 2013. Physical and chemical characterization of ambient aerosol by HR-ToF-AMS at a suburban site in Hong Kong during springtime 2011. *Journal of Geophysical Research: Atmospheres,* 118**,** 8625-8639.

LEE, B. P., LI, Y. J., YU, J. Z., LOUIE, P. K. & CHAN, C. K. 2015. Characteristics of submicron particulate matter at the urban roadside in downtown Hong Kong—Overview of 4 months of continuous high-resolution aerosol mass spectrometer measurements. *Journal of Geophysical Research: Atmospheres,* 120**,** 7040-7058.

LEE, E., CHAN, C. K. & PAATERO, P. 1999. Application of positive matrix factorization in source apportionment of particulate pollutants in Hong Kong. *Atmospheric environment,* 33**,** 3201-3212.

LEE, S.-C., GUO, H., LI, W.-M. & CHAN, L.-Y. 2002a. Inter-comparison of air pollutant concentrations in different indoor environments in Hong Kong. *Atmospheric Environment,* 36**,** 1929-1940.

LEE, S.-C. & WANG, B. 2004. Characteristics of emissions of air pollutants from burning of incense in a large environmental chamber. *Atmospheric Environment,* 38**,** 941-951.

LEE, S. & WANG, B. 2006. Characteristics of emissions of air pollutants from mosquito coils and candles burning in a large environmental chamber. *Atmospheric Environment,* 40**,** 2128-2138.

LEE, S. C., LI, W.-M. & AO, C.-H. 2002b. Investigation of indoor air quality at residential homes in Hong Kong—case study. *Atmospheric Environment,* 36**,** 225-237.

LI, J., XU, W., LI, Z., DUAN, M., OUYANG, B., ZHOU, S., LEI, L., HE, Y., SUN, J. & WANG, Z. 2021. Real-time characterization of aerosol particle composition, sources and influences of increased ventilation and humidity in an office. *Indoor Air,* 31**,** 1364-1376.

LI, N., HAO, M., PHALEN, R. F., HINDS, W. C. & NEL, A. E. 2003. Particulate air pollutants and asthma: a paradigm for the role of oxidative stress in PM-induced adverse health effects. *Clinical immunology,* 109**,** 250-265.

LI, Y., LEE, B., SU, L., FUNG, J. C. H. & CHAN, C. K. 2015. Seasonal characteristics of fine particulate matter (PM) based on high-resolution time-of-flight aerosol mass spectrometric (HR-ToF-AMS) measurements at the HKUST Supersite in

Hong Kong. *Atmospheric Chemistry and Physics,* 15**,** 37-53.

LI, Y. J., LEE, B., YU, J., NG, N. & CHAN, C. K. 2013. Evaluating the degree of oxygenation of organic aerosol during foggy and hazy days in Hong Kong using high-resolution time-of-flight aerosol mass spectrometry (HR-ToF-AMS). *Atmospheric Chemistry and Physics,* 13**,** 8739-8753.

LI, Y. J., YEUNG, J. W., LEUNG, T. P., LAU, A. P. & CHAN, C. K. 2012. Characterization of organic particles from incense burning using an aerodyne high-resolution time-of-flight aerosol mass spectrometer. *Aerosol science and technology,* 46**,** 654-665.

LI, Z., WEN, Q. & ZHANG, R. 2017. Sources, health effects and control strategies of indoor fine particulate matter (PM2. 5): A review. *Science of the Total Environment,* 586**,** 610-622.

LIAO, K., WANG, Q., WANG, S. & YU, J. Z. 2023. Bayesian Inference Approach to Quantify Primary and Secondary Organic Carbon in Fine Particulate Matter Using Major Species Measurements. *Environmental Science & Technology,* 57**,** 5169-5179.

LIAO, K. & YU, J. Z. 2020. Abundance and sources of benzo [a] pyrene and other PAHs in ambient air in Hong Kong: A review of 20-year measurements (1997–2016). *Chemosphere,* 259**,** 127518.

LIU, J., ZHOU, S., ZHANG, Z., KAWAMURA, K., ZHAO, W., WANG, X., SHAO, M., JIANG, F., LIU, J. & SUN, X. 2021. Characterization of dicarboxylic acids, oxoacids, and α-dicarbonyls in PM2. 5 within the urban boundary layer in southern China: Sources and formation pathways. *Environmental Pollution,* 285**,** 117185.

LIU, T., ZHOU, L., LIU, Q., LEE, B. P., YAO, D., LU, H., LYU, X., GUO, H. & CHAN, C. K. 2019. Secondary organic aerosol formation from urban roadside air in Hong Kong. *Environmental science & technology,* 53**,** 3001-3009.

LIU, Y., XING, J., WANG, S., FU, X. & ZHENG, H. 2018. Source-specific speciation profiles of PM2. 5 for heavy metals and their anthropogenic emissions in China. *Environmental Pollution,* 239**,** 544-553.

LONG, C. M. & SARNAT, J. A. 2004. Indoor-outdoor relationships and infiltration behavior of elemental components of outdoor PM2. 5 for Boston-area homes. *Aerosol science and technology,* 38**,** 91-104.

LOUIE, P. K., WATSON, J. G., CHOW, J. C., CHEN, A., SIN, D. W. & LAU, A. K. 2005. Seasonal characteristics and regional transport of PM2. 5 in Hong Kong. *Atmospheric Environment,* 39**,** 1695-1710.

LOUPA, G., ZAROGIANNI, A.-M., KARALI, D., KOSMADAKIS, I. & RAPSOMANIKIS, S. 2016. Indoor/outdoor PM2. 5 elemental composition and organic fraction medications, in a Greek hospital. *Science of the Total Environment,* 550**,** 727-735.

LUI, K., BANDOWE, B. A. M., HO, S. S. H., CHUANG, H.-C., CAO, J.-J., CHUANG, K.-J., LEE, S., HU, D. & HO, K. 2016. Characterization of chemical components and bioreactivity of fine particulate matter (PM2. 5) during incense burning. *Environmental pollution,* 213**,** 524-532.

LUNDEN, M. M., REVZAN, K. L., FISCHER, M. L., THATCHER, T. L., LITTLEJOHN, D., HERING, S. V. & BROWN, N. J. 2003. The transformation of outdoor ammonium nitrate aerosols in the indoor environment. *Atmospheric Environment,* 37**,** 5633-5644.

LUNDERBERG, D. M., KRISTENSEN, K., LIU, Y., MISZTAL, P. K., TIAN, Y., ARATA, C., WERNIS, R., KREISBERG, N., NAZAROFF, W. W. & GOLDSTEIN, A. H. 2019. Characterizing airborne phthalate concentrations and dynamics in a normally occupied residence. *Environmental science & technology,* 53**,** 7337-7346.

LUNDERBERG, D. M., KRISTENSEN, K., TIAN, Y., ARATA, C., MISZTAL, P. K., LIU, Y., KREISBERG, N., KATZ, E. F., DECARLO, P. F. & PATEL, S. 2020. Surface emissions modulate indoor SVOC concentrations through volatility-dependent partitioning. *Environmental science & technology,* 54**,** 6751-6760.

LYU, X., GUO, H., CHENG, H., WANG, X., DING, X., LU, H., YAO, D. & XU, C. 2017. Observation of SOA tracers at a mountainous site in Hong Kong: Chemical characteristics, origins and implication on particle growth. *Science of the Total Environment,* 605**,** 180-189.

LYU, X., GUO, H., YAO, D., LU, H., HUO, Y., XU, W., KREISBERG, N., GOLDSTEIN, A. H., JAYNE, J. & WORSNOP, D. 2020. In situ measurements of molecular markers facilitate understanding of dynamic sources of atmospheric organic aerosols. *Environmental Science & Technology,* 54**,** 11058-11069.

LYU, X., HUO, Y., YANG, J., YAO, D., LI, K., LU, H., ZEREN, Y. & GUO, H. 2021. Real-time molecular characterization of air pollutants in a Hong Kong residence: Implication of indoor source emissions and heterogeneous chemistry. *Indoor air,* 31**,** 1340-1352.

LYU, X., LI, K., GUO, H., MORAWSKA, L., ZHOU, B., ZEREN, Y., JIANG, F., CHEN, C., GOLDSTEIN, A. H. & XU, X. 2023. A synergistic ozone-climate control to address emerging ozone pollution challenges. *One Earth,* 6**,** 964-977.

MA, F., WANG, H., DING, Y., ZHANG, S., WU, G., LI, Y., GONG, D., RISTOVSKI, Z., HE, C. & WANG, B. 2024. Amplified secondary organic aerosol formation induced by anthropogenic–biogenic interactions in forests around megacities. *Journal of Geophysical Research: Atmospheres,* 129**,** e2024JD041679.

MANISALIDIS, I., STAVROPOULOU, E., STAVROPOULOS, A. & BEZIRTZOGLOU, E. 2020. Environmental and health impacts of air pollution: a review. *Frontiers in public health,* 8**,** 14.

MANOUKIAN, A., QUIVET, E., TEMIME-ROUSSEL, B., NICOLAS, M., MAUPETIT, F. & WORTHAM, H. 2013. Emission characteristics of air pollutants from incense and candle burning in indoor atmospheres. *Environmental Science and Pollution Research,* 20**,** 4659-4670.

MARAIS, E. A., JACOB, D. J., JIMENEZ, J. L., CAMPUZANO-JOST, P., DAY, D. A., HU, W., KRECHMER, J., ZHU, L., KIM, P. S. & MILLER, C. C. 2016. Aqueous-phase mechanism for secondary organic aerosol formation from isoprene: application to the southeast United States and co-benefit of SO 2 emission controls. *Atmospheric Chemistry and Physics,* 16**,** 1603-1618.

MASSOLI, P., LAMBE, A., AHERN, A., WILLIAMS, L., EHN, M., MIKKILä, J., CANAGARATNA, M., BRUNE, W., ONASCH, T. & JAYNE, J. 2010. Relationship between aerosol oxidation level and hygroscopic properties of laboratory generated secondary organic aerosol (SOA) particles. *Geophysical Research Letters,* 37.

MATSUI, H., KOIKE, M., KONDO, Y., TAKAMI, A., FAST, J. D., KANAYA, Y. & TAKIGAWA, M. 2014. Volatility basis-set approach simulation of organic aerosol formation in East Asia: implications for anthropogenic–biogenic interaction and controllable amounts. *Atmospheric Chemistry and Physics,* 14**,** 9513-9535.

MCDONALD, B. C., DE GOUW, J. A., GILMAN, J. B., JATHAR, S. H., AKHERATI, A., CAPPA, C. D., JIMENEZ, J. L., LEE-TAYLOR, J., HAYES, P. L. & MCKEEN, S. A. 2018. Volatile chemical products emerging as largest petrochemical source of urban organic emissions. *Science,* 359**,** 760-764.

MCGUIRE, M., CHANG, R.-W., SLOWIK, J., JEONG, C.-H., HEALY, R., LU, G., MIHELE, C., ABBATT, J., BROOK, J. & EVANS, G. 2014. Enhancing non-refractory aerosol apportionment from an urban industrial site through receptor modeling of complete high time-resolution aerosol mass spectra. *Atmospheric Chemistry and Physics,* 14**,** 8017-8042.

MCNEILL, V. F. 2015. Aqueous organic chemistry in the atmosphere: Sources and chemical processing of organic aerosols. ACS Publications.

MENG, Z. & SEINFELD, J. H. 1994. On the source of the submicrometer droplet mode of urban and regional aerosols. *Aerosol Science and Technology,* 20**,** 253-265.

MONOD, A., SIVE, B. C., AVINO, P., CHEN, T., BLAKE, D. R. & ROWLAND, F. S. 2001. Monoaromatic compounds in ambient air of various cities: a focus on correlations between the xylenes and ethylbenzene. *Atmospheric Environment,* 35**,** 135-149.

MORRISON, G., LAKEY, P. S., ABBATT, J. & SHIRAIWA, M. 2019. Indoor boundary layer chemistry modeling. *Indoor Air,* 29**,** 956-967.

MüLLER, L., REINNIG, M.-C., NAUMANN, K., SAATHOFF, H., MENTEL, T., DONAHUE, N. & HOFFMANN, T. 2012. Formation of 3-methyl-1, 2, 3-

butanetricarboxylic acid via gas phase oxidation of pinonic acid–a mass spectrometric study of SOA aging. *Atmospheric chemistry and physics,* 12**,** 1483-1496.

MURPHY, B., DONAHUE, N. M., FOUNTOUKIS, C. & PANDIS, S. N. 2011. Simulating the oxygen content of ambient organic aerosol with the 2D volatility basis set. *Atmospheric Chemistry and Physics,* 11**,** 7859-7873.

MUTZEL, A., RODIGAST, M., IINUMA, Y., BöGE, O. & HERRMANN, H. 2016. Monoterpene SOA–Contribution of first-generation oxidation products to formation and chemical composition. *Atmospheric environment,* 130**,** 136-144.

NAH, T., KESSLER, S. H., DAUMIT, K. E., KROLL, J. H., LEONE, S. R. & WILSON, K. R. 2013. OH-initiated oxidation of sub-micron unsaturated fatty acid particles. *Physical Chemistry Chemical Physics,* 15**,** 18649-18663.

NAKAYAMA, T., SATO, K., TSUGE, M., IMAMURA, T. & MATSUMI, Y. 2015. Complex refractive index of secondary organic aerosol generated from isoprene/NOx photooxidation in the presence and absence of SO2. *Journal of Geophysical Research: Atmospheres,* 120**,** 7777-7787.

NGUYEN, D. L., KAWAMURA, K., ONO, K., RAM, S. S., ENGLING, G., LEE, C.-T., LIN, N.-H., CHANG, S.-C., CHUANG, M.-T. & HSIAO, T.-C. 2016. Comprehensive PM2. 5 organic molecular composition and stable carbon isotope ratios at Sonla, Vietnam: Fingerprint of biomass burning components. *Aerosol and Air Quality Research,* 16**,** 2618-2634.

NIU, S., LIU, R., ZHAO, Q., GAGAN, S., DODERO, A., YING, Q., MA, X., CHENG, Z., CHINA, S. & CANAGARATNA, M. 2024. Quantifying the Chemical Composition and Real-Time Mass Loading of Nanoplastic Particles in the Atmosphere Using Aerosol Mass Spectrometry. *Environmental Science & Technology,* 58**,** 3363-3374.

NOVAKOV, T. & PENNER, J. 1993. Large contribution of organic aerosols to cloud-condensation-nuclei concentrations. *Nature,* 365**,** 823-826.

NOZIèRE, B., GONZáLEZ, N. J., BORG-KARLSON, A. K., PEI, Y., REDEBY, J. P., KREJCI, R., DOMMEN, J., PREVOT, A. S. & ANTHONSEN, T. 2011. Atmospheric chemistry in stereo: A new look at secondary organic aerosols from isoprene. *Geophysical Research Letters,* 38.

OFFENBERG, J. H., LEWANDOWSKI, M., EDNEY, E. O., KLEINDIENST, T. E. & JAOUI, M. 2009. Influence of aerosol acidity on the formation of secondary organic aerosol from biogenic precursor hydrocarbons. *Environmental science & technology,* 43**,** 7742-7747.

OVADNEVAITE, J., CEBURNIS, D., CANAGARATNA, M., BERRESHEIM, H., BIALEK, J., MARTUCCI, G., WORSNOP, D. R. & O'DOWD, C. 2012. On the effect of wind speed on submicron sea salt mass concentrations and source fluxes. *Journal of Geophysical Research: Atmospheres,* 117.

PAATERO, P. & HOPKE, P. K. 2009. Rotational tools for factor analytic models. *Journal of Chemometrics: A Journal of the Chemometrics Society,* 23**,** 91-100.

PAATERO, P. & TAPPER, U. 1994. Positive matrix factorization: A non-negative factor model with optimal utilization of error estimates of data values. *Environmetrics,* 5**,** 111-126.

PACINI, E. 2000. From anther and pollen ripening to pollen presentation. *Pollen and pollination***,** 19-43.

PAULOT, F., CROUNSE, J. D., KJAERGAARD, H. G., KüRTEN, A., ST. CLAIR, J. M., SEINFELD, J. H. & WENNBERG, P. O. 2009. Unexpected epoxide formation in the gas-phase photooxidation of isoprene. *science,* 325**,** 730-733.

PENG, X., WANG, T., WANG, W., RAVISHANKARA, A., GEORGE, C., XIA, M., CAI, M., LI, Q., SALVADOR, C. M. & LAU, C. 2022. Photodissociation of particulate nitrate as a source of daytime tropospheric Cl2. *Nature communications,* 13**,** 939.

PENNINGTON, E. A., SELTZER, K. M., MURPHY, B. N., QIN, M., SEINFELD, J. H. & PYE, H. O. 2021. Modeling secondary organic aerosol formation from volatile chemical products. *Atmospheric chemistry and physics,* 21**,** 18247-18261.

PETRICK, L. M., SVIDOVSKY, A. & DUBOWSKI, Y. 2011. Thirdhand smoke: heterogeneous oxidation of nicotine and secondary aerosol formation in the indoor environment. *Environmental science & technology,* 45**,** 328-333.

POPE, C. A., DOCKERY, D. W. & SCHWARTZ, J. 1995. Review of epidemiological evidence of health effects of particulate air pollution. *Inhalation toxicology,* 7**,** 1-18.

PYE, H. O., PINDER, R. W., PILETIC, I. R., XIE, Y., CAPPS, S. L., LIN, Y.-H., SURRATT, J. D., ZHANG, Z., GOLD, A. & LUECKEN, D. J. 2013. Epoxide pathways improve model predictions of isoprene markers and reveal key role of acidity in aerosol formation. *Environmental science & technology,* 47**,** 11056-11064.

PYE, H. O., WARD-CAVINESS, C. K., MURPHY, B. N., APPEL, K. W. & SELTZER, K. M. 2021. Secondary organic aerosol association with cardiorespiratory disease mortality in the United States. *Nature Communications,* 12**,** 7215.

QIN, Y. M., LI, Y. J., WANG, H., LEE, B. P. Y. L., HUANG, D. D. & CHAN, C. K. 2016. Particulate matter (PM) episodes at a suburban site in Hong Kong: evolution of PM characteristics and role of photochemistry in secondary aerosol formation. *Atmospheric Chemistry and Physics,* 16**,** 14131-14145.

RAMANATHAN, V., CRUTZEN, P. J., KIEHL, J. & ROSENFELD, D. 2001. Aerosols, climate, and the hydrological cycle. *science,* 294**,** 2119-2124.

REFF, A., EBERLY, S. I. & BHAVE, P. V. 2007. Receptor modeling of ambient particulate matter data using positive matrix factorization: review of existing

methods. *Journal of the Air & Waste Management Association,* 57**,** 146-154.

REID, J. P., BERTRAM, A. K., TOPPING, D. O., LASKIN, A., MARTIN, S. T., PETTERS, M. D., POPE, F. D. & ROVELLI, G. 2018. The viscosity of atmospherically relevant organic particles. *Nature communications,* 9**,** 956.

RIVAS, I., VIANA, M., MORENO, T., PANDOLFI, M., AMATO, F., RECHE, C., BOUSO, L., ÀLVAREZ-PEDREROL, M., ALASTUEY, A. & SUNYER, J. 2014. Child exposure to indoor and outdoor air pollutants in schools in Barcelona, Spain. *Environment international,* 69**,** 200-212.

ROBINSON, A. L., SUBRAMANIAN, R., DONAHUE, N. M., BERNARDO-BRICKER, A. & ROGGE, W. F. 2006. Source apportionment of molecular markers and organic aerosol. 3. Food cooking emissions. *Environmental science & technology,* 40**,** 7820-7827.

ROTHFUSS, N. E. & PETTERS, M. D. 2017. Influence of functional groups on the viscosity of organic aerosol. *Environmental science & technology,* 51**,** 271-279.

SARRAFZADEH, M., WILDT, J., PULLINEN, I., SPRINGER, M., KLEIST, E., TILLMANN, R., SCHMITT, S. H., WU, C., MENTEL, T. F. & ZHAO, D. 2016. Impact of NO x and OH on secondary organic aerosol formation from β-pinene photooxidation. *Atmospheric chemistry and physics,* 16**,** 11237-11248.

SATO, K., HATAKEYAMA, S. & IMAMURA, T. 2007. Secondary organic aerosol formation during the photooxidation of toluene: NO x dependence of chemical composition. *The Journal of Physical Chemistry A,* 111**,** 9796-9808.

SCHAUER, J. J., KLEEMAN, M. J., CASS, G. R. & SIMONEIT, B. R. 2002. Measurement of emissions from air pollution sources. 4. C1− C27 organic compounds from cooking with seed oils. *Environmental Science & Technology,* 36**,** 567-575.

SCHAUER, J. J., ROGGE, W. F., HILDEMANN, L. M., MAZUREK, M. A., CASS, G. R. & SIMONEIT, B. R. 1996. Source apportionment of airborne particulate matter using organic compounds as tracers. *Atmospheric Environment,* 30**,** 3837-3855.

SCHLESINGER, R. B. 2007. The health impact of common inorganic components of fine particulate matter (PM2. 5) in ambient air: a critical review. *Inhalation toxicology,* 19**,** 811-832.

SEGUEL, J. M., MERRILL, R., SEGUEL, D. & CAMPAGNA, A. C. 2017. Indoor air quality. *American journal of lifestyle medicine,* 11**,** 284-295.

SEINFELD, J. H. & PANDIS, S. N. 2016. *Atmospheric chemistry and physics: from air pollution to climate change*, John Wiley & Sons.

SHEESLEY, R. J., DEMINTER, J. T., MEIRITZ, M., SNYDER, D. C. & SCHAUER, J. J. 2010. Temporal trends in motor vehicle and secondary organic tracers using in situ methylation thermal desorption GCMS. *Environmental science & technology,* 44**,** 9398-9404.

SHI, Z., ZHANG, D., HAYASHI, M., OGATA, H., JI, H. & FUJIIE, W. 2008. Influences of sulfate and nitrate on the hygroscopic behaviour of coarse dust particles. *Atmospheric Environment,* 42**,** 822-827.

SHILLING, J. E., ZAVERI, R. A., FAST, J. D., KLEINMAN, L., ALEXANDER, M., CANAGARATNA, M. R., FORTNER, E., HUBBE, J. M., JAYNE, J. T. & SEDLACEK, A. 2013. Enhanced SOA formation from mixed anthropogenic and biogenic emissions during the CARES campaign. *Atmospheric Chemistry and Physics,* 13**,** 2091-2113.

SHIRAIWA, M., ZUEND, A., BERTRAM, A. K. & SEINFELD, J. H. 2013. Gas–particle partitioning of atmospheric aerosols: interplay of physical state, non-ideal mixing and morphology. *Physical Chemistry Chemical Physics,* 15**,** 11441-11453.

SHRIVASTAVA, M., ANDREAE, M. O., ARTAXO, P., BARBOSA, H. M., BERG, L. K., BRITO, J., CHING, J., EASTER, R. C., FAN, J. & FAST, J. D. 2019. Urban pollution greatly enhances formation of natural aerosols over the Amazon rainforest. *Nature communications,* 10**,** 1046.

SHRIVASTAVA, M., FAST, J., EASTER, R., GUSTAFSON JR, W., ZAVERI, R. A., JIMENEZ, J. L., SAIDE, P. & HODZIC, A. 2011. Modeling organic aerosols in a megacity: comparison of simple and complex representations of the volatility basis set approach. *Atmospheric Chemistry and Physics,* 11**,** 6639-6662.

SIMONEIT, B. R., ROGGE, W., MAZUREK, M., STANDLEY, L., HILDEMANN, L. & CASS, G. 1993. Lignin pyrolysis products, lignans, and resin acids as specific tracers of plant classes in emissions from biomass combustion. *Environmental science & technology,* 27**,** 2533-2541.

SMITH, K. R. & MEHTA, S. 2003. The burden of disease from indoor air pollution in developing countries: comparison of estimates. *International journal of hygiene and environmental health,* 206**,** 279-289.

SONG, Y., ZHANG, Y., XIE, S., ZENG, L., ZHENG, M., SALMON, L. G., SHAO, M. & SLANINA, S. 2006. Source apportionment of PM2. 5 in Beijing by positive matrix factorization. *Atmospheric Environment,* 40**,** 1526-1537.

SRIVASTAVA, D., VU, T. V., TONG, S., SHI, Z. & HARRISON, R. M. 2022. Formation of secondary organic aerosols from anthropogenic precursors in laboratory studies. *npj Climate and Atmospheric Science,* 5**,** 22.

STANGL, C. M., KRASNOMOWITZ, J. M., APSOKARDU, M. J., TISZENKEL, L., OUYANG, Q., LEE, S. & JOHNSTON, M. V. 2019. Sulfur dioxide modifies aerosol particle formation and growth by ozonolysis of monoterpenes and isoprene. *Journal of Geophysical Research: Atmospheres,* 124**,** 4800-4811.

SURRATT, J. D., CHAN, A. W., EDDINGSAAS, N. C., CHAN, M., LOZA, C. L., KWAN, A. J., HERSEY, S. P., FLAGAN, R. C., WENNBERG, P. O. & SEINFELD, J. H. 2010. Reactive intermediates revealed in secondary organic

aerosol formation from isoprene. *Proceedings of the National Academy of Sciences,* 107**,** 6640-6645.

SURRATT, J. D., LEWANDOWSKI, M., OFFENBERG, J. H., JAOUI, M., KLEINDIENST, T. E., EDNEY, E. O. & SEINFELD, J. H. 2007. Effect of acidity on secondary organic aerosol formation from isoprene. *Environmental science & technology,* 41**,** 5363-5369.

SZMIGIELSKI, R., SURRATT, J. D., GóMEZ-GONZáLEZ, Y., VAN DER VEKEN, P., KOURTCHEV, I., VERMEYLEN, R., BLOCKHUYS, F., JAOUI, M., KLEINDIENST, T. E. & LEWANDOWSKI, M. 2007. 3-methyl-1, 2, 3-butanetricarboxylic acid: An atmospheric tracer for terpene secondary organic aerosol. *Geophysical Research Letters,* 34.

TAI, A. P., MICKLEY, L. J. & JACOB, D. J. 2010. Correlations between fine particulate matter (PM2. 5) and meteorological variables in the United States: Implications for the sensitivity of PM2. 5 to climate change. *Atmospheric environment,* 44**,** 3976-3984.

TALBOT, N., KUBELOVA, L., MAKES, O., CUSACK, M., ONDRACEK, J., VODIČKA, P., SCHWARZ, J. & ZDIMAL, V. 2016. Outdoor and indoor aerosol size, number, mass and compositional dynamics at an urban background site during warm season. *Atmospheric Environment,* 131**,** 171-184.

TAN, Y., HAN, S., CHEN, Y., WU, Z. & LEE, S.-C. 2023. Long-term variation and evaluation of air quality across Hong Kong. *Journal of Environmental Sciences,* 127**,** 284-294.

TO, W. M., YEUNG, L. L. & CHAO, C. Y. 2000. Characterisation of gas phase organic emissions from hot cooking oil in commercial kitchens. *Indoor and Built Environment,* 9**,** 228-232.

TSIMPIDI, A., KARYDIS, V., ZAVALA, M., LEI, W., MOLINA, L., ULBRICH, I., JIMENEZ, J. & PANDIS, S. N. 2010. Evaluation of the volatility basis-set approach for the simulation of organic aerosol formation in the Mexico City metropolitan area. *Atmospheric Chemistry and Physics,* 10**,** 525-546.

VARGA, Z., KISS, G. & HANSSON, H.-C. 2007. Modelling the cloud condensation nucleus activity of organic acids on the basis of surface tension and osmolality measurements. *Atmospheric Chemistry and Physics,* 7**,** 4601-4611.

VESNA, O., SAX, M., KALBERER, M., GASCHEN, A. & AMMANN, M. 2009. Product study of oleic acid ozonolysis as function of humidity. *Atmospheric environment,* 43**,** 3662-3669.

VOLKAMER, R., JIMENEZ, J. L., SAN MARTINI, F., DZEPINA, K., ZHANG, Q., SALCEDO, D., MOLINA, L. T., WORSNOP, D. R. & MOLINA, M. J. 2006. Secondary organic aerosol formation from anthropogenic air pollution: Rapid and higher than expected. *Geophysical Research Letters,* 33.

VU, T. V. & HARRISON, R. M. 2019. Chemical and physical properties of indoor

aerosols.
WANG, D. S., MASOUD, C. G., MODI, M. & HILDEBRANDT RUIZ, L. 2022a. Isoprene–Chlorine Oxidation in the Presence of NO x and Implications for Urban Atmospheric Chemistry. *Environmental Science & Technology,* 56**,** 9251-9264.
WANG, G., ZHANG, R., GOMEZ, M. E., YANG, L., LEVY ZAMORA, M., HU, M., LIN, Y., PENG, J., GUO, S. & MENG, J. 2016. Persistent sulfate formation from London Fog to Chinese haze. *Proceedings of the National Academy of Sciences,* 113**,** 13630-13635.
WANG, J., WANG, G., GAO, J., WANG, H., REN, Y., LI, J., ZHOU, B., WU, C., ZHANG, L. & WANG, S. 2017a. Concentrations and stable carbon isotope compositions of oxalic acid and related SOA in Beijing before, during, and after the 2014 APEC. *Atmospheric Chemistry and Physics,* 17**,** 981-992.
WANG, L., ATKINSON, R. & AREY, J. 2007. Dicarbonyl products of the OH radical-initiated reactions of naphthalene and the C1-and C2-alkylnaphthalenes. *Environmental science & technology,* 41**,** 2803-2810.
WANG, Q., HE, X., HUANG, X. H., GRIFFITH, S. M., FENG, Y., ZHANG, T., ZHANG, Q., WU, D. & YU, J. Z. 2017b. Impact of secondary organic aerosol tracers on tracer-based source apportionment of organic carbon and PM2. 5: A case study in the Pearl River Delta, China. *ACS Earth and Space Chemistry,* 1**,** 562-571.
WANG, Q., HE, X., ZHOU, M., HUANG, D. D., QIAO, L., ZHU, S., MA, Y.-G., WANG, H.-L., LI, L. & HUANG, C. 2020. Hourly measurements of organic molecular markers in urban Shanghai, China: primary organic aerosol source identification and observation of cooking aerosol aging. *ACS Earth and Space Chemistry,* 4**,** 1670-1685.
WANG, Q., QIAO, L., ZHOU, M., ZHU, S., GRIFFITH, S., LI, L. & YU, J. Z. 2018. Source apportionment of PM2. 5 using hourly measurements of elemental tracers and major constituents in an urban environment: Investigation of time-resolution influence. *Journal of Geophysical Research: Atmospheres,* 123**,** 5284-5300.
WANG, Q., WANG, S., CHENG, Y. Y., CHEN, H., ZHANG, Z., LI, J., GU, D., WANG, Z. & YU, J. Z. 2022b. Chemical evolution of secondary organic aerosol tracers during high-PM 2.5 episodes at a suburban site in Hong Kong over 4 months of continuous measurement. *Atmospheric Chemistry and Physics,* 22**,** 11239-11253.
WANG, Q. & YU, J. Z. 2021. Ambient measurements of heterogeneous ozone oxidation rates of oleic, elaidic, and linoleic acid using a relative rate constant approach in an urban environment. *Geophysical Research Letters,* 48**,** e2021GL095130.

WANG, S., WANG, Q., ZHU, S., ZHOU, M., QIAO, L., HUANG, D., MA, Y., LU, Y., HUANG, C. & FU, Q. 2022c. Hourly organic tracers-based source apportionment of PM2. 5 before and during the Covid-19 lockdown in suburban Shanghai, China: Insights into regional transport influences and response to urban emission reductions. *Atmospheric Environment,* 289**,** 119308.

WANG, T., DAI, J., LAM, K. S., NAN POON, C. & BRASSEUR, G. P. 2019. Twenty-five years of lower tropospheric ozone observations in tropical East Asia: The influence of emissions and weather patterns. *Geophysical Research Letters,* 46**,** 11463-11470.

WANG, W., WU, M., LI, L., ZHANG, T., LIU, X., FENG, J., LI, H., WANG, Y., SHENG, G. & CLAEYS, M. 2008. Polar organic tracers in PM 2.5 aerosols from forests in eastern China. *Atmospheric Chemistry and Physics,* 8**,** 7507-7518.

WEBER, R. J., SULLIVAN, A. P., PELTIER, R. E., RUSSELL, A., YAN, B., ZHENG, M., DE GOUW, J., WARNEKE, C., BROCK, C. & HOLLOWAY, J. S. 2007. A study of secondary organic aerosol formation in the anthropogenic-influenced southeastern United States. *Journal of Geophysical Research: Atmospheres,* 112.

WEI, W., MANDIN, C., BLANCHARD, O., MERCIER, F., PELLETIER, M., LE BOT, B., GLORENNEC, P. & RAMALHO, O. 2016. Temperature dependence of the particle/gas partition coefficient: An application to predict indoor gas-phase concentrations of semi-volatile organic compounds. *Science of the Total Environment,* 563**,** 506-512.

WEXLER, A. S. & CLEGG, S. L. 2002. Atmospheric aerosol models for systems including the ions H+, NH4+, Na+, SO42−, NO3−, Cl−, Br−, and H2O. *Journal of Geophysical Research: Atmospheres,* 107**,** ACH 14-1-ACH 14-14.

WILDT, J., MENTEL, T., KIENDLER-SCHARR, A., HOFFMANN, T., ANDRES, S., EHN, M., KLEIST, E., MüSGEN, P., ROHRER, F. & RUDICH, Y. 2014. Suppression of new particle formation from monoterpene oxidation by NO x. *Atmospheric chemistry and physics,* 14**,** 2789-2804.

WILLIAMS, B. J., GOLDSTEIN, A. H., KREISBERG, N. M. & HERING, S. V. 2006. An in-situ instrument for speciated organic composition of atmospheric aerosols: T hermal desorption a erosol GC/MS-FID (TAG). *Aerosol Science and Technology,* 40**,** 627-638.

WILLIAMS, B. J., GOLDSTEIN, A. H., KREISBERG, N. M. & HERING, S. V. 2010. In situ measurements of gas/particle-phase transitions for atmospheric semivolatile organic compounds. *Proceedings of the National Academy of Sciences,* 107**,** 6676-6681.

WILLIAMS, B. J., GOLDSTEIN, A. H., MILLET, D. B., HOLZINGER, R., KREISBERG, N. M., HERING, S. V., WHITE, A. B., WORSNOP, D. R., ALLAN, J. D. & JIMENEZ, J. L. 2007. Chemical speciation of organic aerosol

during the International Consortium for Atmospheric Research on Transport and Transformation 2004: Results from in situ measurements. *Journal of Geophysical Research: Atmospheres,* 112.

WONG, J. P., LEE, A. K. & ABBATT, J. P. 2015. Impacts of sulfate seed acidity and water content on isoprene secondary organic aerosol formation. *Environmental Science & Technology,* 49**,** 13215-13221.

WORTON, D. R., SURRATT, J. D., LAFRANCHI, B. W., CHAN, A. W., ZHAO, Y., WEBER, R. J., PARK, J.-H., GILMAN, J. B., DE GOUW, J. & PARK, C. 2013. Observational insights into aerosol formation from isoprene. *Environmental science & technology,* 47**,** 11403-11413.

WU, K., YANG, X., CHEN, D., GU, S., LU, Y., JIANG, Q., WANG, K., OU, Y., QIAN, Y. & SHAO, P. 2020a. Estimation of biogenic VOC emissions and their corresponding impact on ozone and secondary organic aerosol formation in China. *Atmospheric Research,* 231**,** 104656.

WU, X., CAO, F., HAQUE, M., FAN, M.-Y., ZHANG, S.-C. & ZHANG, Y.-L. 2020b. Molecular composition and source apportionment of fine organic aerosols in Northeast China. *Atmospheric Environment,* 239**,** 117722.

WU, Y., EICHLER, C. M., CAO, J., BENNING, J., OLSON, A., CHEN, S., LIU, C., VEJERANO, E. P., MARR, L. C. & LITTLE, J. C. 2018. Particle/gas partitioning of phthalates to organic and inorganic airborne particles in the indoor environment. *Environmental science & technology,* 52**,** 3583-3590.

XIAO, R., TAKEGAWA, N., ZHENG, M., KONDO, Y., MIYAZAKI, Y., MIYAKAWA, T., HU, M., SHAO, M., ZENG, L. & GONG, Y. 2011. Characterization and source apportionment of submicron aerosol with aerosol mass spectrometer during the PRIDE-PRD 2006 campaign. *Atmospheric Chemistry and Physics,* 11**,** 6911-6929.

XIE, Y.-L., HOPKE, P. K., PAATERO, P., BARRIE, L. A. & LI, S.-M. 1999. Identification of source nature and seasonal variations of arctic aerosol byPositive matrix factorization. *Journal of the Atmospheric Sciences,* 56**,** 249-260.

XU, B., ZHANG, G., GUSTAFSSON, Ö., KAWAMURA, K., LI, J., ANDERSSON, A., BIKKINA, S., KUNWAR, B., POKHREL, A. & ZHONG, G. 2022. Large contribution of fossil-derived components to aqueous secondary organic aerosols in China. *Nature Communications,* 13**,** 5115.

XU, L., GUO, H., BOYD, C. M., KLEIN, M., BOUGIATIOTI, A., CERULLY, K. M., HITE, J. R., ISAACMAN-VANWERTZ, G., KREISBERG, N. M. & KNOTE, C. 2015. Effects of anthropogenic emissions on aerosol formation from isoprene and monoterpenes in the southeastern United States. *Proceedings of the National Academy of Sciences,* 112**,** 37-42.

XU, L., MIDDLEBROOK, A. M., LIAO, J., DE GOUW, J. A., GUO, H., WEBER, R.

J., NENES, A., LOPEZ-HILFIKER, F. D., LEE, B. H. & THORNTON, J. A. 2016. Enhanced formation of isoprene-derived organic aerosol in sulfur-rich power plant plumes during Southeast Nexus. *Journal of Geophysical Research: Atmospheres,* 121**,** 11,137-11,153.

XUE, L., SAUNDERS, S., WANG, T., GAO, R., WANG, X., ZHANG, Q. & WANG, W. 2015. Development of a chlorine chemistry module for the Master Chemical Mechanism. *Geoscientific model development,* 8**,** 3151-3162.

YANG, C., ZHOU, S., ZHANG, C., YU, M., CAO, F. & ZHANG, Y. 2022. Atmospheric chemistry of oxalate: Insight into the role of relative humidity and aerosol acidity from high-resolution observation. *Journal of Geophysical Research: Atmospheres,* 127**,** e2021JD035364.

YANG, K., CHEN, D.-H., DING, X., LI, J., ZHANG, Y.-Q., ZHANG, T., WANG, Q.-Y., WANG, J.-Q., CHENG, Q. & JIANG, H. 2023. Different roles of primary and secondary sources in reducing PM2. 5: Insights from molecular markers in Pearl River Delta, South China. *Atmospheric Environment,* 294**,** 119487.

YANG, L., YOU, B., ZHOU, W., XU, W., LI, Z., ZHANG, Z., ZHANG, Z., ZHANG, Y., LI, Y. & SUN, Y. 2024. Rapid evolution of indoor primary and secondary organic aerosols from human activities. *Building and Environment***,** 111736.

YAO, D., GUO, H., LYU, X., LU, H. & HUO, Y. 2022. Secondary organic aerosol formation at an urban background site on the coastline of South China: Precursors and aging processes. *Environmental Pollution,* 309**,** 119778.

YAO, D., LYU, X., LU, H., ZENG, L., LIU, T., CHAN, C. K. & GUO, H. 2021. Characteristics, sources and evolution processes of atmospheric organic aerosols at a roadside site in Hong Kong. *Atmospheric Environment,* 252**,** 118298.

YAO, X., FANG, M., CHAN, C. K., HO, K. & LEE, S. 2004. Characterization of dicarboxylic acids in PM2. 5 in Hong Kong. *Atmospheric Environment,* 38**,** 963-970.

YE, Z., ZHUANG, Y., CHEN, Y., ZHAO, Z., MA, S., HUANG, H., CHEN, Y. & GE, X. 2020. Aqueous-phase oxidation of three phenolic compounds by hydroxyl radical: Insight into secondary organic aerosol formation yields, mechanisms, products and optical properties. *Atmospheric Environment,* 223**,** 117240.

YEE, L. D., ISAACMAN-VANWERTZ, G., WERNIS, R. A., KREISBERG, N. M., GLASIUS, M., RIVA, M., SURRATT, J. D., DE SÁ, S. S., MARTIN, S. T. & ALEXANDER, M. L. 2020. Natural and anthropogenically influenced isoprene oxidation in southeastern United States and central Amazon. *Environmental Science & Technology,* 54**,** 5980-5991.

YEE, L. D., ISAACMAN-VANWERTZ, G., WERNIS, R. A., MENG, M., RIVERA, V., KREISBERG, N. M., HERING, S. V., BERING, M. S., GLASIUS, M. & UPSHUR, M. A. 2018. Observations of sesquiterpenes and their oxidation

products in central Amazonia during the wet and dry seasons. *Atmospheric Chemistry and Physics,* 18**,** 10433-10457.

YIM, S. H. L., FUNG, J. C. H., LAU, A. K. H. & KOT, S. C. 2009. Air ventilation impacts of the "wall effect" resulting from the alignment of high-rise buildings. *Atmospheric Environment,* 43**,** 4982-4994.

YIN, S., ZHENG, J., LU, Q., YUAN, Z., HUANG, Z., ZHONG, L. & LIN, H. 2015. A refined 2010-based VOC emission inventory and its improvement on modeling regional ozone in the Pearl River Delta Region, China. *Science of the Total Environment,* 514**,** 426-438.

YU, J., COCKER, D. R., GRIFFIN, R. J., FLAGAN, R. C. & SEINFELD, J. H. 1999. Gas-phase ozone oxidation of monoterpenes: Gaseous and particulate products. *Journal of Atmospheric Chemistry,* 34**,** 207-258.

YU, J. Z., HUANG, X.-F., XU, J. & HU, M. 2005. When aerosol sulfate goes up, so does oxalate: Implication for the formation mechanisms of oxalate. *Environmental science & technology,* 39**,** 128-133.

YU, J. Z., YANG, H., ZHANG, H. & LAU, A. K. 2004. Size distributions of water-soluble organic carbon in ambient aerosols and its size-resolved thermal characteristics. *Atmospheric Environment,* 38**,** 1061-1071.

YU, L., SMITH, J., LASKIN, A., ANASTASIO, C., LASKIN, J. & ZHANG, Q. 2014. Chemical characterization of SOA formed from aqueous-phase reactions of phenols with the triplet excited state of carbonyl and hydroxyl radical. *Atmospheric Chemistry and Physics,* 14**,** 13801-13816.

YU, L., WANG, G., ZHANG, R., ZHANG, L., SONG, Y., WU, B., LI, X., AN, K. & CHU, J. 2013. Characterization and source apportionment of PM2. 5 in an urban environment in Beijing. *Aerosol and air quality research,* 13**,** 574-583.

YU, Q., CHEN, J., CHENG, S., QIN, W., ZHANG, Y., SUN, Y. & AHMAD, M. 2021. Seasonal variation of dicarboxylic acids in PM2. 5 in Beijing: Implications for the formation and aging processes of secondary organic aerosols. *Science of the Total Environment,* 763**,** 142964.

YUAN, Q., LAI, S., SONG, J., DING, X., ZHENG, L., WANG, X., ZHAO, Y., ZHENG, J., YUE, D. & ZHONG, L. 2018. Seasonal cycles of secondary organic aerosol tracers in rural Guangzhou, Southern China: The importance of atmospheric oxidants. *Environmental Pollution,* 240**,** 884-893.

YUAN, Z., YU, J., LAU, A. K. H., LOUIE, P. K. K. & FUNG, J. C. H. 2006. Application of positive matrix factorization in estimating aerosol secondary organic carbon in Hong Kong and its relationship with secondary sulfate. *Atmospheric Chemistry and Physics,* 6**,** 25-34.

ZAHARDIS, J. & PETRUCCI, G. 2007. The oleic acid-ozone heterogeneous reaction system: products, kinetics, secondary chemistry, and atmospheric implications of a model system–a review. *Atmospheric Chemistry and Physics,* 7**,** 1237-1274.

ZENG, J., YU, Z., MEKIC, M., LIU, J., LI, S., LOISEL, G., GAO, W., GANDOLFO, A., ZHOU, Z. & WANG, X. 2020. Evolution of indoor cooking emissions captured by using secondary electrospray ionization high-resolution mass spectrometry. *Environmental science & technology letters,* 7**,** 76-81.

ZHANG, H., LI, J., YING, Q., YU, J. Z., WU, D., CHENG, Y., HE, K. & JIANG, J. 2012. Source apportionment of PM2. 5 nitrate and sulfate in China using a source-oriented chemical transport model. *Atmospheric environment,* 62**,** 228-242.

ZHANG, H., YEE, L. D., LEE, B. H., CURTIS, M. P., WORTON, D. R., ISAACMAN-VANWERTZ, G., OFFENBERG, J. H., LEWANDOWSKI, M., KLEINDIENST, T. E. & BEAVER, M. R. 2018. Monoterpenes are the largest source of summertime organic aerosol in the southeastern United States. *Proceedings of the National Academy of Sciences,* 115**,** 2038-2043.

ZHANG, K., YANG, L., LI, Q., LI, R., ZHANG, D., XU, W., FENG, J., WANG, Q., WANG, W. & HUANG, L. 2021. Hourly measurement of PM2. 5-bound nonpolar organic compounds in Shanghai: Characteristics, sources and health risk assessment. *Science of The Total Environment,* 789**,** 148070.

ZHANG, Q., ALFARRA, M. R., WORSNOP, D. R., ALLAN, J. D., COE, H., CANAGARATNA, M. R. & JIMENEZ, J. L. 2005a. Deconvolution and quantification of hydrocarbon-like and oxygenated organic aerosols based on aerosol mass spectrometry. *Environmental science & technology,* 39**,** 4938-4952.

ZHANG, Q., WORSNOP, D., CANAGARATNA, M. & JIMENEZ, J. 2005b. Hydrocarbon-like and oxygenated organic aerosols in Pittsburgh: insights into sources and processes of organic aerosols. *Atmospheric Chemistry and Physics,* 5**,** 3289-3311.

ZHANG, Y. & HATAKEYAMA, S. 2016. New directions: Need for better understanding of source and formation process of phthalic acid in aerosols as inferred from. *Atmos. Environ,* 140**,** 147-149.

ZHAO, D., SCHMITT, S. H., WANG, M., ACIR, I.-H., TILLMANN, R., TAN, Z., NOVELLI, A., FUCHS, H., PULLINEN, I. & WEGENER, R. 2018. Effects of NO x and SO 2 on the secondary organic aerosol formation from photooxidation of α-pinene and limonene. *Atmospheric Chemistry and Physics,* 18**,** 1611-1628.

ZHAO, S., TIAN, H., LUO, L., LIU, H., WU, B., LIU, S., BAI, X., LIU, W., LIU, X. & WU, Y. 2021. Temporal variation characteristics and source apportionment of metal elements in PM2. 5 in urban Beijing during 2018–2019. *Environmental Pollution,* 268**,** 115856.

ZHAO, Y., HU, M., SLANINA, S. & ZHANG, Y. 2007. Chemical compositions of fine particulate organic matter emitted from Chinese cooking. *Environmental science & technology,* 41**,** 99-105.

ZHAO, Y., KREISBERG, N. M., WORTON, D. R., TENG, A. P., HERING, S. V. &

GOLDSTEIN, A. H. 2013. Development of an in situ thermal desorption gas chromatography instrument for quantifying atmospheric semi-volatile organic compounds. *Aerosol Science and Technology,* 47**,** 258-266.

ZHENG, J., SHAO, M., CHE, W., ZHANG, L., ZHONG, L., ZHANG, Y. & STREETS, D. 2009. Speciated VOC emission inventory and spatial patterns of ozone formation potential in the Pearl River Delta, China. *Environmental science & technology,* 43**,** 8580-8586.

ZHENG, M., HAGLER, G. S., KE, L., BERGIN, M. H., WANG, F., LOUIE, P. K., SALMON, L., SIN, D. W., YU, J. Z. & SCHAUER, J. J. 2006. Composition and sources of carbonaceous aerosols at three contrasting sites in Hong Kong. *Journal of Geophysical Research: Atmospheres,* 111.

ZHENG, M., KESTER, D. R., WANG, F., SHI, X. & GUO, Z. 2008. Size distribution of organic and inorganic species in Hong Kong aerosols during the wet and dry seasons. *Journal of Geophysical Research: Atmospheres,* 113.

ZHONG, Z., ZHENG, J., ZHU, M., HUANG, Z., ZHANG, Z., JIA, G., WANG, X., BIAN, Y., WANG, Y. & LI, N. 2018. Recent developments of anthropogenic air pollutant emission inventories in Guangdong province, China. *Science of the total environment,* 627**,** 1080-1092.

ZHOU, R., AN, Q., PAN, X., YANG, B., HU, J. & WANG, Y. 2015a. Higher cytotoxicity and genotoxicity of burning incense than cigarette. *Environmental chemistry letters,* 13**,** 465-471.

ZHOU, Y., HUANG, X. H., BIAN, Q., GRIFFITH, S. M., LOUIE, P. K. & YU, J. Z. 2015b. Sources and atmospheric processes impacting oxalate at a suburban coastal site in Hong Kong: Insights inferred from 1 year hourly measurements. *Journal of Geophysical Research: Atmospheres,* 120**,** 9772-9788.

ZHU, J., PENNER, J. E., LIN, G., ZHOU, C., XU, L. & ZHUANG, B. 2017. Mechanism of SOA formation determines magnitude of radiative effects. *Proceedings of the National Academy of Sciences,* 114**,** 12685-12690.

ZHU, S., ZHOU, M., QIAO, L., HUANG, D. D., WANG, Q., WANG, S., GAO, Y., JING, S., WANG, Q. & WANG, H. 2023. Evolution and chemical characteristics of organic aerosols during wintertime PM 2.5 episodes in Shanghai, China: insights gained from online measurements of organic molecular markers. *Atmospheric Chemistry and Physics,* 23**,** 7551-7568.

ZHU, W., LUO, L., CHENG, Z., YAN, N., LOU, S. & MA, Y. 2018. Characteristics and contributions of biogenic secondary organic aerosol tracers to PM2. 5 in Shanghai, China. *Atmospheric Pollution Research,* 9**,** 179-188.

ZHU, Y., TILGNER, A., HOFFMANN, E. H., HERRMANN, H., KAWAMURA, K., YANG, L., XUE, L. & WANG, W. 2020. Multiphase MCM–CAPRAM modeling of the formation and processing of secondary aerosol constituents observed during the Mt. Tai summer campaign in 2014. *Atmospheric Chemistry*

and Physics, 20**,** 6725-6747.
ZIEMANN, P. 2011. Effects of molecular structure on the chemistry of aerosol formation from the OH-radical-initiated oxidation of alkanes and alkenes. *International Reviews in Physical Chemistry,* 30**,** 161-195.
ZIEMANN, P. J. 2005. Aerosol products, mechanisms, and kinetics of heterogeneous reactions of ozone with oleic acid in pure and mixed particles. *Faraday Discussions,* 130**,** 469-490.
ZIEMANN, P. J. & ATKINSON, R. 2012. Kinetics, products, and mechanisms of secondary organic aerosol formation. *Chemical Society Reviews,* 41**,** 6582-6605.